Bucknell University
Bucknell Digital Commons

Master's Theses   Student Theses

2010

A Microfluidic Method to Measure Diffusion in Hydrogels

Andrew Lee Litzenberger
Bucknell University

Follow this and additional works at: https://digitalcommons.bucknell.edu/masters_theses

Part of the Chemical Engineering Commons

A MICROFLUIDIC METHOD TO MEASURE DIFFUSION IN HYDROGELS

By

Andrew Litzenberger
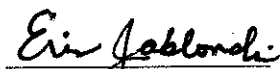
A Thesis

Presented to the Faculty of

Bucknell University

In Partial Fulfillment of the Requirements for the Degree of

Master of Science in Chemical Engineering
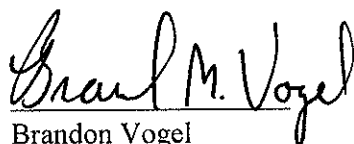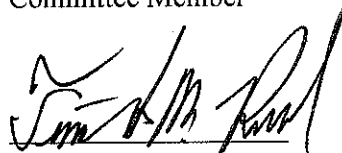
Approved:

Erin Jablonksi
Co-Advisor

James Maneval
Co-Advisor

Brandon Vogel
Committee Member

Timothy Raymond
Department Chairperson

5/13/2010
Date

I, Andrew Litzenberger, do grant permission for my thesis to be copied

_____

Acknowledgements

I owe thanks to the many individuals who helped me during this project. First, I would like thank my co-advisors Dr. Erin Jablonski and Dr. James Maneval for their help and guidance over the past two years. Dr. Jablonski first introduced me to the world of microfluidics, and Dr. Maneval showed me the capability of nuclear magnetic resonance technology. Both provided support and encouragement; without them, this project would have never come to fruition. I would like to thank committee member Dr. Brandon Vogel for his interest in the project and thorough review of the manuscript. I would like to thank Janet Tesfai, Stephanie Evans, and Drew Hackman for their assistance both in and out of the lab during the past two years.

I would like to thank all my professors over the past five years at Bucknell for their time and patience while teaching me. The chemical engineering department deserves thanks for giving me the opportunity to continue learning and for funding me through the summer. I would like to thank Diane Hall for her help with lab equipment and ordering supplies. Nancy Lamay deserves special thanks for her encouragement and the steady supply of candy from her desk. I would also like to thank all the chemical engineering graduate students for providing countless hours of commiseration and entertainment while in the grad office. My girlfriend Tara Pedersen deserves special thanks for her constant support, and encouragement. Her cookies, cupcakes, and dinners helped me through the long hours spent on this project. Finally I would like to thank my family for supporting and encouraging me.

Table of Contents

List of Figures

List of Tables

List of Abbreviations

DI-H2O   De-ionized water

DPI   Dots per inch

DSS   4,4-dimethyl-4-silapentane-1-sulfonic acid

ECM   Extra cellular matrix

FRAP   Fluorescence recovery after photo bleaching

FRP   Free radical polymerization

FTIR   Fourier Transform Infrared

HSV   Hue, Saturation, Value

Irgacure 2959   4-(2-hydroxyethoxy)phenyl-(2-hydroxy-2-propyl)ketone

MDS   multidimensional scaling

NMR   Nuclear Magnetic Resonance

NTSC   National Television System Committee

PCA   Principle component analysis

PDI   Polydispersity index

PEG   poly(ethylene glycol)

PEG-DA   Poly(ethylene glycol) diacrylate

RGB   Red, Green, Blue

SAM   Self assembled monolayer

TPM   3-(trimethoxysilyl)propyl methacrylate

UV   Ultraviolet long wave (365 nm)

Abstract

A novel microfluidic method is proposed for studying diffusion of small molecules in a hydrogel. Microfluidic devices were prepared with semi-permeable microchannels defined by crosslinked poly(ethylene glycol) (PEG). Uptake of dye molecules from aqueous solutions flowing through the microchannels was observed optically and diffusion of the dye into the hydrogel was quantified. To complement the diffusion measurements from the microfluidic studies, nuclear magnetic resonance (NMR) characterization of the diffusion of dye in the PEG hydrogels was performed.

The diffusion of small molecules in a hydrogel is relevant to applications such as drug delivery and modeling transport for tissue-engineering applications. The diffusion of small molecules in a hydrogel is dependent on the extent of crosslinking within the gel, gel structure, and interactions between the diffusive species and the hydrogel network. These effects were studied in a model environment (semi-infinite slab) at the hydrogel-fluid boundary in a microfluidic device.

The microfluidic devices containing PEG microchannels were fabricated using photolithography. The unsteady diffusion of small molecules (dyes) within the microfluidic device was monitored and recorded using a digital microscope. The information was analyzed with techniques drawn from digital microscopy and image analysis to obtain concentration profiles with time. Using a diffusion model to fit this concentration vs. position data, a diffusion coefficient was obtained. This diffusion coefficient was compared to those from complementary NMR analysis. A pulsed field

gradient (PFG) method was used to investigate and quantify small molecule diffusion in hydrogels.

There is good agreement between the diffusion coefficients obtained from the microfluidic methods and those found from the NMR studies. The microfluidic approach used in this research enables the study of diffusion at length scales that approach those of vasculature, facilitating models for studying drug elution from hydrogels in blood-contacting applications.

Introduction

Hydrogels are unique because of their tunable transport properties and high degree of biocompatibility. Because of these properties, hydrogels have found widespread applications in the medical and pharmaceutical industries. One such application of hydrogels is their use in diffusion-controlled drug delivery systems. These systems can provide extended delivery of therapeutic agents, which is both more efficient and more effective than many current delivery methods. Controlled drug delivery systems rely on knowledge of the therapeutic agent transport properties in the hydrogel in order to function properly. However, the complexity of hydrogel networks makes these transport properties difficult, or impossible, to predict.

Diffusion is a transport process driven by thermodynamic forces on the molecular level. The first diffusive model was proposed by Fick in the 19th century. First described as an empirical parameter, the diffusion coefficient is central to describing and predicting diffusive behavior in Fick's model. Due to the importance of diffusion coefficients, theories have been developed to predict them in gases, liquids, and solids. For simple systems these models work reasonably well. With increasingly complex systems, however, these models become inaccurate and more reliant on empirical parameters.

More precise understanding of the mechanisms of diffusion in hydrogels would serve a practical need in designing drug delivery devices. This understanding would also provide a stepping stone to describing diffusion in natural tissues. Hydrogels and natural

tissues share many of the same structural features, and some natural tissues such as the extra cellular matrix (ECM), can be classified as a hydrogel.

Transport properties in hydrogels are dependent on factors describing the individual solute and the hydrogel system. Factors known to affect transport properties include gel composition, structure, solute size, hydrophobicity, ionic charge, hydrodynamic interactions, tortuosity, and surface modifications. These factors and the interactions between them can create increasingly complex behavior. Current diffusion models are beginning to take these factors into account, however a unified theory has yet to be developed, and the need for experimental data remains high. Current methods of quantifying diffusion focus on bulk transport and are ill suited to study the effects of surface modification or transient flow patterns. Furthermore, diffusion experiments may require large amounts of time or expensive equipment to conduct.

Microfluidic devices have been of interest in the last two decades of scientific inquiry because they can manipulate fluids on a small scale and offer an unrestrained slate of possibilities to researchers. The myriad unit operations available on a microfluidic platform have inspired researchers to create the proverbial "lab-on-a-chip." Microfluidic technology includes fluid channels, flow controllers, micro-reactors, and a plethora of chemical and biological indicators. Factors inherent to microfluidic technology, such as small scale and low cost make them an ideal platform for investigating diffusion.

In this thesis, a simple microfluidic device is developed to investigate diffusion in hydrogels. It is designed to be robust and allow for further modification. An

experimental procedure is developed for determining a diffusivity value for optical dyes in hydrogels using this microfluidic device. Diffusivities obtained from the microfluidic device are compared with those obtained using nuclear magnetic resonance (NMR) procedures. Some models available in the literature are evaluated for consistency.

The thesis is outlined as follows. First, a review of hydrogels, diffusion models, and microfluidic fabrication techniques is presented in chapter two. Chapter three outlines the device's design and fabrication methods, as well as experimental procedures used to determine diffusivities. Chapter four describes the methods of analysis used in this thesis. Chapter five presents the results and includes a discussion concerning experiments carried out in this research. Chapter six provides a summary and chapter seven suggests an outline for future work.

Background

To develop a microfluidic technique for measuring diffusion in hydrogels, a review of the materials, experimental methods, theoretical concepts, and results from literature must be conducted. First, a discussion of hydrogels is presented as hydrogels are the primary material of interest. A section on diffusion considering theoretical, experimental, and modeling aspects follows thereafter. Finally, there is a discussion of emerging microfluidic technology.

2.1 Hydrogels

Hydrogels are polymeric networks that absorb large quantities of water while remaining insoluble in aqueous solutions due to chemical or physical crosslinking of individual polymer chains.[1] Hydrogels can be formed from natural or synthetic polymers and could be of a single composition, a mixture, or a copolymer of two or more monomers. As hydrogels absorb water, they swell. This swelling behavior can be exploited and applied as sensors, pumps, and valves in microfluidic devices[2], as well as in controlled drug release platforms.[3] Hydrogels can be highly biocompatible and resemble natural living tissue due to their high water content. Hydrogels are used extensively in the medical and pharmaceutical industries for applications in contact lenses, drug delivery devices, tissue scaffolds, and linings for artificial implants.[4, 5]

The hydrogel used in this research is poly (ethylene glycol) di-acrylate (PEG-DA) shown in Figure 2.1. PEG-DA is formed by functionalizing the end groups of poly(ethylene glycol) (PEG) with acrylate groups, shown in Figure 2.2. PEG-DA is a

unique hydrogel because the polymer forms a gel from physical entanglements and

crosslinking. [6] Also, PEG hydrogels are biocompatible, nontoxic and non-immunogenic.[7]

PEG has been approved by the FDA for human intravenous, oral, and dermal

applications.[8] This approval has led to the widespread use of PEG in pharmaceutical and

biomaterial applications[9], such as surface modification of implants and grafting to

biological particles and proteins. Grafting PEG increases biocompatibility and residence

time in the body.[9, 10] PEG has been used in tissue scaffolds[11] and controlled drug delivery

devices.[4, 12] PEG's unique properties have been combined with other polymers to form

highly specialized block copolymers, or polymer composites. PEG has a lower swelling

percentage compared to similar hydrogel systems, making it ideal for use in a confined

microfluidic system.[13]
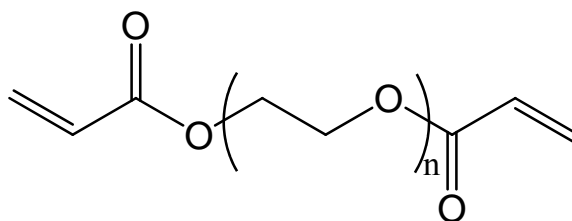
Figure 2.1**:** Chemical structure of PEG-DA polymer
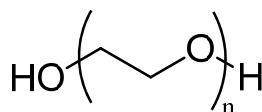
Figure 2.2: Chemical structure of PEG polymer

2.1.1 Hydrogel Properties

There are several parameters used to describe hydrogel polymeric networks.[1, 3] These parameters are: the polymer fraction in the swollen state, $v_{2,s}$; the number average molecular weight between crosslinks, $\bar{M}_C$; and the network mesh size, ξ.

The polymer fraction in the swollen state characterizes how well the polymer absorbs water. It can be expressed as the ratio of the volume of dry polymer, V_P, to the volume of the swollen polymer gel, V_g, and is the reciprocal of the degree of swelling, Q.

$$v_{2,s} = \frac{V_P}{V_g} = \frac{1}{Q} \tag{2.1}$$

The polymer fraction in the swollen state can easily be determined with equilibrium swelling and lyophilization experiments using equation (2.1) above. If the volume of the polymer and solute can be assumed to be additive,

$$V_{gel} = V_{polymer} + V_{solvent} \tag{2.2}$$

then the dry and swollen mass of the gel can be used to find the polymer volume fraction in the swollen state:

$$v_{2,s} = \frac{1}{1 + \dfrac{\rho_{polymer}}{\rho_{solvent}}\left(\dfrac{m_{swollen}}{m_{dry}} - 1\right)} \tag{2.3}$$

where $\rho_{solvent}$ is the density of the solvent, $\rho_{polymer}$ is the density of the polymer (ρ_{PEG} = 1.12 g/mol), $m_{swollen}$ is the mass of the swollen hydrogel, and m_{dry} is the mass of the dry hydrogel after lyophilization. This method is often easier to implement experimentally and widely used in literature.[6, 14, 15]

The number average molecular weight between crosslinks, $\bar{M}_C$, is a measure of the degree of crosslinking within the polymer, and can be related to physical properties including swelling behavior and stiffness. The relationship between $\bar{M}_C$ and swelling behaviour was first quantified through the Flory-Rehner equation.[3] This equation quantifies the molecular weight between crosslinks for a neutral hydrogel prepared in the absence of water or any other solvent.[1, 3]

$$\frac{1}{\bar{M}_C} = \frac{2}{\bar{M}_n} - \frac{\left(\frac{\bar{v}}{V_1}\right)\left[\ln(1-v_{2,s}) + v_{2,s} + \chi_{12}v_{2,s}^{2}\right]}{v_{2,s}^{1/3} - \frac{v_{2,s}}{2}} \tag{2.4}$$

where $\bar{M}_n$ is the molecular weight of the polymer chains prepared in the absence of a crosslinking agent, $v_{2,s}$ is the polymer fraction in the swollen state, χ_{12} is the polymer-solvent interaction parameter, $\bar{v}$ is the specific volume of the polymer, and V_1 is the molar volume of water.

If the polymer hydrogel was prepared in water, equation (2.4) can be modified to account for the presence of water during crosslinking:

$$\frac{1}{\bar{M}_C} = \frac{2}{\bar{M}_n} - \frac{\left(\frac{\bar{v}}{V_1}\right)\left[\ln(1-v_{2,s}) + v_{2,s} + \chi_{12}v_{2,s}^{2}\right]}{v_{2,r}\left[\left(\frac{v_{2,s}}{v_{2,r}}\right)^{1/3} - \frac{1}{2}\left(\frac{v_{2,s}}{v_{2,r}}\right)\right]} \tag{2.5}$$

where $v_{2,r}$ is the polymer volume fraction in the relaxed state, which is defined as the state of the polymer after crosslinking, but before swelling.

Using the theory of rubber elasticity[16, 17], relationships can be derived between material properties and hydrogel parameters. Most hydrogels display some degree of rubbery deformability, and experimental tests can quantify this behavior. The molecular weight between crosslinks can be related to the shear modulus by the expression:[17]

$$\frac{1}{M_C} = \frac{G}{\rho RT \left(\dfrac{\overline{r_0^2}}{r_f^2} \right)} + \frac{2}{M_n} \tag{2.6}$$

where Mc is the molecular weight between crosslinks, ρ is the density of the swollen polymer, G is the shear modulus, R is the ideal gas constant, T is the thermodynamic temperature, M_n is the number average molecular weight before crosslinking, and $\left(\dfrac{\overline{r_0^2}}{r_f^2} \right)$ is the 'front factor,' or the ratio of the end-to-end distance of the chain in a real network with the end-to-end distance of isolated chains. In the absence of information regarding this factor, it is often approximated as 1.0.[17] The model assumes the network is ideal; i.e. all chains are elastically active. Imperfections such as loops, unreacted cross links, and chain entanglements are not taken into account.

An expression has also been developed for relating the molecular weight between crosslinks, M_c and the elastic, or Young's, modulus E'.[16] The equation is given below:

$$M_C = \frac{3\rho RT}{E'} \tag{2.7}$$

where ρ is the polymer density, R is the ideal gas constant, and T is the thermodynamic temperature. The relationship should be taken as a rough estimation which often underestimates M_c since it does not take into account physical crosslinks or chain ends.[18]

The final parameter used to describe hydrogels is the mesh size, or characteristic length, ξ, which is a characteristic distance between cross links, or tie points in a polymer. This parameter, ξ, is easy to visualize, as shown in Figure 2.3 below.

Figure 2.3: Crosslinks (a) between chains (b), and the mesh size, ξ, shown in a crosslinked network[19]

The mesh size can be related to other parameters discussed above via scaling relationships, which produce the following:[1]

$$\xi = v_{2,s}^{-1/3} \left(\overline{r_0^2} \right)^{1/2} \tag{2.8}$$

where $\left(\overline{r_0^2} \right)^{1/2}$ is the unperturbed (solvent free) end to end distance of the polymer chain between two adjacent crosslinks. This statistical parameter can be found via a relationship first developed by Flory:[20]

$$\left(\overline{r_0^2} \right) = C_n x l^2 \tag{2.9}$$

where C_n is the characteristic ratio, x is the number of links in the chain, and l is the length of each link. This relationship can be modified slightly by making two assumptions. First, the total number of links, x, is equal to the number of repeat units, n, multiplied by the number of links per repeat unit n_r. Second, the average bond length, l, is equal to the length along the backbone of the repeat unit, l_r, divided by the number of links per repeat unit, n_r. Using these assumptions with Equations (2.8) and (2.9) produce the following:

$$\xi = v_{2,s}{}^{-1/3} \left(\frac{C_n n}{n_r} \right)^{1/2} l_r \qquad\qquad (2.10)$$

For this equation, l_r is the length of the backbone for one repeat unit, n is the number of repeat units between crosslinks, n_r is the number of bonds per repeat unit, and C_n is the Flory characteristic ratio. For vinyl polymers $l_r = (2 \times 1.54)$Å, while for PEG $l_r = (2 \times 1.54 + 1.50)$ Å. For an end functionalized polymer like PEG-DA where crosslinks can only occur at the end of the chain, n can be taken as the degree of polymerization. The number of bonds per repeat units, n_r, is 2 for vinyl polymers and 3 for PEG. The characteristic ratio depends on the polymer system which has been taken to be 3.8,[17] 4.0,[20] or 4.0 - 5.2 [21] for PEG.

Equation (2.10) does not take into account any extension offered by end groups, which is negligible for long polymer chains. For smaller chains, one way to take into account chain extension due to end groups is to assume the end groups have similar properties to the polymer repeat unit and add 2 to the degree of polymerization. This

gives a relation for the mesh size for small polymers with end group crosslinking functionalization:

$$\xi = v_{2,s}{}^{-1/3} \left(\frac{C_n\left(n+2\right)}{n_r} \right)^{1/2} l_m \qquad\qquad (2.11)$$

The characteristic length, or mesh size is an important factor in solute transport in hydrogels. The mesh size also affects properties such as mechanical strength, degradability, and diffusivity within a hydrogel. If a solute molecule is larger than the mesh size, it is theoretically impossible for the solute molecule to move through the hydrogel. The mesh size of a hydrogel is affected by the degree of crosslinking, chemical structure of the monomer, and other external stimuli, such as pH, temperature, and the presence of ions.

A crosslinked hydrogel can have multiple structural features on the molecular level. These features dictate the behavior of the polymer network and affect physical properties such as swelling ratio and mesh size. These features are typically spoken of in the framework of an ideal chemically crosslinked network. In an ideal network, chain entanglement, chain loops, and unreacted crosslink sites do not contribute to the degree of crosslinking. For an ideal PEG-DA network, one can assume that every chain forms two crosslinks. It follows that the theoretical maximum molecular weight between crosslinks is simply the number average molecular weight divided by the number of junctions per chain (2 in the case of PEG-DA).[18] This approximation does not take into account physical crosslinks, chain loops, or unreacted end groups since an ideal network was assumed. In a real network, these features will affect network properties such as

swelling ratio and mesh size, as well as material properties such as bulk and shear moduli and yield strain. These imperfections will also affect the polymer's elastic and viscoelastic behavior.

2.1.2 Mechanisms and Structure

The structure or architecture of a crosslinked polymer network determines many of its physical properties. The chemical mechanisms behind crosslinking are of importance. The mechanism of the crosslinking reaction depends on the molecular functionality of the crosslinking group. For polymers with a vinyl functionalized crosslinking group, the mechanism is similar to that of chain growth vinyl polymerization. Multiple methods exist to perform cross linking in polymer systems with vinyl functionalizations, however for the purposes of this research, only the free radical method is discussed, since it is the only one employed.

Free radical polymerization has proven useful for multiple polymer systems, especially in vinyl polymerization.[22] The free radical crosslinking mechanism for polymers with vinyl functional groups occurs via the same mechanism as that for conventional free radical polymerization (FRP).[23]

Crosslinking via free radical polymerization is a process that involves three basic steps. First, a free radical must be formed through the initiation step. For the PEG-DA system used in this research, the initiator is Igacure 2959, which forms a free radical under UV light as shown in Figure 2.4.
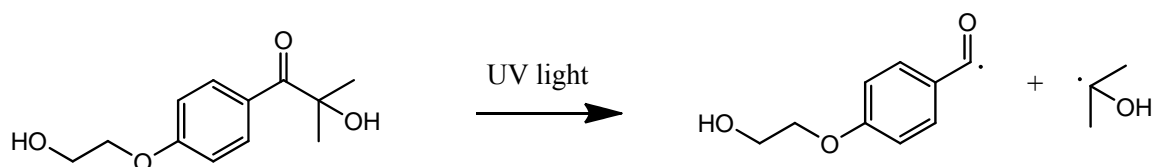
Figure 2.4: Initiation mechanism in free radical polymerization

The next step is known as propagation, where the free radical from the initiator comes into contact with the end of a PEG-DA molecule and reacts with the carbon-carbon double bond in the acrylate functional group, shown in Figure 2.5.
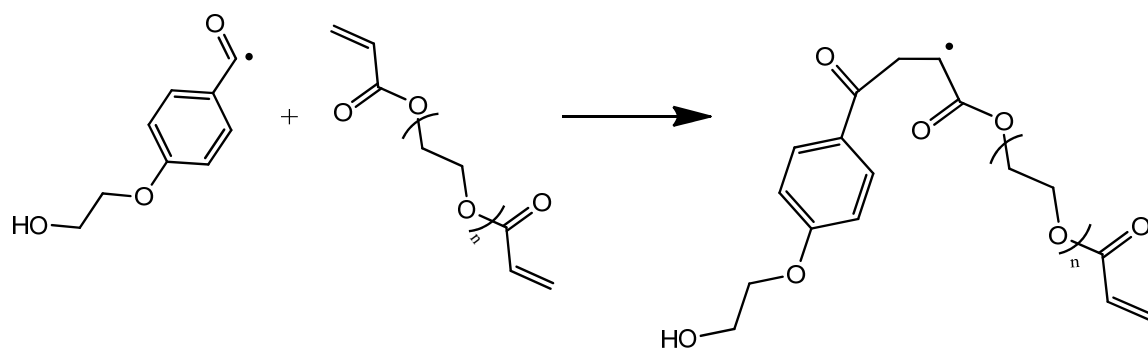
Figure 2.5: Propagation mechanism in free radical polymerization

This step produces a second free radical species, which can go on to react with more PEG-DA polymers propagating the crosslink. The final step in the process of this polymerization is termination, which occurs when two radical species meet and a bond forms between them.

What makes the free radical polymerization of PEG-DA different from traditional vinyl polymerization is that each 'monomer', or PEG-DA chain, has two vinyl groups, and both can form a bond, or crosslink. The majority of polymers in solution become

interconnected and form a single network. A general reaction scheme for a di-functional

polymer forming a network is presented in Figure 2.6 below.
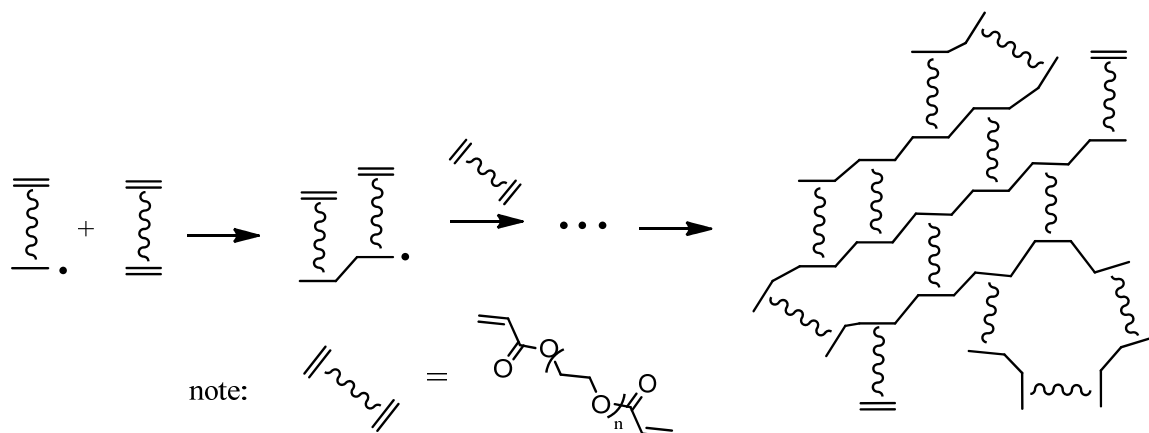
Figure 2.6: Formation of a crosslinked polymer network from a difunctional polymer like PEG-DA

The reaction shown in Figure 2.6 can easily form non-idealities, such as unreacted

end groups, physical entanglements, and rings. The formation of an ideal three-

dimensional network is theoretically possible (but highly unlikely) and one potential

structure is shown in Figure 2.7. The network junctions are formed by a 12 carbon ring

with PEG chains extending in both ways for all three dimensions. Non-idealities like

chain entanglements, loops, and unreacted vinyl groups will exist for a few reasons.

First, cyclization (intramolecular crosslinking) and microheterogeneities are characteristic

of free radical polymerization because of the rapid initial chain growth.[24] Second, the

addition of a solvent to the system further increases cyclization.[25] These factors make the

PEG-DA network structure a unique system to investigate.
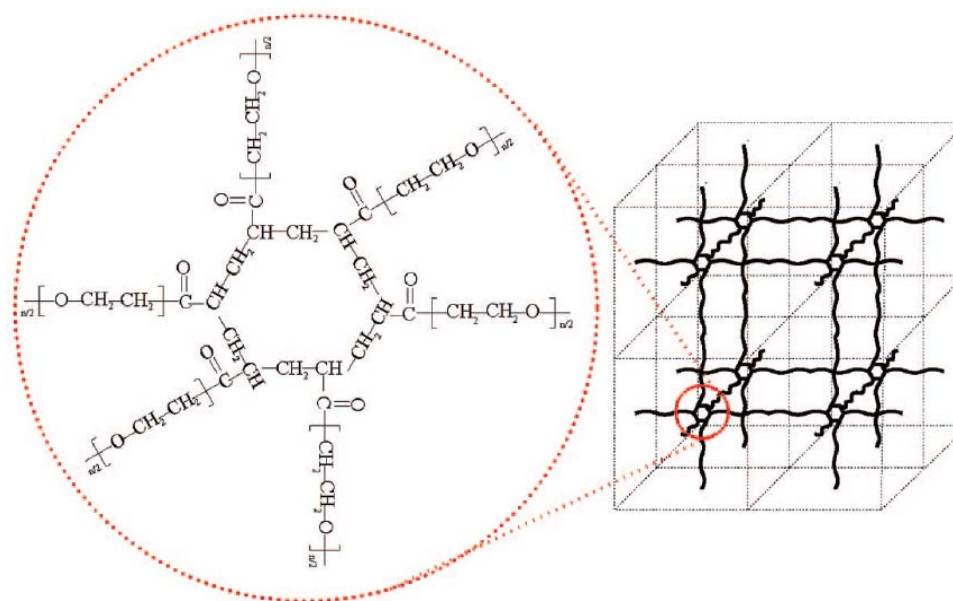
Figure 2.7: A potentially ideal network of crosslinked PEG-DA[26]

2.2 Diffusion

2.2.1 Modelling Diffusion

Diffusion is commonly referred to the process of mass transfer due to a concentration gradient.[27] Although this may not be a thermodynamically exact definition, it does capture the essence of the process. This section will develop diffusion from thermodynamic concepts, and examine diffusion under a mathematical context, including solutions to the diffusion equation. Experimental methods will be explored, and afterwards, models for predicting diffusivity in liquids and gels will be examined.

The mass flux of a species is the rate at which mass of a species passes through a unit cross sectional area per unit time. Mathematically, the one dimensional flux of a species, Φ_A can be defined as:

$$\phi_A = \frac{m_A}{A_x t} \tag{2.12}$$

where m_A is the mass of the species that has passed through the cross sectional area, A_x, and t is time. The mass flux of species A can be related to the density of A, and the velocity of species A:

$$\phi_A = \rho_A v \tag{2.13}$$

Generalizing the flux of a species into three dimensions using vector notation, the general three dimensional flux can be defined as the following:

$$\vec{\phi}_A = \left(\phi_{A,x}, \phi_{A,y}, \phi_{A,z} \right) = \rho_A \vec{v} \tag{2.14}$$

Diffusion can be defined as the process where mass transfer originates from spatial differences in chemical potential, temperature, pressure or other external forces. The total diffusive flux of a species can be thought of as the sum of the four terms originating from the spatial differences in concentration, pressure, temperature, or other external forces:[28]

$$\phi_A = \phi_A^C + \phi_A^P + \phi_A^T + \phi_A^f \tag{2.15}$$

where Φ_A is the total flux of species A; $\Phi_A{}^C$, $\Phi_A{}^P$, $\Phi_A{}^T$, and $\Phi_A{}^f$ are the flux due to concentration, pressure, temperature, and other external forces respectively. Under the

case of negligible pressure, temperature, and external fields, the resulting diffusive flux originates purely from chemical potential and is often called "ordinary diffusion".

Working within the framework of the Chapman-Enskog solution of the Boltzmann's kinetic theory for dilute gases, Curtiss developed a useful expression for the diffusive flux in a multicomponent mixture. [29] In the case of a binary mixture, the flux of species A is shown below:

$$\vec{\phi}_A \equiv -\frac{c^2}{\rho} M_A M_B D_{AB} \left(\frac{\partial \ln a_A}{\partial \ln x_A} \right)_{T,P} \nabla x_A \tag{2.16}$$

where c is the total number of moles per volume, ρ is the overall density of the solution a_A is the molar activity of species A, x_A is the mole fraction of species A, D_{AB} is the Maxwell − Stefan diffusion coefficient, or the binary diffusion coefficient, M_A and M_B are the molar masses for species A and B respectively, and Φ_A is the mass flux of species A.

The molar activity of a species is related to its chemical potential via the defining equation:

$$\ln(a_A) \equiv \frac{\hat{\mu}_A - \mu_A}{RT} \tag{2.17}$$

where a_A is the activity of species A, $\hat{\mu}_A$ is the chemical potential of species A in the mixture, μ_A is the chemical potential of pure A at the same temperature and pressure, R is the ideal gas law constant 8.314 J/mol K, and T is the absolute temperature.

A thermodynamically ideal solution can be defined as one where the activity coefficients of all species are unity when at constant temperature and pressure.[30] Mathematically an ideal solution is one that obeys the following relation:[28]

$$\left(\frac{\partial \ln a_A}{\partial \ln x_A}\right)_{T,P} = 1 \qquad (2.18)$$

This implies that for ideal solutions, the diffusive flux can be expressed as:

$$\vec{\phi}_A = -\frac{c^2}{\rho} M_A M_B D_{AB} \nabla x_A \qquad (2.19)$$

Under dilute conditions, the concentration of species A is much lower than that

for species B ($c_A/c_B \ll 1$), and the relationship simplifies to the following:

$$\vec{\phi}_{mol,A} = -D_{AB} \nabla C_A \qquad (2.20)$$

Or for one dimension:

$$\phi_{mol,A} = -D_{AB} \frac{\partial C_A}{\partial x} \qquad (2.21)$$

where $\Phi_{mol,A}$ is the molar flux of species A, D_{AB} is the diffusion coefficient, or diffusivity,

and C_A is the concentration of species A. This form of the diffusive flux equation

matches Fick's first law. The relationship in Equation (2.21) was first hypothesized by

Fick in 1855 and has been used extensively ever since.[31] Equation (2.21) is often used in

experimental determination of diffusive coefficients. Diffusion coefficients are

sometimes reported as apparent diffusivities, since the systems studied may not be dilute

or ideal. It is much easier for experimentalists to report an apparent diffusivity rather than

taking concentration and non-idealities into consideration.

Using the continuity equation and Fick's law as a constitutive equation for

relating flux to concentration, a partial differential equation can be constructed to model

diffusion processes with no chemical reaction.[32]

$$\frac{\partial C_A}{\partial t} = \frac{\partial}{\partial x}\left(D(C_A)\frac{\partial C_A}{\partial x} \right) \tag{2.22}$$

The diffusion coefficient, or diffusivity, D, is, in general, a function of concentration of the solute. Most of the time, the diffusivity is assumed to be constant; however this is only true for dilute and/or ideal solutions. If the solute is not dilute, or is in a complex, non-homogenous environment, the assumption of constant diffusivity may not be appropriate.

If the diffusivity is assumed constant, the above equation simplifies greatly and analytical solutions for diffusion processes are available. Methods for obtaining analytical solutions in this case include the use of a similarity variable ($\eta = \dfrac{x}{\sqrt{4Dt}}$) and the separation of variables technique among others.[32, 33]

For the case of 1-dimensional, planar diffusion in a semi-infinite slab with a constant source of solute at the border of the slab, the use of a similarity variable can be used to obtain the following relationship:

$$\frac{C}{C_0} = erfc\left(\frac{x}{\sqrt{4Dt}} \right) \tag{2.23}$$

Equation (2.23) is useful for short times as the solute penetrates a slab. Under similar assumptions, diffusion into a finite slab of length L can be solved using the separation of variables technique to obtain the following:

$$C(x,t) = \frac{4C_0}{\pi}\sum_{n=0}^{\infty}\frac{1}{2n+1}\exp\left(\frac{-D(2n+1)^2\pi^2 t}{L^2} \right)\sin\left(\frac{(2n+1)\pi x}{L} \right) \tag{2.24}$$

When the diffusion coefficient is not constant, analytical solutions are difficult to obtain, although not impossible.[34] Under semi-infinite slab conditions, the similarity variable technique is useful in simplifying the partial differential equation into an ordinary differential equation. In general, however, numerical methods such as finite differences are used to model diffusion processes with non-constant diffusion coefficients. Concentration dependent diffusion has been observed in metallic systems, gas diffusing through vitreous silica,[35] as well as polymer systems.

2.2.2 Experimental Methods

Determining the diffusion coefficient experimentally can be accomplished using steady state or transient diffusive processes. For steady state experiments one generally determines concentration of the diffusing species as a function of location. For transient processes the goal is to find concentration as a function of location and time. The realities of most diffusive processes make obtaining this data difficult. Either long times, short distances, or both are required to monitor significant diffusive processes. For most processes, the diffusivity is assumed constant; however this may not be the case for diffusion in some situations. In addition, a non-invasive method is, in most cases, required to monitor concentration as a function of time and space. Currently, non-invasive methods include, but are not limited to fluorescence, optical, and NMR methods. Once the data has been collected, it may be fit to a predictive model and the diffusivities may be calculated.

In traditional diffusometry experiments, the objective is to collect the concentration of the relevant species as a function of space and time. Once the relevant

data has been collected, an appropriate analytical solution curve can be fitted to the data to determine the diffusion coefficient. If the experiment was done with semi-infinite slab geometry, and the diffusion coefficient is constant, the data can be compared with Equation (2.22).[36]

Different methods have been used to measure diffusion coefficients of solutes in hydrogels. One common example is the diaphragm tank method[37] shown in Figure 2.8 below. This method applies a concentration gradient across a hydrogel and monitors the concentration in both tanks as a function of time. The collected data is fitted to a predictive equation to find the diffusion coefficient.
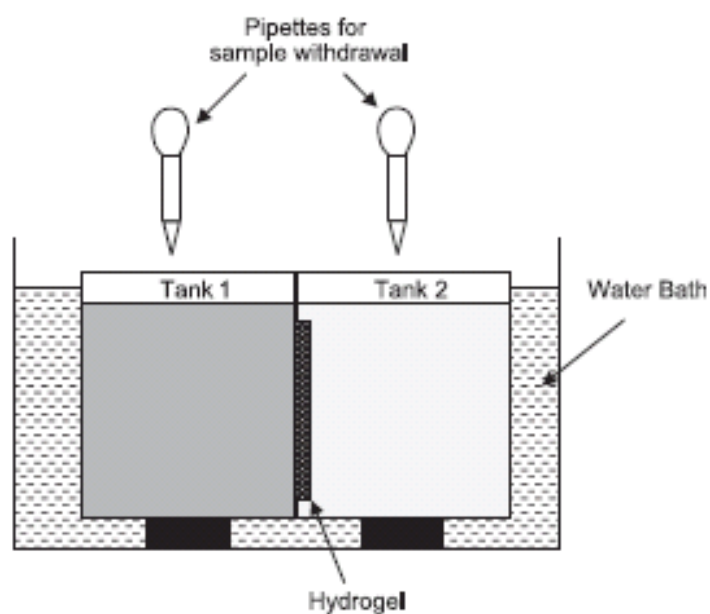
Figure 2.8: A setup to determine the diffusion coefficient of a hydrogel slab.[37]

One can use the following equation to analyze the above system.[27]

$$D = \frac{1}{\beta t} \ln \left(\frac{C_1(t) - C_2(t)}{C_1^0 - C_2^0} \right) \qquad (2.25)$$

and

$$\beta = \frac{A_H}{W_H}\left(\frac{1}{V_1} + \frac{1}{V_2}\right)$$
(2.26)

Where A_H is the cross section of the hydrogel slab, W_H is the width of the hydrogel slab, t is time, V_1 is the volume of the first chamber, V_2 is the volume of the second chamber, $C_1(t)$ is the concentration of the first chamber at time t, $C_2(t)$ is the concentration of the second chamber at time t, C_1^0 is the concentration of the first chamber at $t=0$, and C_2^0 is the concentration of the second chamber at $t=0$.

A second method employed is known as fluorescence recovery after photobleaching, or FRAP. FRAP works by bleaching a small area of fluorescent dye and monitoring dye concentration levels as a function of location and time. A schematic of the FRAP process is shown in Figure 2.9. A diffusion coefficient can be found by matching data to theoretical expressions. FRAP has been used to measure diffusivity of fluorescent solutes in hydrogels.[38-40]

Top View
Macroscopic

Side View

Microscopic (not to scale)

Initial Fluorescent
Dye Solution

Bleaching

Diffusion

New Equilibrium
Reached
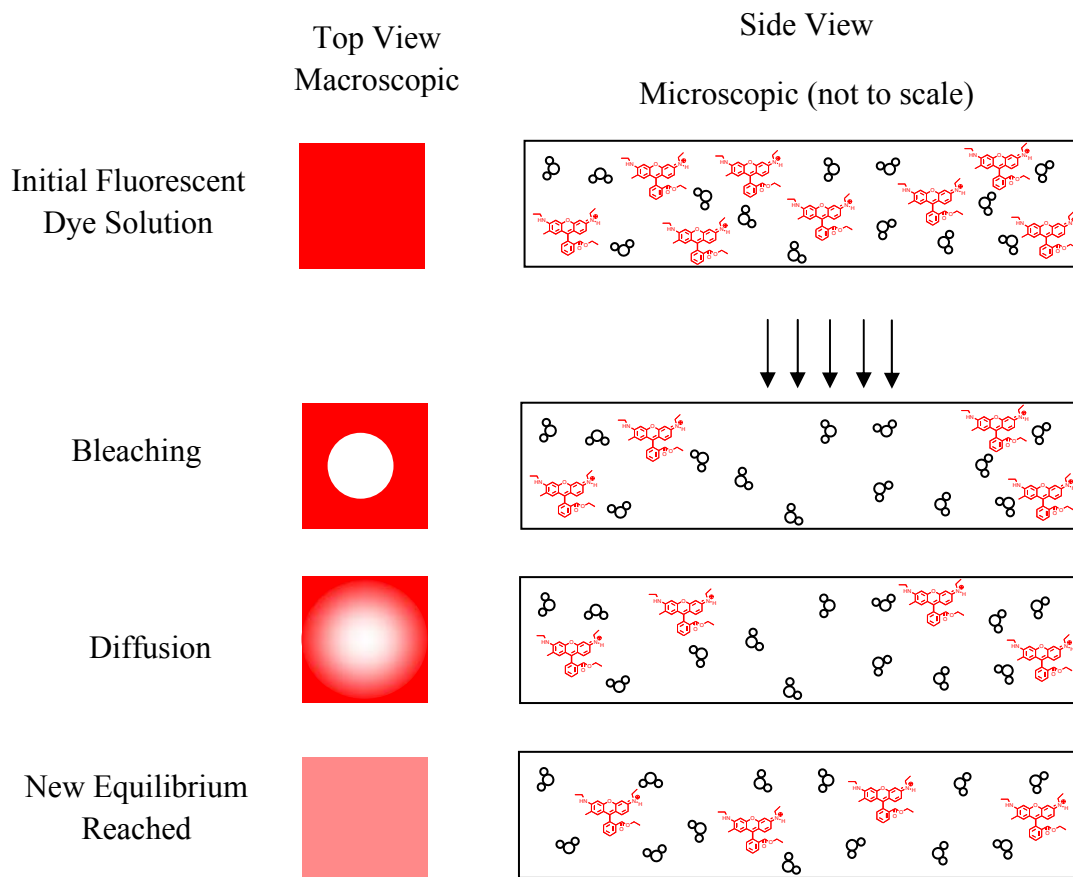
Figure 2.9: Schematic diagram of fluorescence recovery after photobleaching.

Nuclear Magnetic Resonance (NMR) can determine the diffusion characteristics

of solvents on small time scales in a non invasive manner. The technique has proven

useful in simple and complex systems, including gels[41] and biological media.[42] One can

observe the diffusivity on multiple time scales, and, if the observation time is long

enough, one can observe the long-time diffusion coefficient of the analyte in the gel. One

widely used technique to measure the self diffusion coefficient in NMR samples is the

pulsed field gradient (PFG) method. This technique examines the random walk motion

of the analyte under equilibrium conditions (no concentration gradients) and determines

the so called self-diffusion coefficient.[43, 44] Self diffusion coefficients are obtained by fitting the variation of the echo intensity as a function of the applied magnetic field gradient strength G. according to Equation (2.27): [45]

$$\ln\left(\frac{S}{S_0}\right) = -(G\gamma\delta)^2 D_S\left(\Delta - \frac{\delta}{3}\right) \qquad (2.27)$$

In this equation, S and S_0 are the integrated signal with and without a field gradient, γ is the gyromagnetic ratio of the nucleus, δ is the duration of the pulse, G is the field gradient, Δ is the duration between the beginnings of the two gradient pulses, and D_S is the self diffusion coefficient.

A second NMR method monitors the concentration of different species along the length of the sample container.[41] As a concentration gradient is introduced to the system, the concentration of the diffusing solute as a function of time and location can be monitored. This information is recorded as species diffuse through the sample, allowing the diffusion coefficient to be extracted from the data. This NMR method can measure the mutual diffusion coefficient.

The self and mutual diffusion coefficients can be related theoretically. One such relation is the Darken equation:[46]

$$D_{M,i} = D_{S,i}\left(1 + \frac{d\gamma_i}{dx_i}\right) \qquad (2.28)$$

where $D_{M,i}$ is the mutual diffusion coefficient, $D_{S,i}$ is the self diffusion coefficient, γ_i is the activity coefficient of species i, and x_i is the mole fraction of species i.

Values for the self and mutual diffusion coefficients were found via experimentation for a number of solutes in a curdlan hydrogel.[41] An empirical relationship between these two diffusion coefficients was found to have the following form:

$$D_M = (1.1 \pm 0.1)D_S \qquad (2.29)$$

where D_M and D_S are the mutual and self diffusion coefficients, respectively. Although this relation is only verified for curdlan hydrogels, it shows the two values are comparable, and in many cases identical.

Microfluidic techniques have been used to measure the diffusion of analytes in liquids. The physical scale of microfluidic devices has a concrete effect on the flow regime that occurs in them. Fluids in microfluidic devices almost always operate in the laminar region of flow, with the Reynolds number, $Re \ll 1$. The domination of viscous forces over inertial forces means that convective mixing is minimal or nonexistent, and diffusion is the dominant mode of transport in the system. This has lead to some effort in using microfluidic devices to investigate diffusion.[47] Devices employing a T-junction, or plug injection have been used to create concentration gradients which can be observed optically, or using spectroscopic techniques.[47-50] These methods only work to characterize the diffusivity of solutes in water or other liquids. These experimental setups generally analyze the interdiffusion between two liquid samples in a channel on a glass slide or microfluidic device. This technique is simple and resilient enough to have been proposed

for an undergraduate laboratory experiment.[36] Currently, microfluidic devices have not been used to measure the diffusion of solutes within hydrogels.

2.2.3 Modeling Diffusion Coefficients

As diffusion is an important process in many systems, it has been the focus of much research over the last century. Theoretical models for predicting the diffusion coefficient have been developed for non-polar gaseous systems[33] and are within 10% of experimental values. Simple models can be derived from the kinetic theory of gases to describe the diffusion coefficient in terms of properties of the gas. More advanced models incorporate attractive and repulsive forces.

Other theoretical models, although not as accurate, have been made for aqueous, and solid systems. One such model known as the Stokes-Einstein relationship predicts the diffusion of a dilute solution of a spherical particle in a liquid as follows:[33]

$$D = \frac{kT}{6\pi\mu R_S} \tag{2.30}$$

where k is boltzman's constant, T is absolute temperature, μ is the viscosity of the solvent, and R_S is the radius of the solute particle. This equation can predict the diffusivity of a solute based on its size. Alternatively, one can find a solute's "hydrodynamic radius" from experimental diffusivity values.

Another model for diffusion in liquids is Eyring's hole theory where an ideal liquid is treated as a quasi-crystalline lattice where solute and solvent molecules can occupy sites and empty sites are known as holes. To move sites, atoms require a certain amount of energy to overcome a barrier, similar to the theory of chemical reaction rates.

The temperature dependence of diffusion coefficients can often be fitted to Eyring rate expressions. Plotting $\ln(D)$ vs. $1/T$ often yields a linear relationship. One model based on Eyring rate theory predicts diffusion coefficient as follows:[51]

$$D_{AB} = \frac{kT}{\xi_A \mu_B} \left(\frac{N}{V_B} \right)^{1/3} \left(\frac{M_B}{M_A} \right)^{1/2} \exp\left(\frac{E_{\mu B} - E_{DAB}}{RT} \right) \tag{2.31}$$

where ξ_A is the number of solvent molecules around the A molecule, (taken as 6 for a rough approximation), $E_{\mu B}$ is the activation energy for viscosity, E_{DAB} is the activation energy for diffusion, N is Avogadro's number, M_B is the molar mass of the solvent B, and M_A is the molar mass of the diffusing particle A.

Other models for diffusion in liquids include that proposed by Wilke and Chang:[52]

$$D_{AB} = 7.4x10^{-8} \frac{T\sqrt{\Phi_B M_B}}{\mu_B V_A} \tag{2.32}$$

where M_B is the molecular weight of the solvent B in g/mol, V_A is the molar volume of the solute A in cm^3/gmol, μ_B is the viscosity of the solvent B (in centipoises), T is the thermodynamic temperature (K), and Φ_B is an empirical association constant, dependant on the solvent; Φ_B takes a value of 2.26 for water.[53]

2.2.4 Modelling Diffusion Coefficients in Gels

In more complex systems, such as polymers or structured solids, most diffusion modeling depends on empirically determined diffusion coefficients. The lack of predictive equations for diffusivity in hydrogels and other similar structures has led to research on the subject. Models for diffusivity in these environments have been

developed for specific cases including polymer gels. These models generally come in the form[1, 3]:

$$\frac{D}{D_0} = f(r_s, v_{2,s}, \xi) \qquad (2.33)$$

According to these models, the diffusion of a solute depends on properties of the solute and polymer gel. These include the diffusion in pure solvent D_0, the mesh size, ξ, the solute size, r_s, polymer fraction in the swollen state, $v_{2,s}$, polymer-solute interactions, crosslink density, and polymer chain mobility.

For hydrogels, if the characteristic length, ξ, is much larger than the hydrodynamic radius of the solute, ($\xi >> r_s$), then interactions between the solute and the polymer chain are minimized and the diffusion coefficient is related to the porosity and tortuosity of the porous structure. When the characteristic length approaches the size of the solute molecule, interactions between the solute and the hydrogel structure become important.

Multiple theories have been used to model the diffusion process in hydrogels and other polymeric networks. Some predominant theories include hydrodynamic theory, obstruction theory, and free volume theory. These theories sometimes discriminate between homogenous and heterogenous hydrogels.[54] A homogenous hydrogel has a large amount of water in it, relatively little polymer chain interactions, and high chain mobility. Heterogeneous hydrogels are described as polymer networks where there are regions of high polymer density and other regions with high concentrations of water. Examples of

heterogenous hydrogels include alginate and aragose, while PEG and PVA are examples of homogenous hydrogels.

Hydrodynamic theory has been developed from a theoretical framework to describe diffusion in a dilute solution.[33] A predictive model can be derived from hydrodynamic theory to predict diffusion in a heterogenous hydrogel as shown in below:

$$\frac{D}{D_0} = \exp\left[-k_c r_s \varphi^{0.75}\right] \tag{2.34}$$

where k_c is a constant for polymer gel systems, r_s is the radius of the solute, and φ is the volume fraction of polymer in the hydrogel. This theory has been shown to agree with experimental data for diffusion for a variety of cases including homogenous hydrogels. The theory does not take into account polymer-solute interactions, and the solute is assumed to be spherical.

Obstruction theory has been used to model polymer solutions and gels as a random network of negligibly thin, straight polymer fibers. One model borne from this theory predicts the diffusion process to obey the following:[21]

$$\frac{D}{D_0} = \exp\left[-\frac{\pi}{4}\left(\frac{r_s + r_f}{\frac{\xi}{2} + r_f}\right)^2\right] \tag{2.35}$$

where D is the diffusion of the solute in the gel, D_0 is the diffusion coefficient of the solute in water, r_s is the radius of the solute, r_f is the radius of the polymer fiber, and ξ is the characteristic mesh size.

Multiple expressions for ζ have been found drawing from scaling concepts for polymer solutions similar to those used to derive Equation (2.8). One expression for zeta derived under conditions when the polymer chains are rigid cylinders is as follows:[55]

$$\zeta = k_s \varphi^{-1/2} \tag{2.36}$$

where k_s is an empirical parameter and φ is the volume fraction of polymer in the gel. This expression is useful for heterogenous hydrogels, but not for homogenous hydrogels like PEG where the polymer chains have high mobility. For homogenous hydrogels, conditions are probably closer to that of a good solvent near the point where polymer chains just begin to overlap. An expression for the mesh size at this point is the following:

$$\xi \propto a\varphi^{-0.75} C_n^{-0.25} (1 - 2\chi)^{-0.25} \tag{2.37}$$

where a is the equivalent bond length of the monomer, φ is the polymer volume fraction, C_n is the Flory characteristic ratio of the polymer, χ is the Flory-Huggins interaction parameter. For a PEG-water system, a is approximately 1.53 Å, C_n has been taken to be 3.8,[56] 4.0,[20] or 4.0 – 5.2 [21] for PEG, and the interaction parameter, χ has been found to lie in the range of 0.45 – 0.48.[21] This result assumes the gel behaves similar to polymer chains at the solution concentration where they begin to overlap. This relation applies for concentrations near the dilute semi-dilute transition concentration, c^*, shown in Figure 2.10 below:
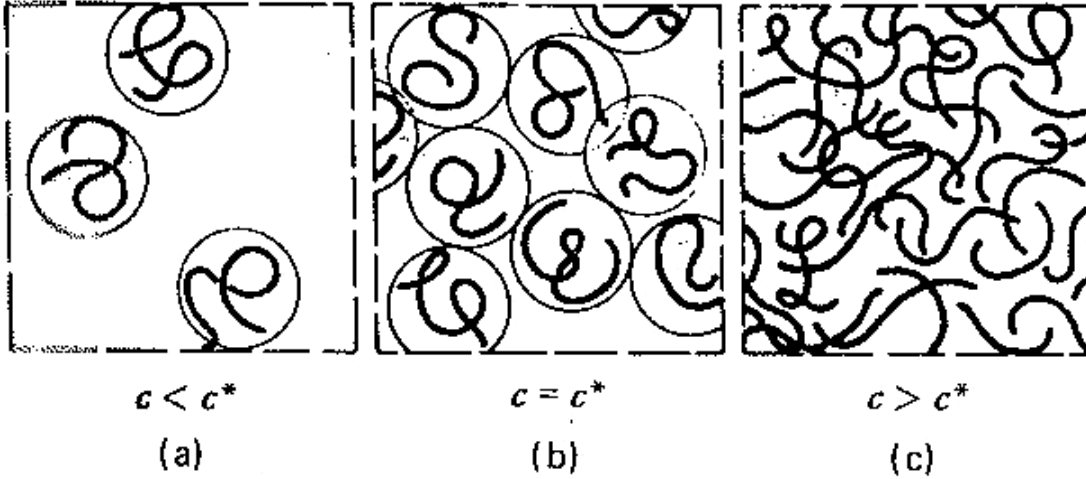
Figure 2.10: The (a) dilute regime, (b) transition point, and (c) semidilute regime for polymers in a solvent.[57]

The critical polymer volume fraction, φ^*, can be found from the relation below[58]:

$$\varphi^* = \frac{3M}{4\pi S_{G,0}^3 N_A \rho} \qquad (2.38)$$

where M is the molecular weight of the polymer, $S_{G,0}$ is the radius of gyration, ρ is the density of the polymer and N_A is Avogadro's number. The radius of gyration is dependent on polymer molecular weight, but can be found experimentally. The radius of gyration for PEG with molecular weight of 575 g/mol is approximately 9.6 Å[54], and the density of PEG is approximately 1.12 g/cm^3. For PEG hydrogels used in this research, the relation gives a value for $\varphi^* \approx 0.23$. Combining Equations (2.35) and (2.37) results in a predictive model for diffusion in homogenous hydrogels as presented below:

$$\frac{D}{D_0} = \exp\left[-\pi\left(\frac{r_s + r_f}{k_s a \varphi^{-0.75} C_n^{-0.25}(1-2\chi)^{-0.25} + 2r_f}\right)^2\right] \qquad (2.39)$$

where k_s is a constant of proportionality for a polymer-solvent system.

Free volume theory is based on the concept that solute particles can diffuse only when other components of the system move out of the way. There is no activation energy to move from site to site; the solute is only restricted by requiring a void space nearby. A free volume theory has been developed and is presented below:[54]

$$\frac{D}{D_0} = \left(1 - k_1 r_s \varphi^{0.75}\right) \exp\left[-k_2 r_s^2 \left(\frac{\varphi}{1-\varphi}\right)\right] \tag{2.40}$$

The effects of obstruction and hydrodynamic drag can be combined mulitplicativly to account for both effects. One model combines obstruction, and hydrodynamic effects for the diffusion of large molecules (proteins and micelles) in hydrogels.[59]

Other models have been developed in the literature,[1, 54, 60, 61] but few have taken into consideration Polar interactions between the hydrogel and the solute. If certain solutes have charge induced attractive forces, then the diffusion process may be affected. Hirota and coworkers studied the diffusion of proteins through polysaccharide hydrogels at different pH values. They found that the diffusion coefficient for myoglobin changed with pH for λ-carrageenan gels, but not in aragose gel. This phenomenon was ascribed to the ionizeable nature of the λ-carrageenan gel caused by ionized sulfonic acid groups. The experiment also showed that the diffusivity in a charged λ-carrageenan gel could be affected by the concentration of a salt in solution. Changing the concentration of salt in a nonpolar aragose gel had no effect. It has also been observed that PVA hydrogels behave remarkably different in electrolytic solutions.[62]

Brownian motion simulations have indicated that obstruction due to polymer chains alone cannot explain the observed diffusion rates in hydrogels.[63]   An interaction between the solute and the gel strands should be included in the model. They calculated that in order for their simulation to match their experimental results, a "sticky wall" time delay on the order of 30 to 250 ns was needed, suggesting a polymer-solute interaction is at work.

2.3 Microfluidics

Microfluidics is the application of fluid flow through devices with lengths between 10 μm and 1000 μm[64] in at least 1 dimension. Much of the past work in fluid dynamics rarely approaches length scales smaller than 1 cm and is usually an order of magnitude larger. At the small length scale of microfluidics, transport phenomena can be much different than fluid dynamics at larger scales. By introducing small length scales, the fluid flow is more often dominated by viscosity and characterized by small Reynolds numbers and laminar flow.[65] The second ramification is that the surface area to volume ratio increases dramatically, and surface effects can become important. Finally, smaller length scales require the use of small amounts of volume, which can be advantageous for dangerous or expensive fluids.

Many have directed their research towards developing the so called "lab-on-a-chip," where small amounts of analyte are evaluated with various microfluidic processing units on an integrated platform. The paradigm of small-scale microfluidic analysis is attractive on many levels. The inherent small scale of microfluidic technology increases

portability, and reduces raw materials needed for production.   The applications for small, portable, and inexpensive analytical devices are widespread. Medical applications include bioassays[66]; DNA analysis[67]; flow cytometry[68]; and optical[69] and rheological[70] measurements. Industrial uses include microreactors[71], bioreactors[72], and high-level integrated flow devices.[73] Military applications include biological and chemical sensors.[74] Other applications include fuel cells[75], the food industry[76], agriculture, emulsifification, liquid-liquid extraction, heat exchangers, and protein crystallization. The scalability of microfluidics also makes simultaneous high throughput possible. The accessibility and customizability of microfluidic technology has promoted rapid growth in the field.

2.3.1 Microfluidic Fabrication Techniques

Microfluidic devices are composed of small scale channels and microstructures which require specialized fabrication methods to produce. Fabrication techniques include lithographic etching, photolithography, x-ray lithography, laser ablation, and polymer molding among others.[77] The primary fabrication method used in this research is photolithography, so it will be the only one discussed.

Photolithography uses a material's sensitivity to light to create chemical modifications. One widespread example is the use of photo-initiated crosslinking polymer solutions. Upon exposure to UV light, these solutions will crosslink and chemically bond to the device substrate and to each other. If a photomask is used to block out light from certain regions, those regions will not polymerize, and small structures or channels can be formed. Chemical structures that cure or harden under the

application of UV light are known as negative-tone photoresists. The use of negative-tone

photo-resists in photolithograpy is shown in Figure 2.11 below:
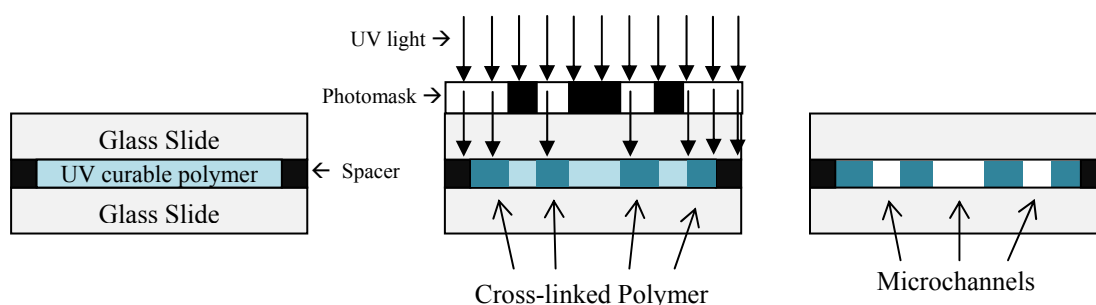
Figure 2.11: Negative tone photolithographic process

Common materials used in negative-tone photolithography include glass as the

substrate; any photoinitiated crosslinkable polymer as the photoresist, a patterned

transparency as the photomask, and small silicon wafers as spacers. One widely used

photoinitiated polymer solution is a thiolene-based optical adhesive. Thiolene optical

adhesives are highly sensitive to UV light, and cure quickly to create a solvent resistant

bond with glass. One common optical adhesive is the proprietary NOA 81 thiolene

optical adhesive. Using NOA 81 it is possible to make structures as tall as 1 mm with

horizontal resolutions of 125 μm.[78] The solution cures within minutes using a

conventional UV (365 nm) light source. The exact composition of NOA 81 is

proprietary, however, studies have shown that it is a binary blend of urethane based thiol

functionalized polymers with molecular weights of 1000 g/mol and 2500 g/mol.[79]

NOA 81 is useful for making rigid precise structures, making it ideal to use on

glass substrates. Other polymers can be used, but their properties will differ, and they

may not bond to glass. To overcome this drawback, researchers have applied self-assembled monolayers (SAMs) to glass substrates for the purpose of chemically binding various polymers to the glass surface. The chemisorption behavior of trichlorosilane to glass is well known and can be used to make SAMs on glass.[80] The silanization process for glass is shown in Figure 2.12 below.
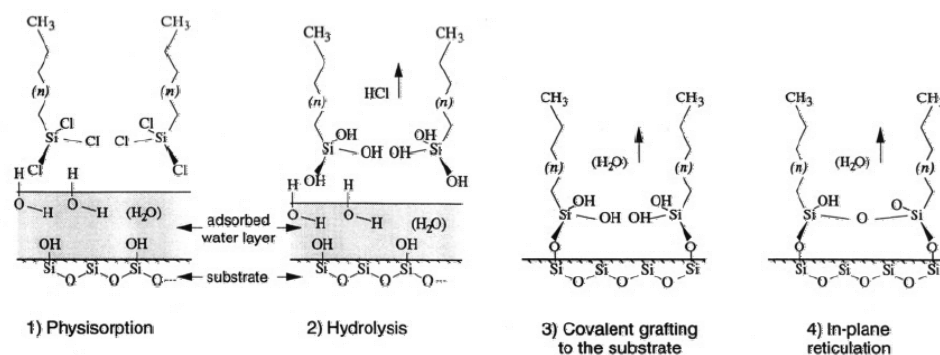
Figure 2.12: General silanization scheme [80]

If the silane is functionalized with an alkene group, it can be used as an intermediary to connect a vinyl polymer to the glass surface. This covalent bond augments surface adhesion. This method of silanization is especially useful for preventing delamination of PEG hydrogels from glass surfaces and is used in microfluidic devices.[81]

2.3.2 Microfluidic Flow Properties

The small scale of microfluidics amplifies the effects of surfaces and viscosity of flow patterns. For this reason, flow in microfluidic devices is prone to high pressure drops and low velocities. Alternatives to pressure driven flow have been developed and

include electro-osmotic, and centrifugal flow. However, these techniques have drawbacks; electro-osmotic flow can only be used for charged fluids and centrifugal flow is unrealistic for integrated multifunctional devices. Pressure driven flow, on the other hand, is easy to implement and control using syringe pumps.

2.4 Summary and Project Objectives

Hydrogels are novel materials with extensive current applications and hold much promise for the future. The key to a hydrogel's unique properties is its behavior in water, which can be traced to the hydrogel's molecular structure. A thorough understanding of diffusive transport in gels is still emerging. The necessity of such knowledge for applications including controlled drug delivery has been a major driving force in the scientific community. Microfluidic technology is a fast emerging field that harnesses effects on the small scale for a wide range of purposes.

The goal of this research is to use microfluidic techniques to create an instrument capable of measuring diffusivity of solutes in hydrogels. Such a device would have advantages over current diffusometry methods and be simple to fabricate. The quantitative results of the device will be compared with contemporary diffusometry methods, specifically NMR diffusometry. The following chapter outlines the materials, instruments, and procedures used to fabricate and test the microfluidic device, as well as measuring properties of the hydrogel.

2. 5 References

1. Lin, C. C.; Metters, A. T. *Adv. Drug Deliv. Rev.* **2006**, *12-13,* 1379-1408.

2. Moorthy, J. Hydrogels in Microfluidics. In *Smart Polymers;* CRC: 2007; pp 437.

3. Peppas, N.,A.; Huang, Y.; Torres-Lugo, M.; Ward, J., H.; Zhang, J. *Annual Reviews in Biomedical Engineering* **2000**, *1,* 9-29.

4. Hoffman, A. S. *Adv. Drug Deliv. Rev.* **2002**, *1,* 3-12.

5. Hoare, T. R.; Kohane, D. S. *Polymer* **2008**, *8,* 1993-2007.

6. Watkins, A. W.; Southard, S. L.; Anseth, K. S. *Acta Biomaterialia* **2007**, *4,* 439-448.

7. Harris, J. M. *Poly(ethylene glycol) chemistry: biotechnical and biomedical applications* **1992**.

8. Greenwald, R. B.; Choe, Y. H.; McGuire, J.; Conover, C. D. *Adv. Drug Deliv. Rev.* **2003**, *2,* 217-250.

9. Ratner, B. D.; Hoffman, A. S.; Schoen, F. J.; Lemons, J. E. *Biomaterials science: an introduction to materials in medicine;* Academic press: 2004.

10. Khandare, J.; Minko, T. *Progress in Polymer Science* **2006**, *4,* 359-397.

11. Zhu, J.; Tang, C.; Kottke-Marchant, K.; Marchant, R. E. *Bioconjug. Chem.* **2009**, *2,* 333.

12. Hamidi, M.; Azadi, A.; Rafiei, P. *Adv. Drug Deliv. Rev.* **2008**, *15,* 1638-1649.

13. Mayo, D. *Calcium Alginate Encapsulation and Continuous Separation of the capsules through co-laminar flow of the Immiscible Fluids;* Bucknell University: **2008**.

14. Geever, L. M.; Cooney, C. C.; Lyons, J. G.; Kennedy, J. E.; Nugent, M. J. D.; Devery, S.; Higginbotham, C. L. *European Journal of Pharmaceutics and Biopharmaceutics* **2008**, *3,* 1147-1159.

15. Bajpai, A.; Giri, A. *React Funct Polym* **2002**, *2-3,* 125-141.

16. Treloar, L. *The physics of rubber elasticity;* Oxford University Press, USA: 2005.

17. Anseth, K. S.; Bowman, C. N.; Brannon-Peppas, L. *Biomaterials* **1996**, *17,* 1647-1657.

18. Lin, H.; Kai, T.; Freeman, B. D.; Kalakkunnath, S.; Kalikas, D. S. *Macromolecules* **2005***, 20,* 8381-8393.

19. Canal, T.; Peppas, N. A. *J. Biomed. Mater. Res.* **1989***, 10,* 1183-1193.

20. Billmeyer, F. *Polymer Science., John Wiley & Sons Inc., New York 1984, 3 rd Edition, xviii 578* **1984**.

21. Amsden, B. *Macromolecules* **1999***, 3,* 874-879.

22. Odian, G. G. *Principles of polymerization;* Wiley-Interscience: 2004.

23. Tan, G.; Wang, Y.; Li, J.; Zhang, S. *Polymer Bulletin* **2008***, 1,* 91-98.

24. Irzhak, V. I. *Russian Chemical Reviews* **2004***, 3,* 251-265.

25. Elliott, J. E.; Anseth, J. W.; Bowman, C. N. *Chemical Engineering Science* **2001***, 10,* 3173-3184.

26. Wu, Y.; Joseph, S.; Aluru, N. *The Journal of Physical Chemistry B* **2009***, 11,* 3512-3520.

27. Cussler, E. L. *Diffusion, mass transfer in fluid systems;* Cambridge University Press: Cambridge [Cambridgeshire]; New York, 1984.

28. Slattery, J. C. *Advanced transport phenomena;* Cambridge Univ Pr: 1999.

29. Curtiss, C. *J. Chem. Phys.* **1968**, 2917.

30. Elliott, J. R.; Lira, C. T. *Introductory chemical engineering thermodynamics;* Prentice Hall: 1999; .

31. Fick, A. *Poggendorff's Annalen der Physik und Chemie* **1855***, 59-86,.*

32. Logan, J. D. *Applied partial differential equations;* Springer Verlag: 2004.

33. R. Byron Bird, Warren E. Stuart, Edwin N. Lightfoot *Transport Phenomena;* John Wiley & Sons Inc: New York, 2007.

34. Crank, J. *The mathematics of diffusion;* Oxford University: London, 1956.

35. Rundgren, J.; Dong, Q.; Hultquist, G. *J. Appl. Phys.* **2006**, 104902.

36. Ray, E.; Bunton, P.; Pojman, J., A. *American Journal of Physics* **2007**, 903.

37. Falk, B.; Garramone, S.; Shivkumar, S. *Mater Lett* **2004**, *26*, 3261-3265.

38. Vermonden, T.; Jena, S. S.; Barriet, D.; Censi, R.; van der Gucht, J.; Hennink, W. E.; Siegel, R. A. *Macromolecules* **2010**, 13-36.

39. De Smedt, S.; Meyvis, T.; Demeester, J.; Van Oostveldt, P.; Blonk, J.; Hennink, W. *Macromolecules* **1997**, *17*, 4863-4870.

40. Burke, M. D.; Park, J. O.; Srinivasarao, M.; Khan, S. A. *Macromolecules* **2000**, *20*, 7500-7507.

41. Gagnon, M. A.; Lafleur, M. *The Journal of Physical Chemistry B* , **2009** 397.

42. Kapellos, G. E.; Alexiou, T. S.; Payatakes, A. C. *Math. Biosci.* **2007**, *1*, 177-237.

43. Le Bihan, D.; Basser, P. J. *Diffusion and perfusion magnetic resonance imaging: applications to functional MRI.Raven Press; New York* **1995**, 5–17.

44. Stallmach, F.; Galvosas, P. *Annual Reports on NMR Spectroscopy* **2007**, 52-133.

45. Tanner, J. *J. Chem. Phys.* **1970**, 2523.

46. Atzmon, M. *Phys. Rev. Lett.* **1990**, *23*, 2889-2892.

47. Kamholz, A. E.; Schilling, E. A.; Yager, P. *Biophys. J.* **2001**, *4*, 1967-1972.

48. Pappaert, K.; Biesemans, J.; Clicq, D.; Vankrunkelsven, S.; Desmet, G. *Lab on a Chip* **2005**, *10*, 1104-1110.

49. Culbertson, C. T.; Jacobson, S. C.; Michael Ramsey, J. *Talanta* **2002**, *2*, 365-373.

50. Estevez-Torres, A.; Gosse, C.; Le Saux, T.; Allemand, J. F.; Croquette, V.; Berthoumieux, H.; Lemarchand, A.; Jullien, L. *Anal. Chem.* **2007**, *21*, 8222-8231.

51. Akgerman, A. *Industrial & Engineering Chemistry Fundamentals* **1976**, *1*, 78-79.

52. Wilke, C.; Chang, P. *AIChE Journal* **1955**, 264.

53. Welty, J.; Wicks, C.; Wilson, R. *Fundamentals of Momentum, Heat, and Mass Transfer;* John Wiley, New York: 1984.

54. Amsden, B. *Macromolecules* **1998**, *23*, 8382-8395.

55. Amsden, B. *Polymer Gels and Networks* **1998**, *1*, 13-43.

56. Stringer, J. L.; Peppas, N. A. *J. Controlled Release* **1996***, 2,* 195-202.

57. de Gennes, P. G. *Scaling concepts in polymer physics;* Cornell Univ Pr: 1979.

58. Noda, I.; Kato, N.; Kitano, T.; Nagasawa, M. *Macromolecules* **1981***, 3,* 668-676.

59. Phillips, R. J. *Biophys. J.* **2000***, 6,* 3350-3353.

60. Masaro, L.; Zhu, X. X. *Progress in Polymer Science* **1999***, 5,* 731-775.

61. Muhr, A. H.; Blanshard, J. M. V. *Polymer* **1982***, 1012,* 154.

62. Patachia, S.; Valente, A. J. M.; Baciu, C. *European Polymer Journal* **2007***, 2,* 460-467.

63. Kvarnstrom, M.; Westergard, A.; Loren, N.; Nyden, M. *J.Chem.Phys Phys Rev E* **2005**.

64. Kockmann, N. *Transport phenomena in micro process engineering;* Springer Verlag: 2008.

65. Kamholz, A. E.; Yager, P. *Biophys. J.* **2001***, 1,* 155-160.

66. Srinivasan, V.; Pamula, V. K.; Fair, R. B. *Lab on a Chip* **2004***, 4,* 310-315.

67. Horsman, K. M.; Bienvenue, J. M.; Blasier, K. R.; Landers, J. P. *J. Forensic Sci.* **2007***, 4,* 784-799.

68. Khademhosseini, A.; Ferreira, L.; Blumling III, J.; Yeh, J.; Karp, J. M.; Fukuda, J.; Langer, R. *Biomaterials* **2006***, 36,* 5968-5977.

69. Wu, J.; Day, D.; Gu, M. *Appl. Phys. Lett.* **2008**,

70. Pipe, C. J.; McKinley, G. H. *Mech. Res. Commun.* **2009***, 1,* 110-120.

71. McMullen, J. P.; Jensen, K. F. *Annu.Rev.Anal.Chem* **2010**, 19-42.

72. Retterer, S. T.; Siuti, P.; Choi, C. K.; Thomas, D. K.; Doktycz, M. J. *Lab Chip* **2010**.

73. Melin, J.; Quake, S. R. **2007**.

74. Waggoner, P. S.; Craighead, H. G. *Lab on a Chip* **2007***, 10,* 1238-1255.

75. Kjeang, E.; Djilali, N.; Sinton, D. *J. Power Sources* **2009***, 2,* 353-369.

76. Skurtys, O.; Aguilera, J. M. *Food Biophysics* **2008***, 1,* 1-15.

77. Ziaie, B.; Baldi, A.; Lei, M.; Gu, Y.; Siegel, R. A. *Adv. Drug Deliv. Rev.* **2004**, *2,* 145-172.

78. Harrison, C.; Cabral, J. *J Micromech Microengineering* **2004**, 153.

79. Khan, S.; Plitz, I.; Frantz, R. *Rheologica Acta* **1992**, *2,* 151-160.

80. Brzoska, J.; Azouz, I. B.; Rondelez, F. *Langmuir* **1994**, *11,* 4367-4373.

81. Revzin, A.; Russell, R. J.; Yadavalli, V. K.; Koh, W. G.; Deister, C.; Hile, D. D.; Mellott, M. B.; Pishko, M. V. *Langmuir* **2001**, *18,* 5440-5447.

Materials and Methods

3.1 Materials

The materials used to make the microfluidic device include glass slides (25 mm x 75 mm x 1 mm, VWR), kimwipes (Kimtech, delicate task), acetone (Krylon Industrial coatings), isopropanol (BDH, ACS grade), thiolene based optical adhesive (NOA 81 resin, Norland Products, Cranbury NJ), silicon wafers (University Wafer – mechanical grade SSP Si), photomasks made from transparencies (3M General Purpose transparency) and/or electrical tape. A radio frequency (RF) plasma cleaner (Harrick) was used with a vacuum pump (SPX RobinAir cool tech). A long wave ultraviolet (UV) light source (Blak-Ray UV Lamp, λ=365 nm) and temperature-controlled oven (ThermoScientific Lindberg Blue M) were also used in the device fabrication.

To create a hydrogel inside the microfluidic device, ethanol (anhydrous, Pharmco-Aaper), 3-(trichlorosilyl)propyl methacrylate (TPM) (Sigma Aldrich), 4-(2-hydroxyethoxy)phenyl-(2-hydroxy-2-propyl)ketone (Irgacure 2959) (Ciba Specialty Chemicals), poly(ethylene glycol) di-acrylate (PEG-DA) (Sigma Aldrich, M_n: 575 g/mol, PDI ~ 3), a UV lightsource (Blak-Ray UV Lamp), and UV lightmeter (290-390 nm Lutron lightmeter) were used. Deionized water (DI-H_2O) was used; DI-H_2O was made by running tap water through an organic / mixed bed DI cartridge (Thermo Scientific, Dubuque, IA).

To secure the device with luer-locking syringe needles (21G 1.5 in, 25G 1.5 in, and 27G, 1.25 in, all from Precision Guide), a wire cutter, a Dremel sanding tool, optical

adhesive (NOA-81 resin, Norland Products, Cranbury NJ), and a UV lightsource (Blak-Ray UV Lamp) were used.

The materials used as optical dyes include methylene blue (Sigma Aldrich), rhodamine 6G (Fluka), brilliant black BN (Sigma Aldrich), and crystal violet (Fluka).

Other materials used pertaining to the microfluidic device include syringe pumps (model NE-100, New Era Pump Systems, Inc; Farmingdale NY), and plastic luer-lock tubing ($D_i = 0.2$ cm, $D_o = 0.3$ cm, Cole-Parmer). Materials used in NMR experimentation not previously listed include 5 mm NMR tubes (5mm 33MHz, Wilmead LabGlass), D_2O (Cambridge Isotope Laboratories), and a H_2O, D_2O, 4,4-dimethyl-4-silapentane-1-sulfonic acid (DSS) standard (Varian Inc.). Other materials include poly(ethylene glycol) (PEG-1000) (Mn: 1000 ± 50 g/mol, Fluka). Surface tension measurements were taken with a Sigma 703D tensiometer (KSV Instruments).

3.2 Instrumentation

Light intensity in the ultra-violet range (290 nm - 390 nm) was measured using a Lutron UV lightmeter. An analytical balance was used to measure the masses (Ohaus Voyager Pro). Nuclear magnetic resonance (NMR) spectroscopy and diffusometry was performed using a Varian VXR 600 MHz spectrometer (Varian Inc). Fourier transform Infrared spectrometry was performed using a ThermoScientific Nicolette 380 (Electron Corporation). Dynamic mechanical testing was performed using a RSAIII Rheometric system analyzer (T.A. instruments, New Castle, DE). Digital images were obtained using a Motic digital microscope in conjunction with Motic software.

3.3 Methods

3.3.1 Fabrication of the Device

The following procedure was developed to fabricate a microfluidic device. Two 25 x 75 x 1 mm glass slides were wiped clean with kimwipes, acetone, and isopropanol. Care was taken to ensure isopropanol was the last solvent used before the slide entered the plasma cleaner. The slides were then cleaned in an oxygen plasma cleaner for 3 min at a low radio frequency (RF) level at a pressure of 200 mTorr. Optical adhesive was poured onto the bottom slide and the second slide was placed on top of the bottom slide, sandwiching the optical adhesive. Small pieces of silicon wafer were used as spacers to keep the slides exactly 600 μm or 1200 μm apart depending on whether one spacer or two were used, respectively. A photomask constructed from UV opaque material (electrical tape) was placed along both of the long (75 mm) sides of the device to make two 2-4 mm wide strips of cured optical adhesive along the edges, leaving 1.7 – 2.1 cm between the optical adhesive strips. The optical adhesive in the device was cured for 3.75 min at 600 μW/cm^2 for a total energy dose of 135 mJ/cm^2. The devices were removed from UV light and the silicon spacers were removed. Excess optical adhesive between the slides was removed by rinsing with DI-H$_2$O, isopropanol and acetone, and mechanical cleaning was used if necessary. Care was taken to rinse the device quickly with isopropanol after an acetone rinse to prevent any dissolution of partially cured optical adhesive. The devices were further cured at 500 μW/cm^2 for 20 min and then placed in an oven at 50° C for 4h to fully cure the optical adhesive. A device with optical adhesive is presented in Figure 3.1 below:
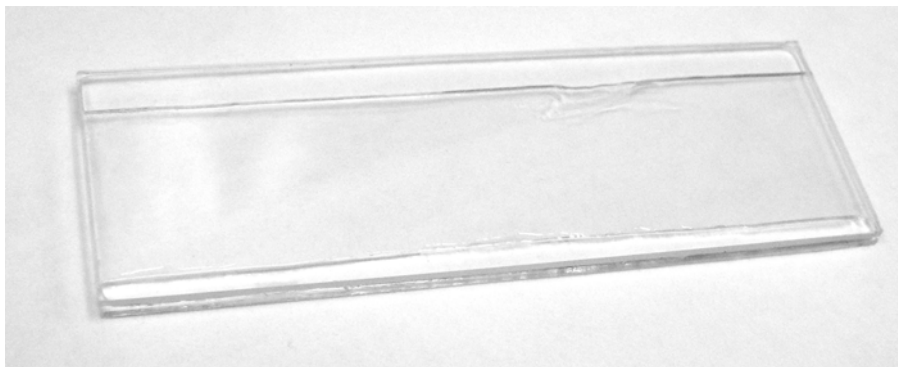
Figure 3.1: Cured optical adhesive in a microfluidic device

To prepare the device for the formation of a hydrogel, the optical adhesive shell was immersed in a 1 mM TPM in ethanol solution for 20 min. The device was then filled with a solution of 30 vol.% PEG-DA and Irgacure 2959, and 70 vol.% DI-H_2O. To make this solution, 0.25 wt/wt % irgacure was first added to pure PEG-DA. DI-H_2O was then added to dilute the PEG-DA and Irgacure mixture to 30 vol%. This PEG-DA/water solution was added between the two slides of the device using a syringe. Two methods were used to imprint a channel into the hydrogel; both are described below. The first method uses a photomask, while the second uses a small diameter wire to achieve a defined channel in the hydrogel portion of the microfluidic device.

The following procedure was used to imprint a channel onto the device using a photomask. First, a photomask was made in Microsoft publisher and printed on transparencies using a laser printer. The photomask was patterned with a 0.5 mm - 1.5 mm thick straight-line channel geometry presented in Figure 3.2 below.
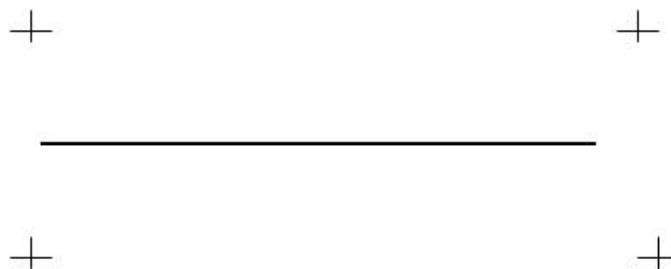
Figure 3.2: Photomask used to imprint a straight channel geometry in a PEG hydrogel microfluidic device system (note: not to scale)

Two copies were printed out and taped over one another to increase the opacity of the photomask. The crosshairs at the corners of the photomask helped achieve alignment. The photomask was secured over the device and both were loaded onto a 12 cm x 12 cm cardboard platform to facilitate movement to and from the UV light source. Using the cardboard platform, the device and photomask were placed under the UV light source at an intensity of 3000 μW/cm^2 (as measured under the photomask). The device was cured uniformly by moving the device under the UV light source as needed. The device was cured for 8 min on the left and right sides, followed by 4 to 8 min in the middle as needed for a total irradiation dose of 3.5 to 4.2 J/cm^2. The movement was necessary to account for spatial inhomogeneities under the UV lamp. Figure 5.1 shows how UV intensity varies with position under the UV lamp. After curing the hydrogel, any blockages in the channel were cleared using a small wire and water in syringes, delivered by 1.5 inch 21-G needles. The channel was then rinsed with DI-H$_2$O and immersed in a beaker of DI-H$_2$O until needles were ready to be attached.

To imprint a channel using a small wire, the following procedure was used. First, a 500 μm diameter wire was placed inside the device with ends protruding from both sides. Adding the wire ensured the hydrogel solution would remain uncured when placed under UV light, resulting in a 500 μm channel. The device was then loaded onto a 15 cm x 15 cm cardboard platform to facilitate movement, and placed directly under a UV lamp at an intensity of 5000 μW/cm^2, centered the left-most edge of the device. The device was moved to the right at a rate of 0.5 cm to 1 cm every 2 min. During this process, 1 inch by 3 inch opaque photomasks were used to cover sections of the device that became cured to prevent the hydrogel from cracking. Curing manifests around 7 or 8 min; however, the first photomask was placed on the device after 10 – 12 min of curing. This coincided to when a third of the device (i.e. the left-most third) became cured. The devices continued to be moved so that the less cured sections were under the most intense UV radiation. This occurred at a rate of 1 cm every 2 min until the length of the device was cured, continuing to apply black or opaque photomasks along fully cured sections of the hydrogel. The whole curing process took about 20 min and imparted a total energy of ~3.6 J. After curing, the device was removed from the UV lamp and the wire was taken out, using caution not to crack the cured hydrogel. The channel was rinsed with DI-H$_2$O using a syringe with a 25 G needle and immersed in a beaker of DI-H$_2$O until needles were ready to be attached.

To complete the device, needles were inserted into the channel and permanently attached using optical adhesive. Needles were cut and sanded using needle-nosed clippers and a handheld Dremel, respectively. Needles were individually inserted and

cured. Once inserted into the channel defined by the cured hydrogel, optical adhesive was used to secure the needle in place and seal the end of the device. Optical adhesive was carefully poured over the side of the device with the needle held in place manually. The device was quickly moved under a UV light source and cured under high intensity (5000 µW/cm^2) UV light for 10 to 30 s while holding the needle in place. Once both needles were adequately secured, the device was placed under mild UV radiation (≈700 µW/cm^2) for 10 to 15 min to cure the optical adhesive surrounding the needles. Care was taken to cover the hydrogel to prevent it from cracking - a result of excess curing. Water was introduced into the device to confirm seals were watertight and to keep the hydrogel inside hydrated and swollen. Finished devices were stored submerged in DI-H$_2$O at 4 °C in darkness until used.

3.3.2 NMR Sample Preparation Procedure

To cure a hydrogel inside an NMR tube, an aliquot of 70 vol% DI-H$_2$O, 30 vol% PEG-DA, and 0.25 wt/wt Irgacure/PEG-DA was placed in an NMR tube. The solution was placed under a UV light source (365 nm) with slow axial rotation of 30 rpm. The tube was cured under an intensity of 650 µW/cm^2 for 39 min to crosslink the PEG hydrogel.

In certain cases, a solution of dye was added to the tube and allowed to diffuse into the hydrogel structure over a week. The volume of dye solution added was roughly the same volume as the PEG hydrogel already in the NMR tube, which ensured the overall concentration of dye in the tube was approximately half of that in the original

solution. The overall dye concentration in the NMR tube for each dye solution is presented in Table 3.1 below.

Table 3.1: Concentrations of various dyes used in the NMR hydrogel samples

Dye	Concentration in NMR tube [mM]
Methylene blue	34
Rhodamine 6G	1.04

After the tubes were filled, they were capped and sealed with Parafilm to prevent evaporation. In some cases, tubes containing hydrogel and dye were placed in temperature controlled ovens for multiple days to help speed up diffusion in the tube. Temperatures used were 30 to 45 ºC, which is well below the thermal decomposition temperature of any dyes used in the study.

Samples of methylene blue, rhodamine 6G, crystal violet, PEG1000, PEG-DA, and brilliant black BN were added to D_2O and DI-H_2O and mixed. A 1 to 2 ml aliquot was taken and placed inside an NMR tube for the purpose of gathering a ^{1}H-NMR, as well as aqueous free diffusion spectra.

3.3.3 Optical Calibration Curve

Hydrogel slabs were placed in 50 ml sealed containers with concentrations of dye ranging from 0 to 100 % (in 10 % increments) of the dye concentration used in the diffusion procedure. After 48h of total immersion at room temperature, the slabs were removed and dried by wiping the surface with a kimwipe. The smallest dimension was

measured with a caliper before the slab was photographed using a Motic digital

microscope. Lighting and exposure settings remained constant for all pictures, and were

as close as possible to those used during diffusion experimentation.

3.3.4 Device Diffusion Procedure

A device was secured in the viewing area of the digital microscope. Risers were

placed under the device if it did not lay flat due to the needles. Care was taken to make

the device as square as possible as viewed from the software. Pictures were taken of the

device with a ruler placed on top before at the beginning of each experiment. A white

sheet of paper was used to calibrate the white balance of the camera before pictures were

taken. A 100 W lamp was placed three feet to the side of the microscope and elevated to

provide additional light.

A small volume of water was pumped through the device to remove any air

bubbles. When the experiment was set to begin, a 60 ml syringe filled with a dye

solution of known concentration was placed in a syringe pump and connected to the

device using plastic luer-lock tubing. Typical concentrations for methylene blue dye

used were approximately 17 μM. Pictures were taken and saved using the digital

microscope and commercial software once every second for a minute as the syringe

pump began to pump dye solution into the device. The small time interval between

pictures helps identify the precise time when dye first enters the device. The brightness

of the digital pictures was adjusted when the dye first filled the channel and remained

constant thereafter. After one or two minutes had elapsed, pictures were taken

approximately once every 60 s for the remainder of the experiment. The syringe pump delivered dye solution at 15 ml/h giving a total run time of approximately 4 h.

3.3.5 NMR diffusion procedure

First, the magnetic field of the NMR instrument was adjusted until homogenous, and spectra of samples were taken using a single pulse experiment. The $\pi/2$ pulse width was found and recorded. Spin-lattice relaxation times, τ_1, were found using an inversion recovery method.

The pulsed field gradient sequence, shown in Figure 3.3, was applied to determine the diffusion coefficient of species in the sample. The sequence was set up by adjusting the magnitude of the gradient pulses, G, and the length of time between the first and second gradient pulses, Δ. Values used for G and Δ range from 5 to 35 G/cm and 0.003 to 0.3 s, respectively. The duration of the gradient pulses, δ remained constant at 0.002 s. The upper limit of Δ was chosen as the point where signal attenuation for the peaks of interest was large enough to decay the signal into the baseline when the gradient strength was at a maximum of 35 G/cm. The pulse sequence typically ran with 4 to 7 values of G and 4 to 6 values of Δ. Multiple scans (32+) at each point were gathered to improve signal resolution. Inter-pulse delay (d1) values were around 10 s, and always greater than 5 times the value of τ_1.
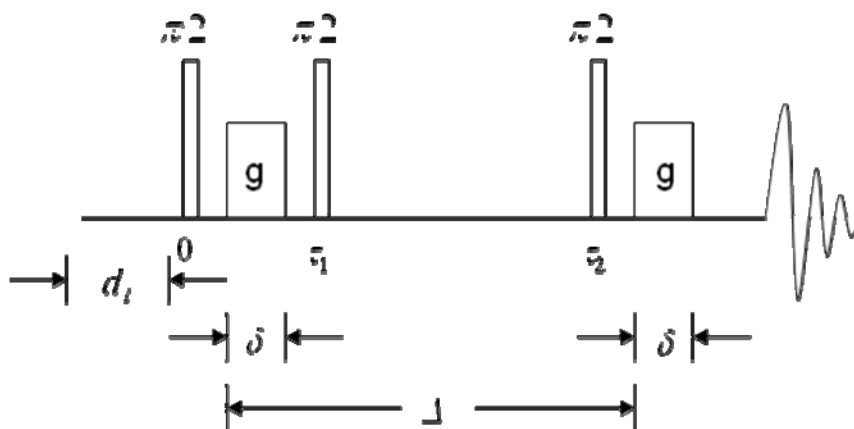
Figure 3.3: Pulse sequence for the pulsed field gradient stimulated echo (pge_ste) pulse

3.3.5.1 Water Suppression Sequences

Once the magnetic field on the NMR instrument had been adjusted, a water suppression sequence was grafted onto the beginning of a single pulse experiment to obtain a solvent free spectra. The water suppression works by applying transverse gradients and eliminating the solvent peak in the spectra.[1] The pulse sequence for the water suppression pulse (wet1d) is shown below in Figure 3.4:
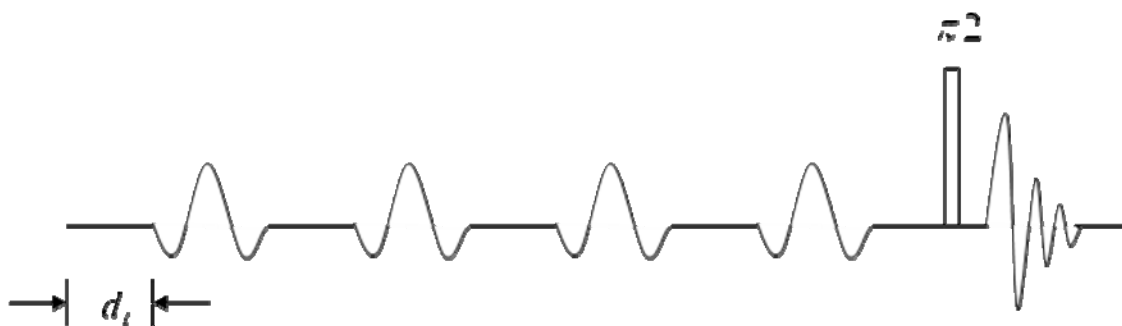
Figure 3.4: Water suppression sequence used (wet1d)

The water suppression sequence required a manual input of the water peak information including peak location and bandwidth. These values were chosen by the user to achieve sufficient water suppression.

The water suppression sequence was combined with a pulsed field gradient stimulated echo experiment to obtain solvent free diffusion spectra. The pulse sequence for the combined solvent suppression pulsed field gradient (pge_wet) experiment is shown in Figure 3.5 below:
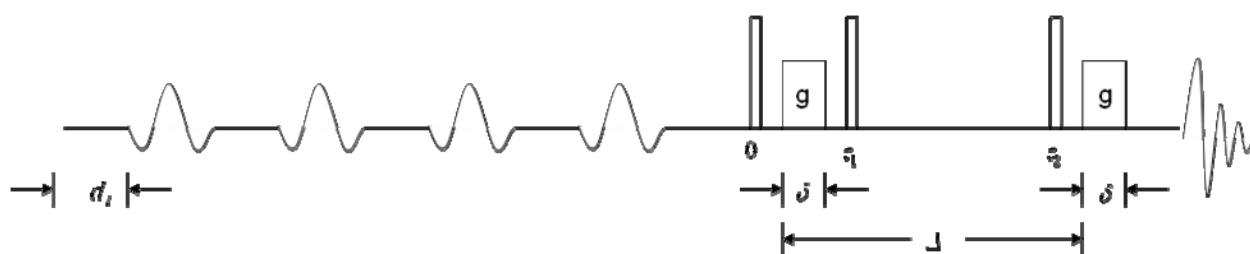
Figure 3.5: Water suppression pulsed field gradient pulse sequence (pge_wet)

The pge_wet sequence was set up using similar parameter values for δ and Δ as those used in the pge_ste sequence. The only exception is the water suppression parameters were taken from the wet1d sequence.

3.3.6 Fabrication of Hydrogel Slabs

3.3.6.1 Fabrication of Wellplate

To make a wellplate to fabricate PEG slabs for general analysis and concentration curve purposes, the following procedure was used. First, a 50 mm x 75 mm x 1 mm glass slide was cleaned with acetone and isopropanol. The slide was then placed in an oxygen plasma cleaner and cleaned for 2 min at a low RF level at a pressure of 200 mbar. The slide was placed over a reservoir of optical adhesive, and a photomask was secured above it. Care was taken to avoid any bubbles at the glass-optical adhesice interface by sliding the glass gently over the surface of the optical adhesive. The photomask outlined four 2.5 cm x 1.5 cm squares and is shown in Figure 3.6. The photomask was made using Microsoft publisher.
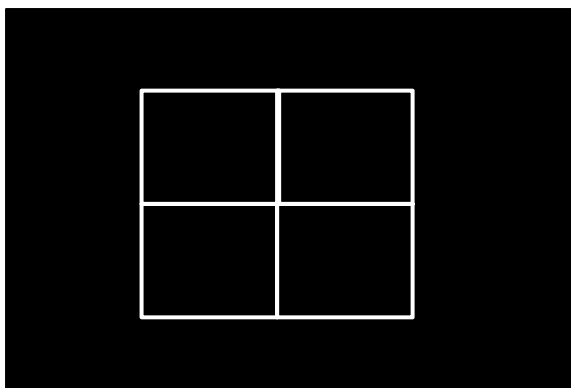
Figure 3.6: Photomask for wellplate (note: not to scale)

Two copies of the photomask were printed onto transparencies and taped together to form the final photomask used in the curing process. The reservoir with slide and photomask attached were exposed to UV light for 6 min at 600 μW/cm^2. This resulted in

a wall height of approximately 1 mm being formed. The wellplate was cleaned using acetone, ethanol, isopropanol, along with mechanical cleaning via spatula. The final wellplate is shown in Figure 3.7.

Figure 3.7: Wellplate for the fabrication of PEG slabs

3.3.6.2 Hydrogel Slab Curing procedure

To make hydrogel slabs, a solution of uncured 30 vol% PEG-DA/ Irgacure (0.25 wt Irgacure / wt PEG-DA %) and 70 vol% DI-H_2O mixture was introduced into the wellplate to make multiple 1.5 cm x 2.5 cm x 0.1 cm slabs. A syringe was used to fill the wellplates, since a sheet of glass was placed over the wells by sliding it from one side to the other. Sliding the glass cover and using a syringe prevented bubbles from forming, as well as minimized the amount of fluid outside the wells. The covered wellplate was placed under UV light (3000 $\mu W/cm^2$) for 22 to 25 min to cure the solution as needed. Curing was finished when the slab became cloudy throughout the wellplate. After removing the wellplate from the UV light, the slabs were cut out with a razor blade and

stored in DI-H$_2$O. Examples of PEG hydrogel slabs created by this procedure are

presented in Figure 3.8 below.

Figure 3.8: Examples of PEG hydrogel slabs fabricated in the wellplate

3.3.7 Characterization of Hydrogel Properties

3.3.7.1 Dynamic Mechanical Analysis

PEG hydrogel slabs were used for dynamic mechanical analysis (DMA). The

slab dimensions were approximately 1.5 cm x 2.5 cm x 0.1 cm, however more precise

measurements were taken for each sample. The slabs were loaded onto a shear sandwich

apparatus for testing. The slabs were covered in petroleum gel to prevent dehydration

during the course of the experiment. The hydrogel's response to a range of frequency

and shear magnitude inputs were recorded. Data was generated using software supplied

by the manufacturer of the instrument.

3.3.7.2 Swelling Ratio

PEG hydrogel slabs were removed from the DI-H$_2$O storage container and patted

dry. The slabs were weighed and their dimensions were recorded. The samples were

allowed to de-swell in atmospheric conditions before being cooled to the temperature of a

commercial freezer ($\approx$ -5 ºC). Afterwards, the samples were cooled with liquid nitrogen

and placed in a low vacuum lyophilizer overnight. This gradual dehydration helped to prevent sample cracking and disintegration. After lyophilization, the samples were reweighed and measured, and immersed in DI-H_2O for six days before being weighed and measured for a third time.

3.4 Concluding Remarks

These procedures describe the fabrication and diffusometry procedures for a microfluidic device. The NMR diffusometry methods used to compare diffusometry values to those determined from the device are developed. Additionally, an array of procedures for evaluating the physical properties of a PEG hydrogel are presented.

3.5 References

1. Smallcombe, S. H.; Patt, S. L.; Keifer, P. A. *Journal of Magnetic Resonance, Series A* **1995**, *2,* 295-303.

Methods of Analysis

4.1 Choice of Solutes
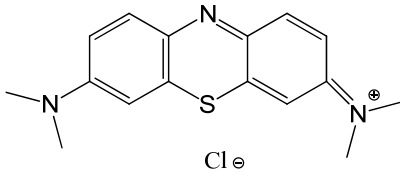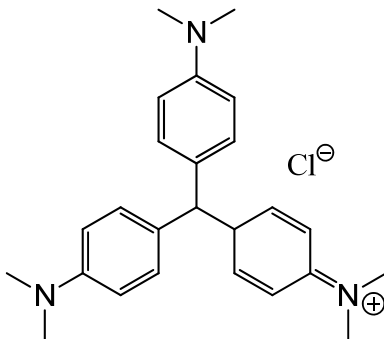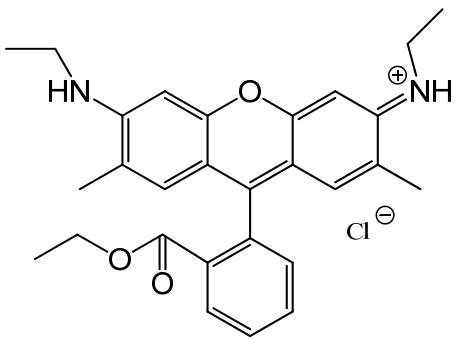
The diffusion study carried out in this research requires the use of solutes as diffusing species. In order to be useful as a solute, a chemical (or biological) species must fulfill several requirements. First, the dye must be water soluble. This is necessary because an insoluble molecule will not diffuse through a hydrogel. Second, the solute must be optically active in the visible range of the electromagnetic spectrum. This requirement is the most difficult to fulfill as most compounds do not color an aqueous solution when they dissolve. Although this requirement limits the number of compounds, there are thousands of dyes and fluorescent molecules that are still potential candidates. Third, the solute must have at least one distinct and visible nuclear magnetic resonance (NMR) sensitive environment when in a hydrogel matrix. This is necessary to monitor diffusion using NMR. If this requirement is not fulfilled, a diffusion coefficient cannot be determined via NMR methods. In this research, the only magnetically susceptible isotope used was hydrogen. Although most organic molecules have numerous hydrogen environments, this requirement is somewhat difficult to fulfill because the poly(ethylene glycol) (PEG-DA) hydrogel has hydrogen peaks that can disturb or block out the peaks of the solute. The final requirement of the solute is that it must be small enough to physically diffuse through the hydrogel matrix. The PEG-DA hydrogel used in this research has a relatively small mesh size, so only small organic molecules were considered. Hydrogels with larger mesh sizes could use proteins or small polymer chains
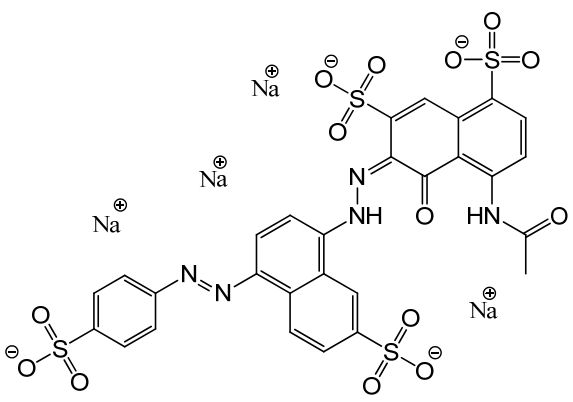
as the solute. Although not strictly a requirement, one should choose solutes that have differing physical properties. This can be used to infer the effect of these properties on the diffusivity value. The properties of solutes can include molecular weight, molar volume, ionic charge, and shape factors.

The dyes used in this research were chosen based on their fulfillment of the above requirements. The solutes selected include methylene blue, crystal violet, rhodamine 6G, and brilliant black BN. The structures and properties of the solutes chosen are presented in Table 4.1 below.

The ionic nature of these solutes is important. Many diffusion theories cannot incorporate ionic charge into their models. Many drugs and therapeutic compounds exist as salts, so the effects of ionic charge should be examined. Methylene blue, rhodamine 6G, and crystal violet have been known to aggregate and form dimers, trimers, or tetramers. This has a practical consequence for diffusion studies as aggregated species will have a larger hydrodynamic radius. Spectroscopic investigations indicate crystal violet dimerizes at concentrations greater than 10^{-5} M,[1] methylene blue dimerizes at concentrations above 4×10^{-5} M,[2] and rhodamine 6G dimerizes at concentrations above 10^{-6} M.[3] These factors will have to be taken into account for diffusion in the microfluidic device, as well as in the NMR studies.

Table 4.1: Solutes chosen for diffusive studies in PEG-DA hydrogels

Name	Structure	Molecular weight [g/mol]	Molar volume [A^3]	Ionic charge
Methylene blue		319.8	264	+1
Crystal violet		407.9	378	+1
Rhodamine 6G		479	424	+1

Brilliant Black BN		867.7	555	-4

The three solutes have similarities to current drugs and pharmacologically active agents. Methlene blue is being investigated as a treatment for malaria[4], and alzheimer's disease.[5] Crystal violet has been used as an antiseptic.[6] Rhodamine 6G and brilliant black BN are non-therapeutic, although Brilliant black BN is used a food dye. All of these compounds have structural similarities with common drug molecules. Trends in the solute's diffusion behavior could be extrapolated for other drug molecules.

4.2 Digital Image Intensity and Concentration Relationship

The key factor in determining solute diffusivity using the microfluidic device is that the solute's concentration can be monitored. One way this can be done is through optical measurements. On a conceptual level, the darker a solution of dye is, the more concentrated it is. This relationship has been quantified mathematically and is known as Beer's law:

$$A = \varepsilon \ell C \qquad\qquad (4.1)$$

where A is absorbance, ε is the extinction coefficient, l is path length, and C is concentration. The extinction coefficient should be determined experimentally, and usually only applies up to a threshold concentration, after which deviations occur and Beer's law is no longer valid. This relationship is widely used in analytical chemistry; however, it requires the use of a spectrophotometer to measure absorbance.

This research uses a digital camera on a microscope to monitor concentration levels in the microfluidic device. This technique uses the same concept behind Beer's law: the darker the image, the more concentrated the dye. When a digital image is taken, information is stored as a two dimensional array of pixels. Each pixel has a number value associated with the red, green, and blue (R, G, and B) component of the color for light entering the pixel area. A digital image stores its information in these red, green, and blue component values. Colors and image intensity can be found given the R, G, and B components of a pixel. Although darkness and color information can be collected with digital photography, there is no direct link from R, G and B values to solute concentration. Information from a digital image is not the same as absorbance; so strictly speaking, Beer's law is not applicable. In order to verify a relationship between image 'darkness' or intensity with solute concentration, a calibration curve was created.

This calibration quantifies the relationship between R, G, and B values (or combinations thereof) to solute concentration, making the link necessary to monitor solute concentration in the microfluidic device. To achieve this, multiple hydrogel slabs

were placed in aqueous solutions of known solute concentration and allowed to come to equilibrium. Digital images were then taken of the slabs, and the R, G, and B information was plotted against the concentration in the hydrogel slabs.

Ideally, solute concentration and image intensity would be directly correlated with a one-to-one relationship. In reality, the R, G, and B values do not always correlate with color darkness, or intensity. To have a calibration curve that described as much of the variance in color as possible, each component (R, G, and B) as well as combinations of the components were tested. For example, the R, G, and B values can be combined to find the grayscale, or black-and-white intensity using equation (4.2):

$$GS = 0.299R + 0.587G + 0.114B \tag{4.2}$$

In addition to testing linear combinations of R, G, and B different colormaps were tested. A colormap is directly comparable to a geometric coordinate system. Just like you can convert between Cartesian and spherical coordinates, you can convert between colormaps. If you know the components of in the RGB colormap (R,G,B), you can find the components in a different colormap. Ultimately, the goal of using other colormaps is to find a strong correlation between some type of information in the digital image and the solute concentration.

4.3 Microfluidic Device Data Analysis

The raw data gathered to analyze diffusion in a hydrogel using a microfluidic device is a set of digital images. Examples of some images taken are shown in Figure 4.1 below.

$t = 48\text{s}$	$t = 3,865\text{s}$	$t = 14,376\text{s}$
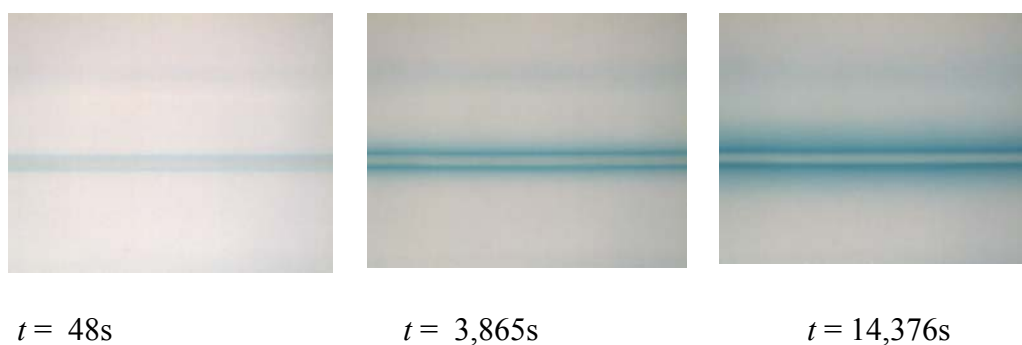
Figure 4.1: Pictures of diffusion in PEG-DA hydrogel in a microfluidic device

The images are taken using a digital microscope and analyzed using custom MATLAB scripts (see appendix 4). To find diffusion coefficients, the scripts take the set of digital images and extract the colormap information (i.e. R, G, and B values) from them. Next, the intensity values are converted into concentration values using a previously determined empirical relationship. Finally, the concentration values are compared with theoretical models to determine diffusion coefficients. A more in-depth examination of how the digital images are analyzed to determine diffusion coefficients is below.

Pictures were imported into MATLAB and converted from color into grayscale using the NTSC algorithm in equation (4.2). A suitable section of the picture where the channel was straight and free of imperfections was chosen for data analysis.

The top left of Figure 4.2 shows an image of a device taken at *t=0* s; the red box is the area chosen for analysis. The intensity values within the red box were averaged to give intensity profiles across the channel and hydrogel sections of the digital image. The intensity profile is shown in the main part of Figure 4.2.
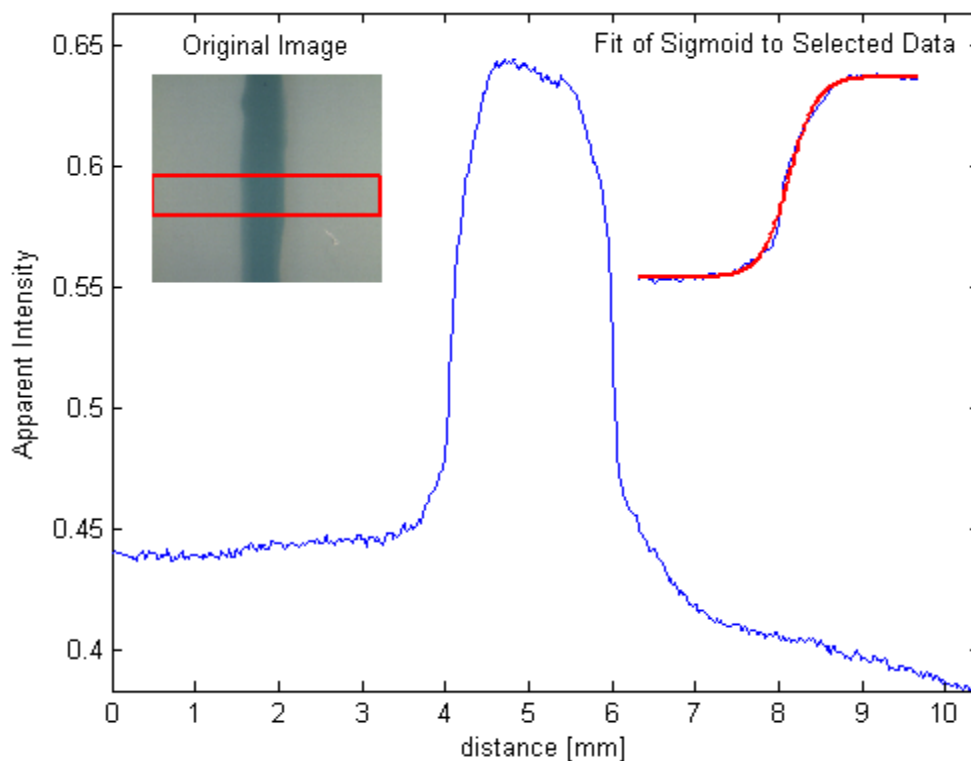
Figure 4.2: Intensity of the optical image across the channel at t=1s

The precise boundary between the hydrogel and the channel was found by fitting the initial dye picture (t=0) to a simple sigmoid equation with parameters for translation and stretching in both x and y directions as shown in equation (4.3).

$$y = \frac{a}{1+\exp(-b(x-c))} + d \tag{4.3}$$

This procedure helped determine an appropriate value for the boundary between the hydrogel wall and the dye in the channel. The sigmoid function did an excellent job fitting selected data around the channel boundary; an example is provided in Figure 4.3. The boundary was defined by the inflection point in the sigmoid function, which corresponds to the parameter c in equation (4.3). The sigmoid function was chosen because it could compensate for varying degrees of resolution caused by the hydrogel water boundary. The boundary location was always reviewed, and sometimes changed before further data processing steps. The boundary was never moved more than a few pixels from the value provided by the sigmoid fit.
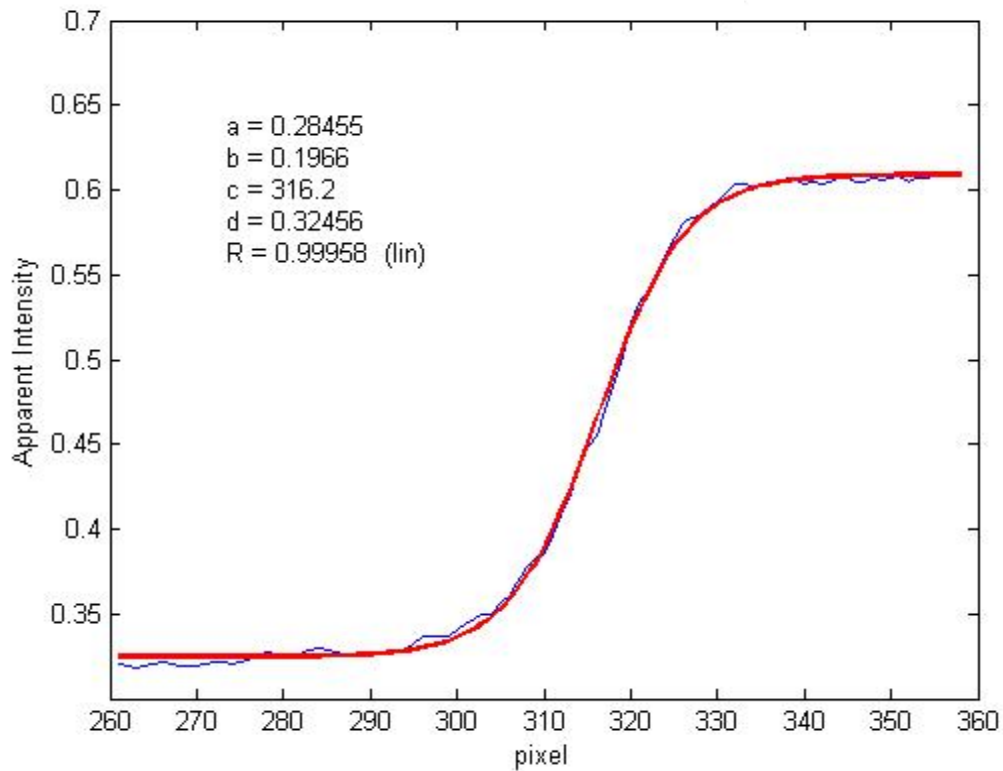
Figure 4.3:Fit of the sigmoid equation to the data around the channel boundary.

Next, the intensity profile was taken from the channel boundary out to the end of the picture for both sides of the channel. Using the empirical relationship between intensity and concentration found by the calibration curve, the intensity values were converted to concentration profiles. At this point, the background of the concentration profile is fitted to a first order polynomial and removed. The concentration profiles are then normalized so that they all range from 0 to 1. The profiles were then plotted against the variable $\eta = x / 2\sqrt{t}$. The analytical penetration solution to the diffusion equation shown in Equation (4.4) was regressed against the data to determine the diffusion coefficient.

$$\frac{C}{C_0} = erfc\left(\frac{\eta}{\sqrt{D}}\right) \qquad (4.4)$$

This solution assumes that the diffusion coefficient is constant with respect to space (homogenous media), time, and solute concentration. Furthermore, the model assumes a negligable mass transfer resistance at the boundary $x=0$. The simplicity of this model is one of its assets. It allows all the data to be conveniently shown at once through the use of a similarity variable, and can be regressed to find a diffusion coefficient. An r^2 value for the fit was calculated as shown in Equation (4.5).

$$r^2 = 1 - \frac{SS_{resid}}{SS_{tot}} = 1 - \frac{\sum_i (y_i - f_i)^2}{\sum_i (y_i - \bar{y})^2} \qquad (4.5)$$

Another method of verifying that the data collected follows normal Fickian behavior is to plot the total amount of solute in the hydrogel, M_t, against the square root of time and see if the resulting trend is linear. Alternatively one can plot M_t and time on a log-log plot and evaluate the slope. Under short time, or semi-infinite slab conditions, diffusive absorption obeys the following general relationship:

$$M_t = kt^n \qquad (4.6)$$

where n is the exponent. For planar geometries, when $n=0.5$, the diffusion is Fickian.[7,8] The parameter k can be shown to be related to the diffusion coefficient (see appendix 2) via:

$$D = \frac{\pi}{4}\left(\frac{k}{C_0}\right)^2 \qquad\qquad (4.7)$$

A log-log plot of total solute uptake, M_t, and time, t, is useful to see if the diffusion process is Fickian or not. The diffusion coefficient can be inferred from this graph as well. These methods were used to analyze data generated from digital images of the diffusion process.

4.4 NMR Data Analysis

Nuclear magnetic resonance (NMR) diffusometry requires that the solute have visible peaks in the hydrogel spectra. If the peaks are not visible, no diffusion analysis can be carried out. The presence of visible peaks belonging to the solute is not trivial. The spectra in the hydrogel can be crowded, and the concentration of solute is typically low. Spectra are gathered for each component individually, as well as for the solute-hydrogel mixture. It is helpful to identify which hydrogen environments the NMR peaks correspond to on the molecule (although it is not necessary).

Once a solute peak is visible in the hydrogel sample, a pulsed field gradient (PFG) pulse sequence is applied to the sample. The success of this sequence depends on monitoring peak attenuation of the solute as it diffuses out of the monitoring window. This requires a clear signal of the peak. If a solute has multiple hydrogen environments visible in the NMR spectra, then more than one peak can be monitored during the PFG

experiment. Looking at more than one peak reduces the error associated with the experiment.

The peak relative intensities, S/S_0, can be plotted against $(\gamma g \delta)^2 (\Delta - \delta/3)$ on a semi-log plot to yield a straight line. The slope of this line is directly related to the diffusion coefficient. A linear regression can provide a value for the slope. The standard deviation of the slope of the line, e, can be calculated from the following expression:[9]

$$e = \sqrt{\frac{\sum_i (y_i - \hat{y}_i)^2}{(n-2)\sum_i (x_i - \bar{x})^2}} \tag{4.8}$$

Where y_i is the y value for point i in the dataset, $\hat{y}_i$ is the predicted value for point i, n is the number of samples, x_i is the x value for point i, and $\bar{x}$ is the mean of the x values in the data-set.

4.5 Swelling Data Analysis

The mass and volume of hydrogel slabs were measured before and after lyophilization. The slabs were also allowed to re-swell in water and mass and volume were re-measured. The polymer volume fraction, $v_{2,S}$, can be calculated from the volume change before and after lyophilization:

$$v_{2,s} = \frac{V_{lyo.}}{V_{swollen}} \qquad (4.9)$$

where $V_{lyo.}$ is the volume after lyophilization, and $V_{swollen}$ is the volume before lyophilization. The polymer volume fraction was also calculated from the mass before and after lyophilization using the following equation:

$$v_{2,s} = \frac{1}{1 + \dfrac{\rho_{polymer}}{\rho_{solvent}}\left(\dfrac{m_{swollen}}{m_{dry}} - 1\right)} \qquad (4.10)$$

The two methods of calculating polymer volume fraction should produce the same value assuming the volume change of mixing is negligible.

4.6 References

1. Stork, W.; Lippits, G.; Mandel, M. *J. Phys. Chem.* **1972**, *12,* 1772-1775.

2. Braswell, E. *J. Phys. Chem.* **1968**, *7,* 2477-2483.

3. Dare-Doyen, S.; Doizi, D.; Guilbaud, P.; Djedaini-Pilard, F.; Perly, B.; Millie, P. *Journal of Physical Chemistry B-Condensed Phase* **2003**, *50,* 13803-13812.

4. Meissner, P. E.; Mandi, G.; Coulibaly, B.; Witte, S.; Tapsoba, T.; Mansmann, U.; Rengelshausen, J.; Schiek, W.; Jahn, A.; Walter-Sack, I. *Malaria J* **2006**, 84.

5. E. Wilkinson *BBC* **2008**.

6. Docampo, R.; Moreno, S.; Muniz, R.; Cruz, F.; Mason, R. *Science* **1983**, *4603,* 1292.

7. Ritger, P.; Peppas, N. *J. Controlled Release* **1987**, *1,* 23-36.

8. Muhr, A. H.; Blanshard, J. M. V. *Polymer* **1982**, *1012,* 154.

9. Devore, J. L.; Farnum, N. R. *Applied statistics for engineers and scientists;* Thomson Brooks/Cole: 2005; .

Results and Discussion

5.1 Device Fabrication

The first result of this study is the fabrication of a microfluidic device to characterize the diffusivity of solutes in hydrogels. Hydrogels have been used in microfluidic devices as valves, microstructures, to biocompatibilize surfaces, or as tissue scaffolds. The imprinting of a hydrogel defined microchannel in a microfluidic device is, to this author's knowledge, a novel concept. The principle follows traditional photolithography, but the design was based on previous studies of poly(ethylene glycol) (PEG) hydrogels inside microfluidic devices.[1] The design is simple, robust, and can incorporate hydrogels that can be thermally or photo-crosslinked.

The procedure, as described in the materials and methods (Chapter 3), for making the optical adhesive shell is straightforward and robust. The optical adhesive cures quickly and remains a liquid in areas covered by the photomask. Excess optical adhesive is easily cleaned out using common solvents, compressed air, and the occasional mechanical cleaning. The optical adhesive shell adds rigidity, and structural stability to device, allowing sensitive materials (like hydrogels) to be used inside.

Optimizing the curing procedure for the PEG-DA hydrogel proved to be more difficult. The hydrogel can be cured without a solvent, but the mesh size of the resulting hydrogel would be too small. The network structure would be too entangled to allow diffusion. To obviate this, PEG-DA was diluted as much as possible while still allowing it to be cured. Studies carried out at different dilutions showed PEG-DA at 20 vol%

would not crosslink to form a network. This agrees well with a calculated value of

23 vol% as the critical volume fraction of polymer at the dilute to semi-dilute transition

point (see section 2.2.4). This transition point corresponds to the volume fraction

necessary for polymer coils to first interact with one another shown in Figure 2.10.

A mixture of 30 vol% PEG-DA and 70% water was chosen to be used since it was

close to the transition point, and thus had a large mesh size, but was still concentrated

enough to be cured. Photopolymerizing PEG-DA at this concentration sometimes

produced hydrogels that cracked, suggesting the mesh structure was being strained. The

crosslinked PEG-DA cracked more often if it remained under the UV light after the

transition from liquid to solid was observed. Unfortunately, the UV light source was not

homogenous over the area of the device allowing certain points to cure (and crack) before

others had cured. A plot of the spatial variation of UV light intensity is shown in Figure

5.1.
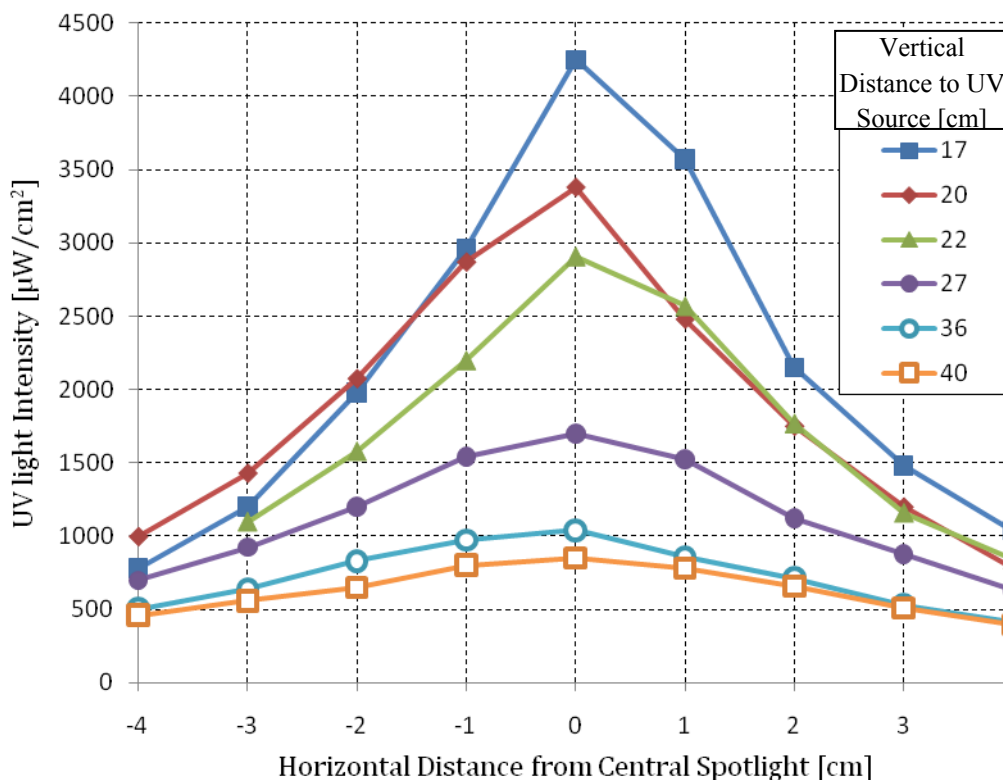
Figure 5.1: Variation of UV light Intensity as a function of location

The non-uniformity of the UV light led to an optimization of the curing regime

for the PEG-DA hydrogel. It was found that a UV intensity of 3000 to 3500 µW/cm^2 (as

measured under the photomask) balanced the time required to cure the device with the

UV inhomogeneities associated with being closer to the UV light source. The curing

regime developed involves placing the left side of the device under the center 'spotlight'

of the light source for some time, followed by placing the right side of the device under

the center spotlight for the same amount of time. Finally, the device was centered under

the spotlight until cured. If one side became cured before the other, a photomask was

placed over the cured areas to block UV light and prevent cracking.

One method used to imprint microchannels in the cured PEG-DA hydrogel was to use a photomask with a linear channel geometry shown in Figure 5. below. After curing, the channel was rinsed out with water, needles, and small diameter wire. It was noticed that if the channel width on the photomask was too small, the hydrogel would cure under the photomask, blocking the channel. If the channels were cured over, it was very difficult to remove PEG-DA material without compromising the device. The cured gel would often crack, or the edge of the carved out channel would be undesirably rough, increasing the need for an optimized photomask geometry. Multiple channel widths were tested to determine the limitation on channel resolution. The channel dimensions tested were 0.5, 0.7, 0.8, and 1.0 mm wide. It was found that the 0.5 mm channel photomask was too thin for reliable device production. Channels using the 1.0 mm photomask were on the order of 0.9 mm. The smallest channel made using a photomask was 0.45 mm.

Figure 5.2: Photomask used to imprint a straight channel geometry in a PEG hydrogel microfluidic device system (note: not to scale)

5.2 Diffusion Limited Channel Resolution

The limitation on channel resolution using the photomask comes mainly from the diffusion of reactive species under the photomask. Another potential source of error is the diffraction of light past the photomask, however, it was found that this would account

for only 10% of the observed limitation in resolution (see Appendix 1). The limiting process in making small channels is diffusion of reactive species under the photomask.

As PEG-DA chains become free radical carriers, they may diffuse as they react with other species. This is possible up until the point where the growing PEG-DA globule becomes part of the overall network. The movement of a growing PEG-DA globule is not improbable, since the volume fraction of PEG-DA is close to the dilute transition concentration, and PEG chains are relatively mobile in water. Using the Stokes-Einstein equation, the diffusivity of PEG-DA ($R_g = 9.6$ Å)^2 in water is approximately 2.3 x 10^{-10} m^2/s. Assuming PEG-DA diffuses at 30 vol% the same as it does in water at infinite dilution, an approximate diffusion length corresponding to the average cure time (22 min) can be found with the following:

$$x = 2\sqrt{Dt}$$ (5.1)

where x is the diffusion length, D is the diffusivity of PEG, and t is time. For 1 polymer chain of PEG-DA ($M_n = 575$ g/mol), this diffusion distance after 22 min (cure time) is approximately 1.4 mm, which is on the same length scale as the width of the channel. As PEG-DA free radicals diffuse under the photomask, they will react with nearby PEG-DA end groups and begin to grow, reducing their overall mobility. This reduction in mobility can be accounted for by looking at the diffusivity of larger PEG molecules. The diffusion coefficient of PEG can be related with molecular weight with the following expression[3]:

$$D_o = 7.0x10^{-9} M_w^{-0.46}$$ (5.2)

where D_o is the diffusivity in water (m^2/s), and M_w is the molecular weight of the PEG

chain (g/mol). The relation was derived using 6 different chain lengths of PEG between

326 and 3978 g/mol. Assuming two connected PEG-DA molecules diffuse similarly to

one PEG chain of equal weight, the above relation can predict how the growing PEG-DA

macromolecules will diffuse as they gain more polymer chains. The diffusion length for

various sized PEG-DA molecules during the 22 min curing process is shown in Figure

5.3:
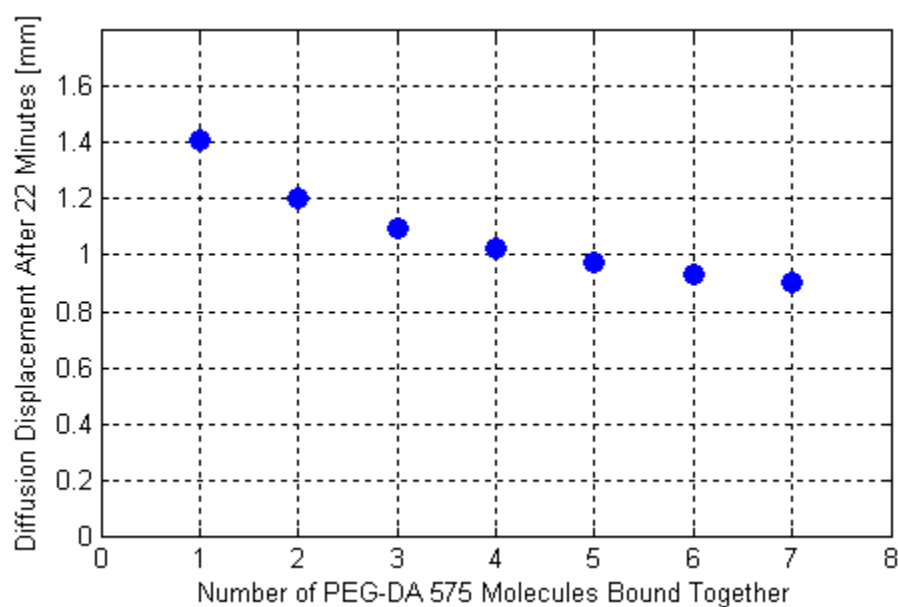
Figure 5.3: Diffusion length as a function of number of PEG-DA molecules connected together

The diffusion length for PEG scales with $M_w^{-0.23}$ and $t^{0.5}$, making reductions in

time, or increases in chain length have less of an effect on diffusion distance than one

might expect. This has large implications for channel resolution, as the diffusion length

does not decrease greatly by reducing cure time or increasing molecular weight.

Extrapolating the relation above, to reduce diffusion distance to 0.5 mm, the molecular

weight would have to exceed 50,000 g/mol with n = 88. Alternatively, to reduce the diffusion distance to 0.5 mm, the curing time would have to be reduced to 2.8 min.

The channel resolution ultimately depends on whether or not the network polymer extends under the photomask enough to combine with the other side and block the channel. The above analysis gives weight to notion that free radical species exist under the photomask, and contribute to the channel overcuring. The mechanisms of this process would have to be examined further, including the evaluation of kinetic parameters to determine the minimum channel resolution more precisely.

Given the limitations of channel resolution using a photomask, a second method of imprinting a channel using a thin wire was developed. This method has some immediate disadvantages from the photomask in that only linear channels can be made. For the purposes of this thesis, being limited to linear channels was not an issue. The method uses a 500 μm diameter wire which is placed between the slides of the device with the PEG-DA water solution. The wire is present during curing, and is removed immediately afterwards. This method proved to be effective and produced channel widths with minimal variability.

5.3 Diffusion in the Microfluidic Device

The second result of this thesis is the development of a procedure to measure diffusion coefficients of dyes in a hydrogel. The following is the procedure developed and applied to various dyes.

5.3.1 Hydrogel Calibration Curve

Slabs of hydrogel were fabricated and placed in various concentrations of dye as described in Chapter 3.3.3. Images of these slabs were taken by a digital microscope and imported into MATLAB. They were processed using a homemade MATLAB script (See Appendix 4). The script took a section of the photograph free of edges or other defects, and calculated the average of the red, green, and blue, components for each picture. The grayscale component for each picture was also calculated using the national television system committee (NTSC) algorithm:

$$GS = 0.299 * R + 0.587 * G + 0.114 * B \qquad\qquad (5.3)$$

where *GS* is the grayscale value and *R*, *G*, and *B* are the red, green, and blue components of the color picture respectively.

These intensity values were plotted against the concentration of the dyed solution multiplied by the slab's thickness. The slabs were about 1.2 mm thick, however, a small variation in slab thickness was present; multiplying the concentration by the measured slab thickness takes this into account. For methylene blue the relationships between red, green, blue, and grayscale intensity versus solution concentration are shown in Figure 5.4.
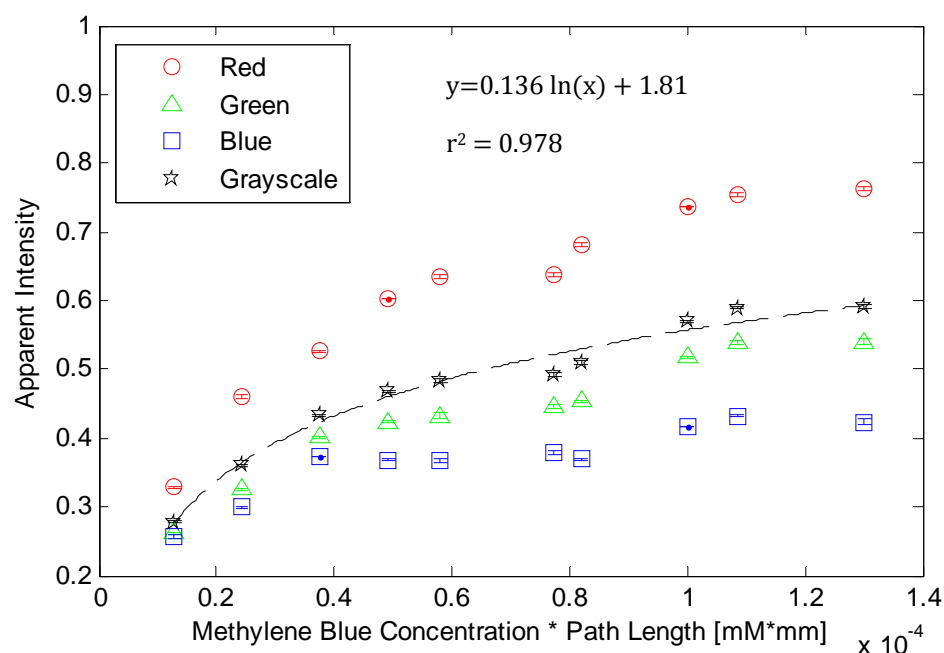
Figure 5.4: Intensity versus concentration and path length for methylene blue.

The data in Figure 5.4 shows the component intensity is generally not a linear function of concentration in the PEG-DA hydrogel. At low dye concentrations, there was a high sensitivity to concentration resulting in a steep part of the curve, while at higher concentrations this was less so. The nonlinear sensitivity of the hydrogel slab to concentration may be related to the hydrogel's cloudy swollen appearance, which affects the transmittance of light.

Digital photography has been used to determine the concentration of analytical species. Both linear[4] and logarithmic functions[5] between concentration and intensity have been observed. The trend between intensity, I, and the mathematical product of solution concentration and slab thickness (path length), x, was approximated by a logarithmic function shown in Equation (4.4) below. This empirical correlation allows

one to connect information collected via digital microscopy, i.e. image intensity or

'darkness', to actual dye concentration in the hydrogel. This is necessary because the

driving force for diffusion is a gradient in concentration, not image intensity.

$$I = a \ln(x) + b \tag{5.4}$$

The fit for the empirical relationship between image intensity and concentration

was relatively good ($r^2 > 0.95$), and was used to correlate grayscale intensity to

concentration in microfluidic devices. Calibration curves were taken in multiple lighting

conditions, and remained the same. In all cases, a logarithmic relationship was found to

fit the data well with correlation coefficients above 0.95. The brightness of the pictures

was held constant by allowing the digital microscope to calibrate an exposure time to a

reference object. Measures were taken to reduce variability due to lighting. These

measures included taking advantage of full room lighting, as well as the use of a 100 W

light illuminating the hydrogel slabs at an angle. Some different values for for

parameters a and b in equation 4.4 for methylene blue in hydrogel slabs are presented in

Table 5.1 below:

Table 5.1: Parameters found for Eq. (4.4) under various conditions

Exposure [ns]	Use of 100 W lamp	a	b	r^2
514.6	Yes	0.18	1.4	0.99
400.0	No	0.092	1.4	0.95
300.0	Yes	0.14	1.8	0.98

The same procedure was carried out for rhodamine 6G in hydrogel slabs. The relationship between intensity and solution concentration for red, green, blue, and grayscale components are shown in Figure 5.5.
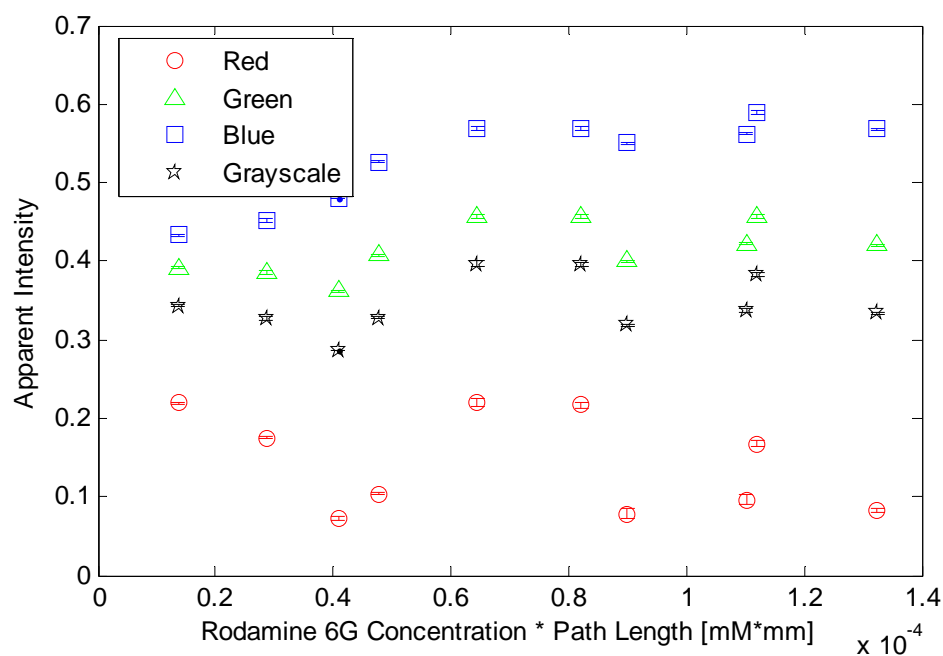
Figure 5.5: Intensity versus concentration and path length for rhodamine 6G.

The red, green, and blue, and grayscale components for rhodamine 6G are not indicative of the concentration of dye in solution. Alternate colormaps were examined including the hue, saturation, and value (HSV) colormap. The relationships between hue, saturation, and value to rhodamine 6G concentration are presented in Figure 5.6:
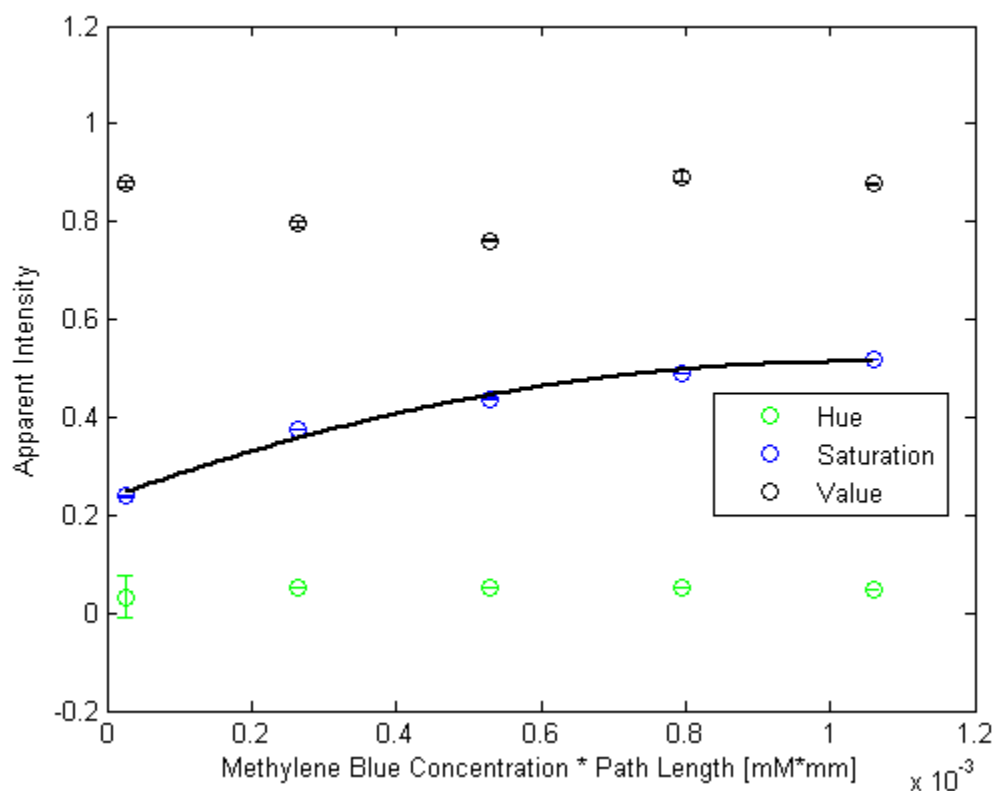
Figure 5.6: Hue, saturation, and value intensity versus concentration and path length for

rhodamine 6G.

In Figure 5.6, the saturation component of the HSV colormap shows a good trend

with rhodamine 6G concentration. A logarithmic function, Equation (5.4), was used to fit

the data; r^2 values were greater than 0.97. The values for a and b for a few different

lighting situations are presented in Table 5.2.

Table 5.2: Constants used in the empirical equation relating image intensity to rhodamine 6G concentration

Exposure [ns]	a	b	r^2
250	0.067	0.93	0.95
400	0.074	1.0	0.98

The relationship between saturation intensity and rhodamine 6G concentration is similar to that for methylene blue. There is a higher sensitivity of saturation value at low rhodamine 6G concentrations; this was less so at higher concentrations. The empirical relationship was used for converting the intensity values in digital images to concentration values.

A calibration curve was created for crystal violet. The curve is presented in Figure 5.7 below. The coefficients of the logarithmic fit are presented in Table 5.3 below.

Table 5.3: Constants used in the empirical equation relating image intensity to crystal violet concentration

Exposure [ns]	a	b	r^2
400	0.14	2.1	0.99
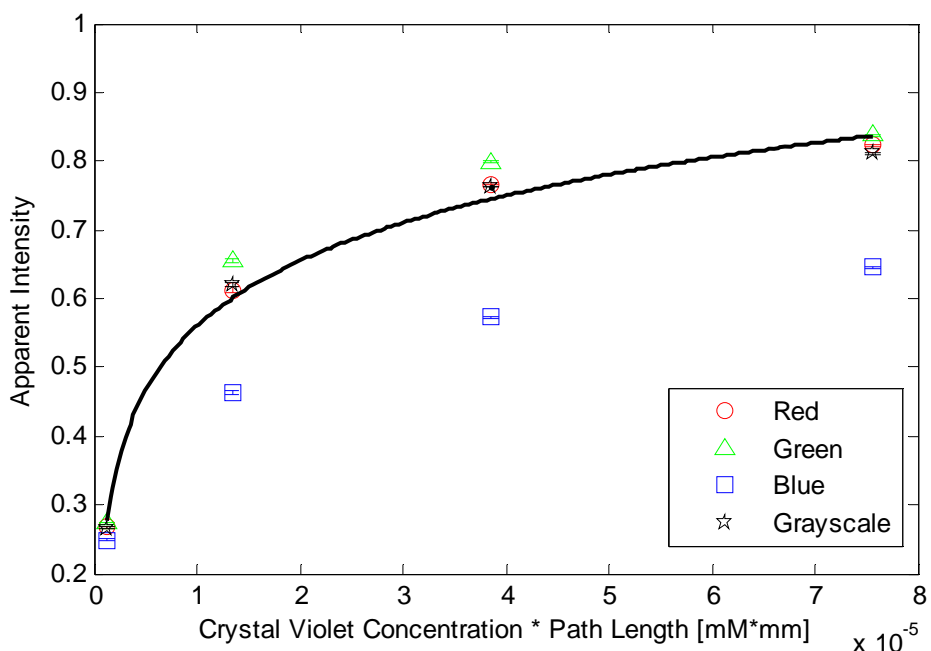
Figure 5.7: Red, green, blue and grayscale components versus concentration and path length for crystal
violet.

5.3.2 Diffusion Data Analysis

The data analysis was carried out using custom MATLAB scripts (see A4). First,
the color levels in the digital images were correlated to concentration levels using a
calibration curve. Second, the concentration distributions were then compared to
theoretical models to extract diffusion coefficients.

The similarity variable penetration solution carries along multiple assumptions,
however, it also fits the data relatively well. Examples of the model being regressed
against the data are shown in Figures 5.8 and 5.9 below.
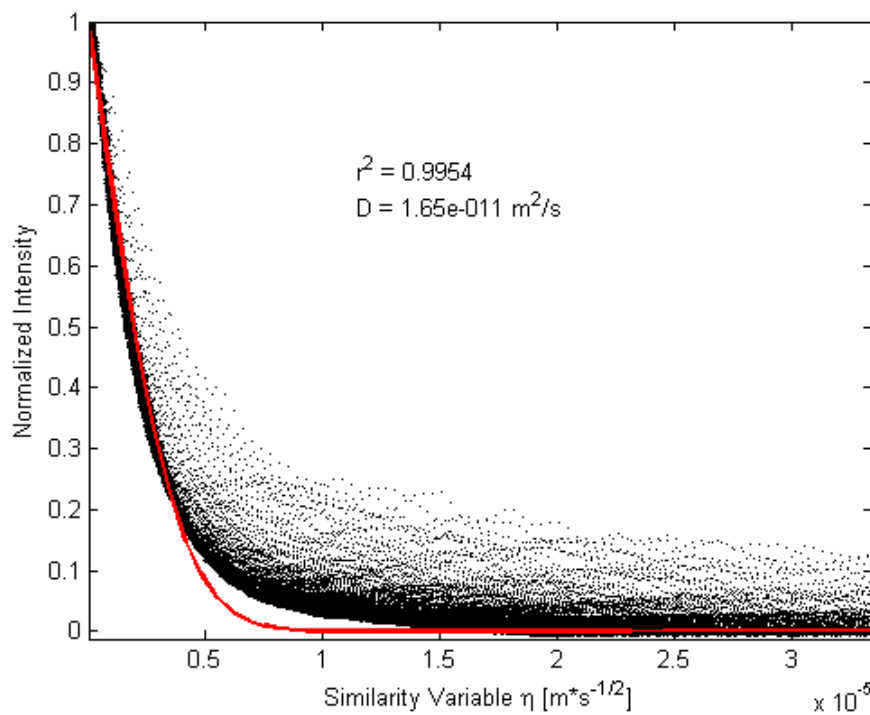
Figure 5.8: Example of the regression of data against equation. Data shown for *t* > 5 min
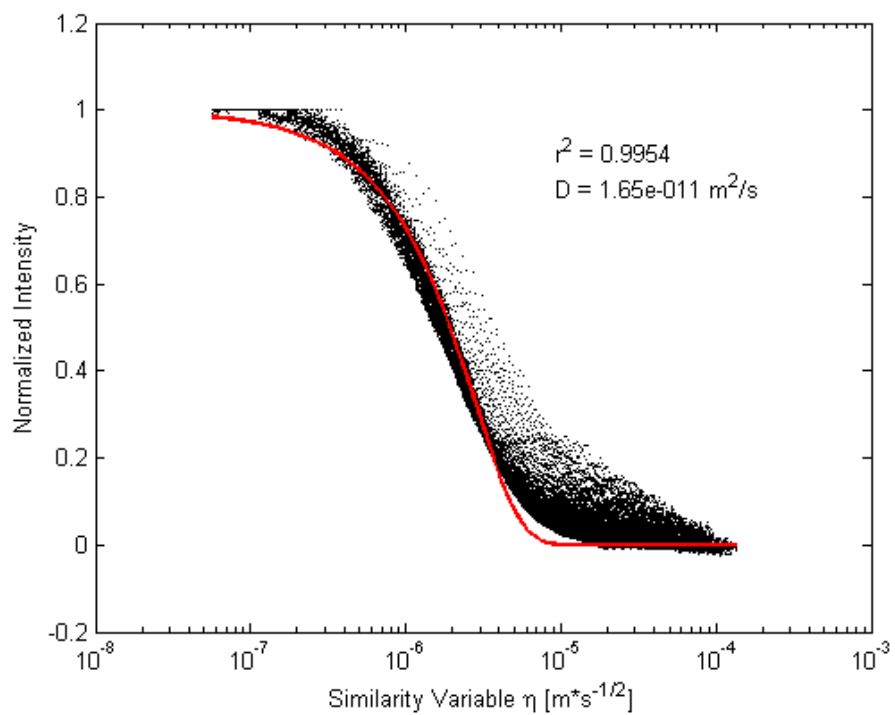
Figure 5.9: Log plot of regression shown in Figure 5.8. Data shown for *t* > 5 min.

The applicability of the use of the similarity variable is supported by the data collapsing reasonably well onto a single line. The scatter present in Figure 5.8 and Figure 5.9 is almost always associated with shorter timescales where inaccuracies in starting time and channel boundary location are amplified in the similarity variable. The majority of the scatter also occurs within about 20 % of the baseline, which may be due to noise.

Another method of examining the data collected to verify that it follows normal Fickian behavior is to plot the total solute uptake, M_t, and time, t, on a log-log plot and evaluate the slope. If the slope is 0.5, the diffusion behavior is Fickian. The diffusion parameter can also be determined from this plot. An example of the relationship between M_t and time is shown in Figure 5.10.
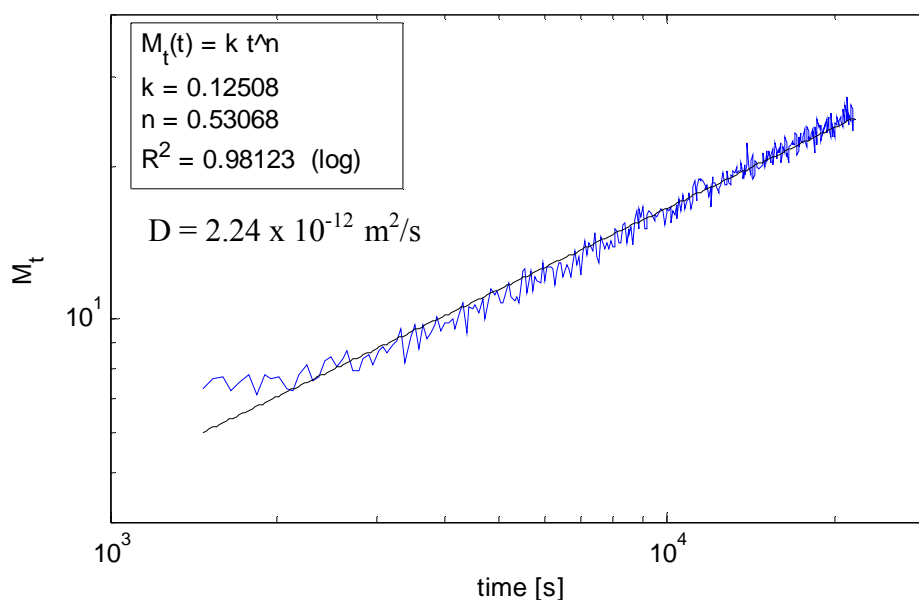
Figure 5.10: An example log-log plot of total solute diffused (M_t) vs. time

The model works well for describing the overall apparent diffusivity of methylene

blue.

5.3.3 Dye Diffusivity Results

The results of different trials of methylene blue diffusing through PEG-DA are

shown in Table 5.4:

Table 5.4: Results of methylene blue diffusion analysis

		$\frac{C}{C_0} = erfc\left(\frac{\eta}{\sqrt{D}}\right)$			$M_t(t) = \frac{C_0}{\sqrt{\pi}} 2\sqrt{D}t^n$	
Device	Side	D x 10^{-11} [m^2/s]	r^2	n	D x 10^{-11} [m^2/s]	r^2
D 60	L	0.68	0.989	0.39	1.3	0.980
	R	1.46	0.942	0.50	1.2	0.982
D 61	L	0.58	0.990	0.48	2.5	0.985
	R	1.10	0.991	0.46	3.4	0.993
D 62	L	2.86	0.995	0.47	4.6	0.989
	R	1.65	0.992	0.50	1.6	0.990
D 63	L	1.39	0.994	0.45	3.9	0.993
	R	4.02	0.974	0.35	48	0.997

The methylene blue diffusiviy was found to be reproducible and gave a mean

value of (1.71 ± 0.15) x 10^{-11} m^2/s using the complementary errorfunction model, and

(2.6 ± 0.2) x 10^{-11} m^2/s using the power law model. The diffusion coefficient determined

from the two models were not statistically different (α=0.05).

The results of the Rhodamine 6G diffusion experiments are presented below in

Table 5.5.

Table 5.5 Results of rhodamine 6G diffusion analysis

		$\frac{C}{C_0} = erfc\left(\frac{\eta}{\sqrt{D}}\right)$			$M_t(t) = \frac{C_0}{\sqrt{\pi}} 2\sqrt{D} t^n$	
Device	Side	D x 10^{-12} [m^2/s]	r^2	n	D x 10^{-12} [m^2/s]	r^2
D 64	L	4.41	0.982	0.52	2.20	0.951
	R	3.43	0.989	0.57	0.76	0.962
D 65	L	5.09	0.981	0.67	2.10	0.975
	R	5.19	0.973	0.48	5.86	0.970
D 66	L	4.90	0.984	0.52	2.78	0.983
	R	5.91	0.977	0.53	2.61	0.985
D 67	L	4.80	0.973	0.55	1.68	0.985
	R	5.37	0.981	0.53	2.38	0.986

The complementary errorfunction model gave a diffusivity value of

(4.89 ± 0.09) x 10^{-12} m^2/s for rhodamine 6g in the hydrogel as measured by the

microfluidic device. The power law model gave a diffusivity value of (2.5 ± 0.2) x

10^{-12} m^2/s. There was a statistically significant difference between the two diffusivities, although they are quite similar.

The crystal violet diffusion results are presented in Table 5.6. The complementary errorfunction gave diffusivity values of (4.7 ± 0.2) x 10^{-12} m^2/s while the power law model gave values of (5.1 ± 0.7) x 10^{-14} m^2/s. The high value for n in the power law model suggests that the diffusive mechanism for crystal violet is non-Fickian, and the diffusion coefficient reported by the power law should be regarded with skepticism. The complementary errorfunction model did report a consistent diffusivity for crystal violet, however, the model's overall fit was not as good as it was with rhodamine 6G or methylene blue. A typical fit for the complementary error function model can be seen in Table 5.9 below. These factors suggest that a more complex diffusion process is occurring for crystal violet in the PEG-DA hydrogel.

Table 5.6: Results of crystal violet diffusion analysis

Device	Side	$\dfrac{C}{C_0} = erfc\left(\dfrac{\eta}{\sqrt{D}}\right)$			$M_t(t) = \dfrac{C_0}{\sqrt{\pi}} 2\sqrt{D}t^n$	
		D x 10^{-12} [m^2/s]	r^2	n	D x 10^{-13} [m^2/s]	r^2
D 68	L	6.53	0.972	0.72	0.809	0.999
	R	7.27	0.964	0.68	1.90	0.998
D 70	L	4.91	0.976	0.69	0.246	0.999
	R	1.99	0.945	0.86	0.152	0.997
D 71	L	3.66	0.975	0.71	0.554	0.993
	R	4.60	0.941	0.71	0.32	0.997
D 72	L	4.06	0.977	0.81	0.0844	0.997
	R	4.22	0.887	0.87	0.0269	0.986
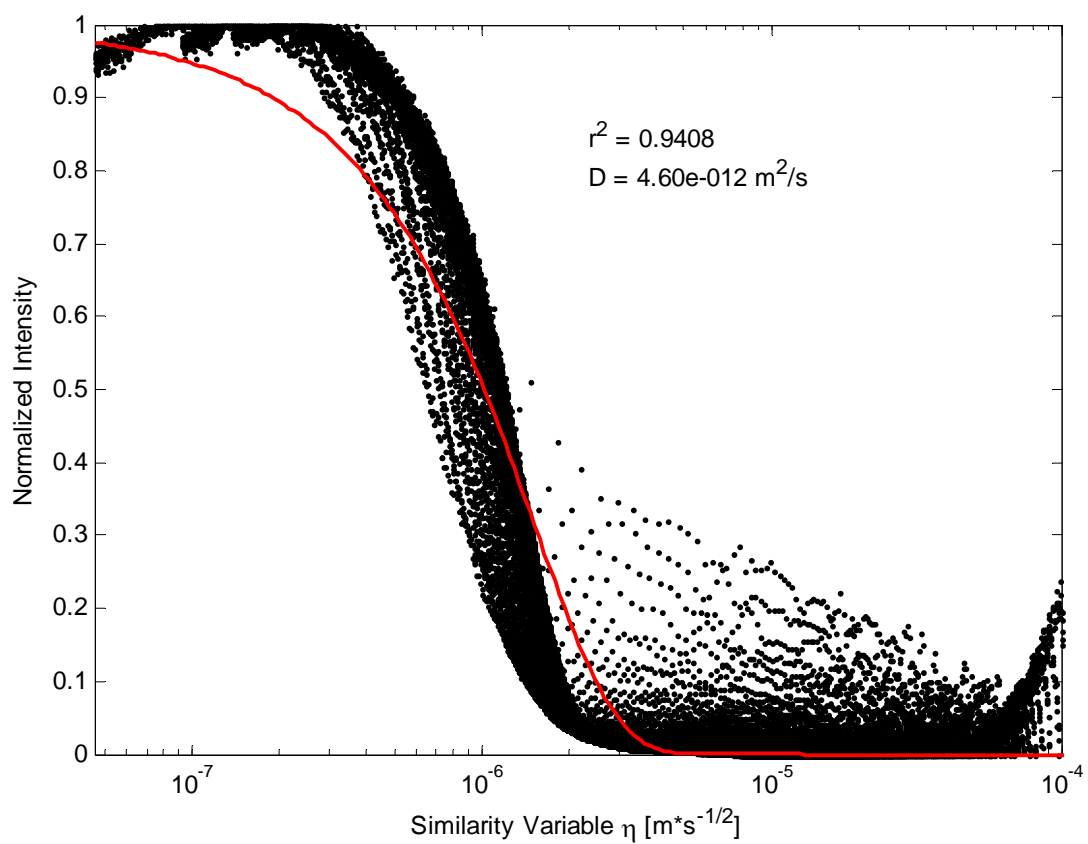
Figure 5.11: Complementary error function model and crystal violet diffusion data

The diffusion results for the three dyes can be summarized with Table 5.7 The diffusivities reported for rhodamine 6G and crystal violet from the complementary errorfunction model are not statistically different ($\alpha = 0.05$).

Table 5.7: Summary of diffusivity values obtained using the microfluidic method

	Diffusion coefficient x 10^{-12} [m^2/s]	
Solute	Complementary error function	Power law model
Methylene blue	17.1 ± 1.5	26 ± 2
Rhodamine 6G	4.89 ± 0.09	2.5 ± 0.2
Crystal violet	4.7 ± 0.2	--

5.4 NMR Results

5.4.1 Spectroscopy and peak assignments

In order to apply nuclear magnetic resonance (NMR) diffusometry techniques, a thorough evaluation and identification of ^{1}HNMR spectrum peaks for the chemicals involved was carried out. De-ionized water (DI-H$_2$O) was widely used as the solvent in order to mimic the conditions found in the hydrogel, although a few spectra were taken in D$_2$O. Spectra were taken using a water suppression pulse sequence to reduce the impact of the large water peak on the rest of the spectra. The water suppression sequence reduced the magnitude of the water peak by at least an order of magnitude. Once spectra were taken, peaks were assigned and compared with those found in the literature. The identification of the peaks for various species was especially necessary to identify dyes in the PEG-DA hydrogel environment.

The ^{1}HNMR spectrum and identification of peaks for pure, uncured PEG-DA is shown in Figure 5.12. The ^{1}HNMR spectrum of PEG-DA was taken without using a solvent. The peak assignments agree with those found in the literature.[6]
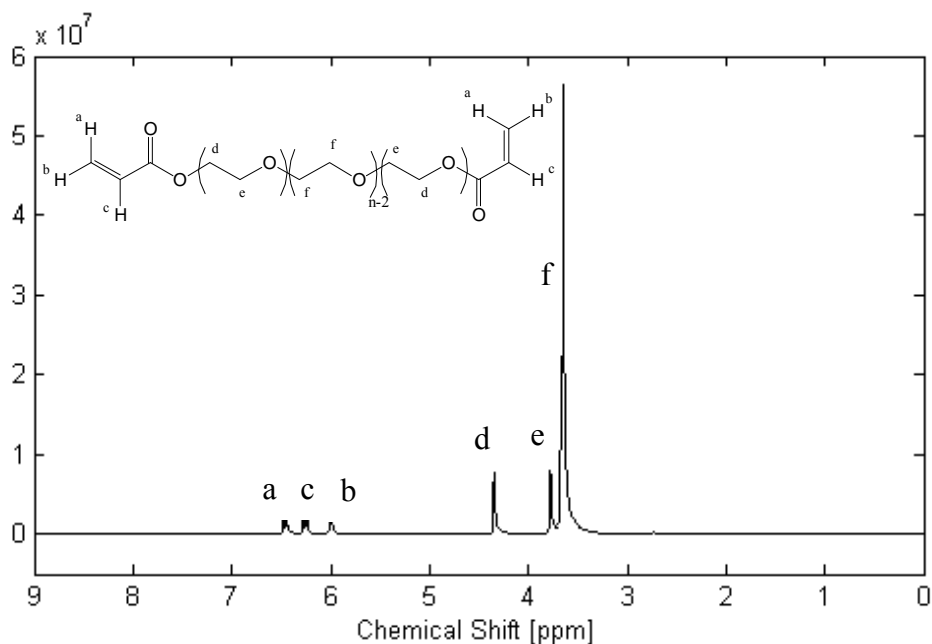
Figure 5.12: ^{1}H-NMR spectrum of uncured dry PEG-DA

The spectrum and peak identification for cured 30 vol% PEG-DA in water are shown in Figure 5.13. Several differences between the cured and uncured spectra of PEG-DA confirm that a crosslinked hydrogel network has formed. First, the vinyl group peaks have essentially disappeared, and aliphatic CH_2 peaks have appeared. This indicates a high conversion of double bonds to single bonds. Second, the CH_2-O backbone peak has broadened. This broadening indicates the movement of PEG chains is more restricted and is indicative of a more solid like environment.
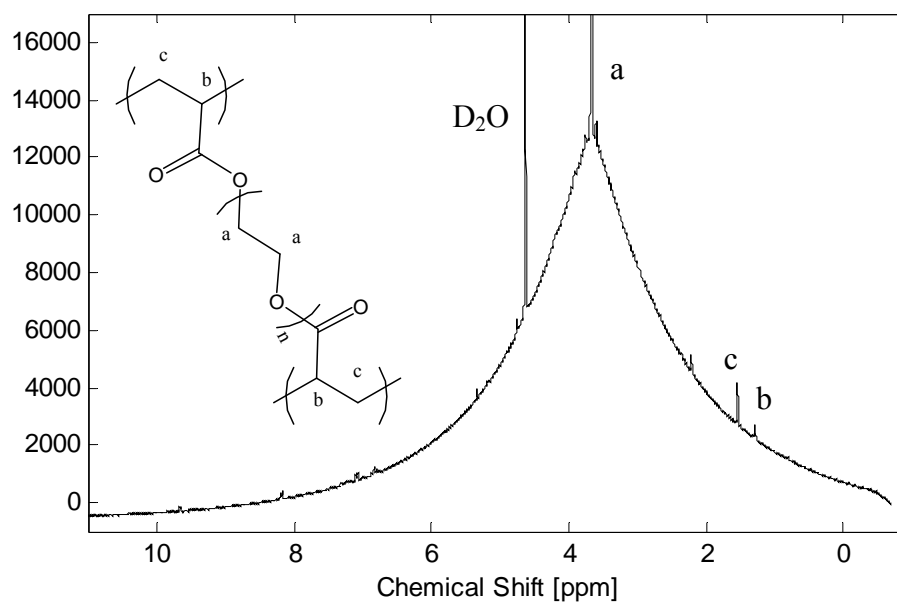
Figure 5.13: ^{1}H-NMR spectrum of cured PEG-DA in D_2O

The ^{1}HNMR spectrum and identified peaks for methylene blue is shown in Figure 5.14. The spectrum is characterized by two large peaks in the 3-4 ppm range, as well as three small aromatic peaks near 7 ppm.

The peak identification for a ^{1}HNMR spectrum of rhodamine 6G is shown in Figure 5.15. The peak assignments agree with those found in the literature.[7] The same was done for crystal violet. The spectrum of crystal violet is presented in Figure 5.16 below.
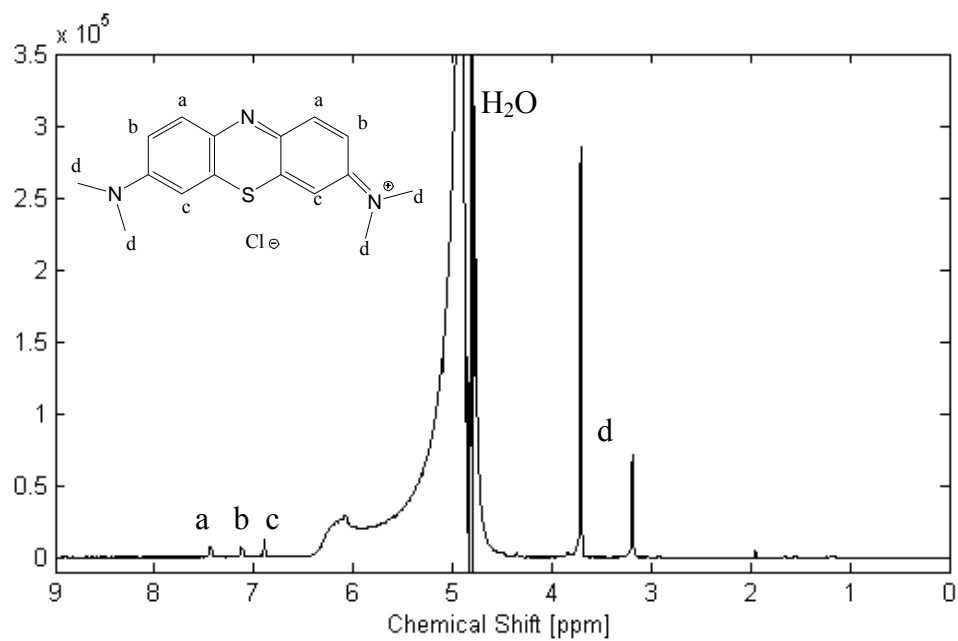
Figure 5.14: ^{1}H-NMR spectrum of methylene blue in H_2O
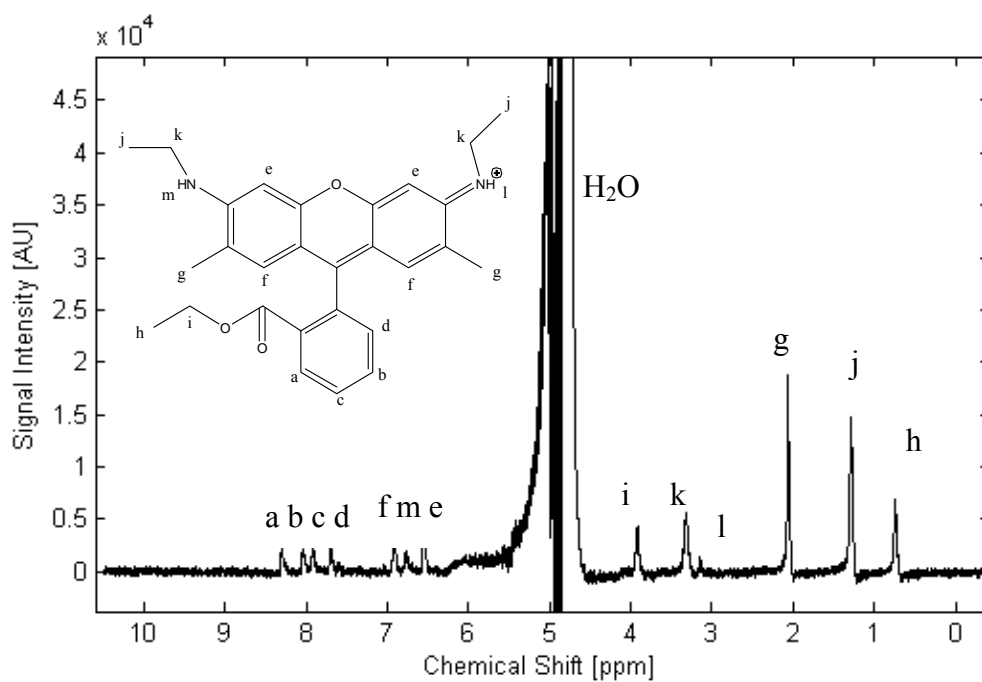
Figure 5.15: ^{1}H-NMR spectrum of rhodamine 6G in H_2O
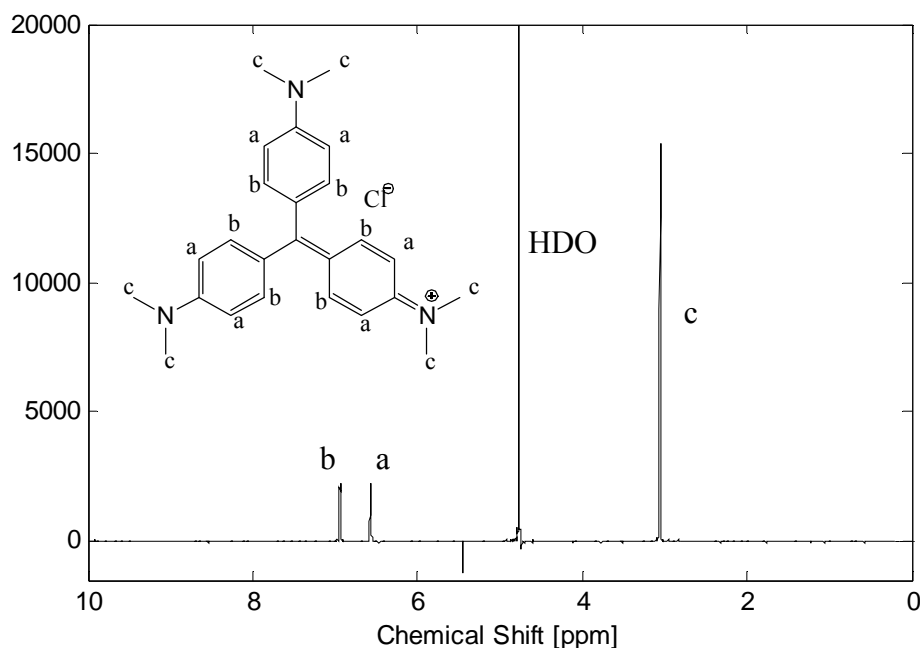
Figure 5.16: ^{1}H-NMR spectrum of crystal violet in D_2O

5.4.2 Free diffusion in water

A high concentration of solute was used to measure the free diffusion of the solutes in water with NMR. A water suppression pulse sequence was grafted onto a standard pulsed field gradient experiment to achieve higher peak resolutions. The experiment gave values for the free diffusion of methylene blue in water at a concentration of 34 mM.

A PFG experiment was carried out on methylene blue in water. The attenuation of peak intensities can describe the diffusivities of the system. The results for the individual

methylene blue peaks are summarized in Table 5.8. The labeled peaks correspond to those in Figure 5.14.

Table 5.8: Summary of methylene blue in water PFG analysis

Peak	D x 10^{-10} [m^2/s]
a	1.43 ± 0.03
b	1.60 ± 0.04
c	1.58 ± 0.05
d	1.46 ± 0.02
All	1.52 ± 0.02

A plot of the logarithm of relative peak intensities, $ln(S/S_0)$, vs. $(\gamma g \delta)^2 (\Delta - \delta/3)$ yields a linear trend, as shown in Figure 5.17. The slope of this trend is used to find the diffusion coefficient. The error was calculated using the following expression for the standard deviation of the slope of a line[8]:

$$ e = \sqrt{\frac{\sum_i (y_i - \hat{y}_i)^2}{(n-2)\sum_i (x_i - \bar{x})^2}} $$

where e is the standard deviation of the slope of a regressed line, y_i is the y value for point i in the dataset, $\hat{y}_i$ is the predicted value for point i, n is the number of samples, x_i is the x value for point i, and $\bar{x}$ is the mean of the x values in the dataset. The individual peak analysis provides a relatively coherent picture of the diffusivity of the species. Plotting all the data on one plot, as shown in Figure 5.17 shows the good agreement. A

global fit carried out on all methylene blue peak attenuation data gives a diffusivity value of 1.52 ± 0.02 x 10^{-10} m^2/s for methylene blue in water.
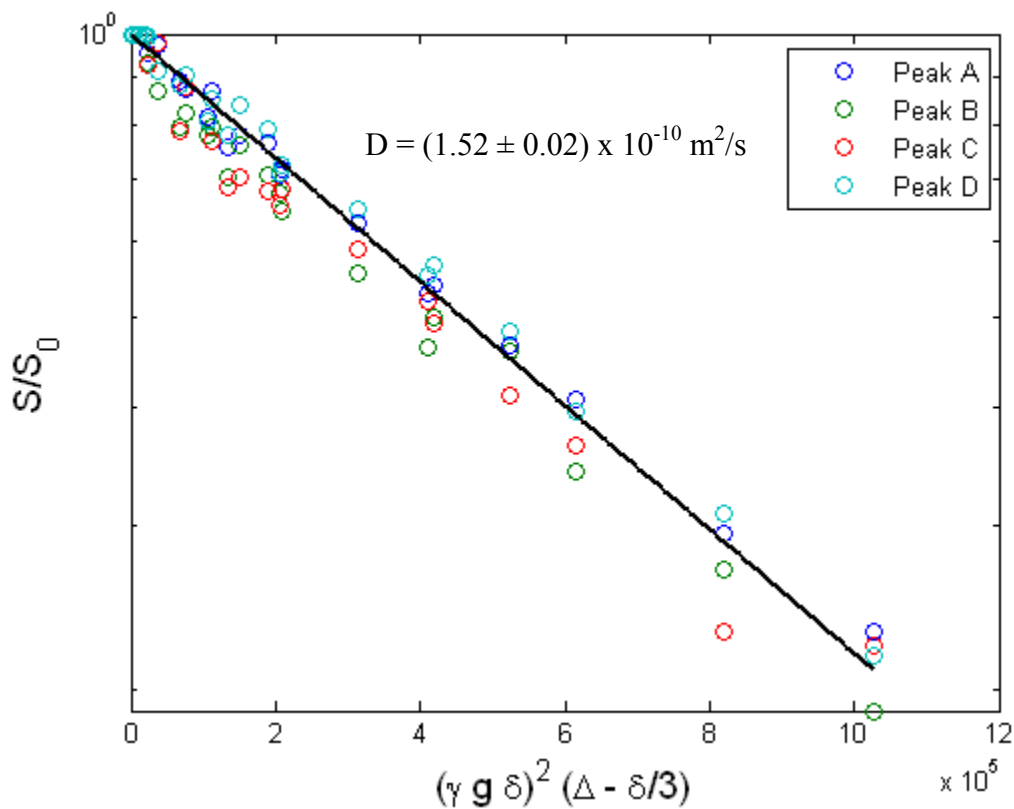
Figure 5.17: PFG plot for methylene blue in water

A PFG experiment was carried out on a sample of rhodamine 6G in water. The results of the individual peak analyses are summarized in Table 5.9 :

Table 5.9 Summary of rhodamine 6G in water PFG analysis

Peak	D x 10^{-11} [m^2/s]
a	1.70 ± 0.06
b	1.6 ± 0.1
c	1.78 ± 0.06
d	1.8 ± 0.1
f	1.62 ± 0.06
m	2.46 ± 0.15
e	1.73 ± 0.06
i	1.67 ± 0.05
k	1.68 ± 0.04
l	1.1 ± 0.4
g	1.79 ± 0.05
j	1.77 ± 0.07
h	1.92 ± 0.07
All	2.464 ± 0.007

The data can be plotted showing *ln*(S/S_0) for rhodamine 6G peaks, shown in Figure 5.18. Peaks *l* and *m* were not included in the global fit as they had high signal to noise ratios and did not fit with the trend of the rest of the data.
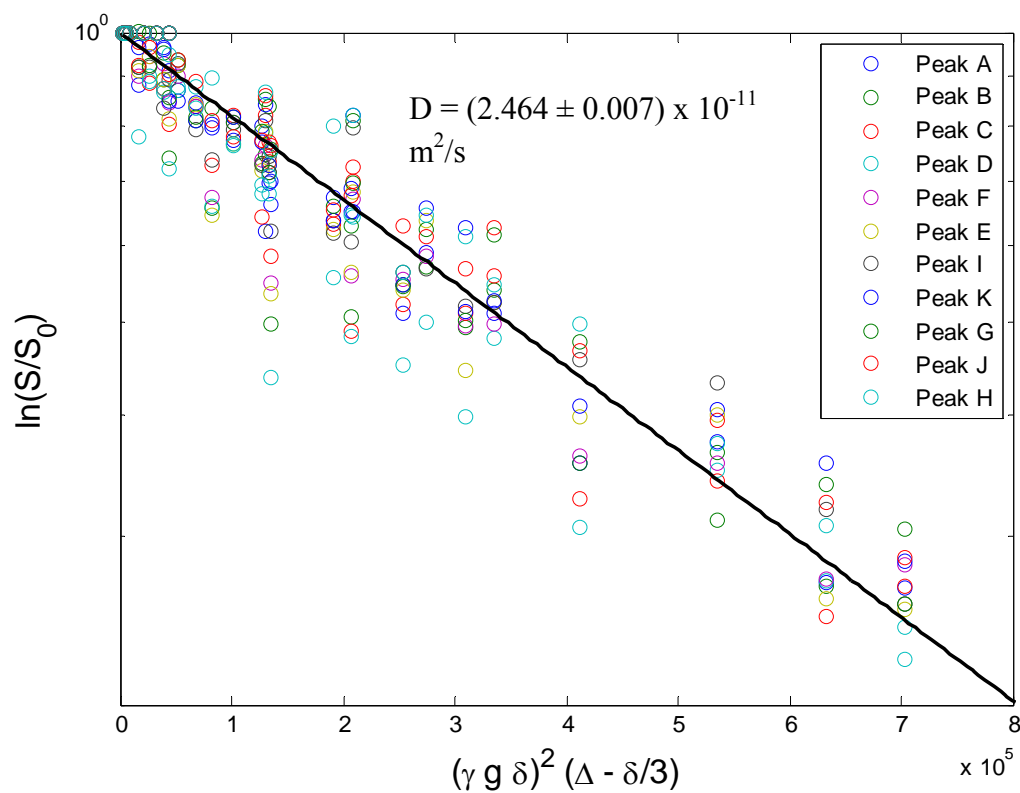
Figure 5.18: Combined PFG plot for rhodamine 6G peaks in water

A PFG experiment was performed on crystal violet in water. The diffusivities for the three peaks are reported in Table 5.10.

Table 5.10: Summary of crystal violet in water PFG analysis

Peak	D x 10^{-10} [m2/s]
a	2.3 ± 0.3
b	3.2 ± 0.1
c	2.9 ± 0.1
All	2.93 ± 0.07
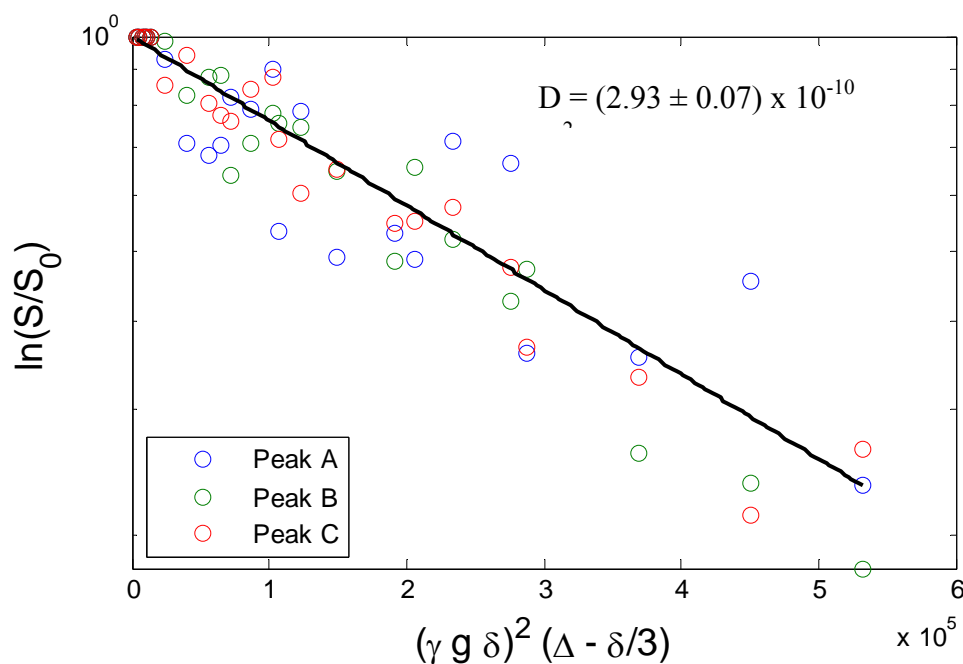
Figure 5.19: Combined PFG plot for crystal violet peaks in water

A summary of the diffusivity values, along with those predicted by the Stokes-Einstein and the Nernst-Haskell models for the three dyes are presented in Table 5.11. The Stokes-Einstein Equation assumes a spherical geometry calculated from the molecular molar volume. The Nernst-Haskell Equation takes into account the ionic nature of the dyes and that local charge neutrality must be obeyed. According to the model, a compound's diffusivity lies somewhere between that of the large dye and its counter-ion. Since the counter-ion is small and can move quickly, the diffusivity of the dye will be slightly increased. Both the Stokes-Einstein and Nernst-Haskell models do not take into account a hydration layer of water, or the potential that the dyes have aggregated. The diffusivities of methylene blue and crystal violet are comparable to

those predicted by these models. The diffusivity of rhodamine 6G is much less than that predicted by the Stokes-Einstein equation, indicating a significant deviation from the assumptions used by the Stokes-Einstein model.

Table 5.11: Summary of diffusivities of solutes in water determined by PFG

Solute	$D \times 10^{-10}$ [m^2/s] (^{1}H-NMR)	$D \times 10^{-10}$ [m^2/s] (Stokes-Einstein)	$D \times 10^{-10}$ [m^2/s] (Nernst-Haskell)
Methylene blue	1.52 ± 0.02	5.5	8.6
Rhodamine 6G	0.2464 ± 0.0007	4.68	8.8
Crystal violet	2.93 ± 0.07	4.9	7.9

5.4.3 Diffusivities in Hydrogel

The data gathered from a PFG experiment for methylene blue in a PEG hydrogel are shown in Table 5.12. Peaks are identified with the letters used in Figure 5.14.   In Figure 5.20, we can see the diffusion coefficient for methylene blue in crosslinked PEG is approximately 3.45 x 10^{-11} m^2/s, significantly less than that for methylene blue in water.

Table 5.12: Summary of methylene blue in PEG-DA PFG analysis

Peak	D x 10^{-11} [m^2/s]
a	2.9 ± 0.2
b	4.9 ± 0.4
c	4.8 ± 0.7
d	3.7 ± 0.1
All	3.45 ± 0.02
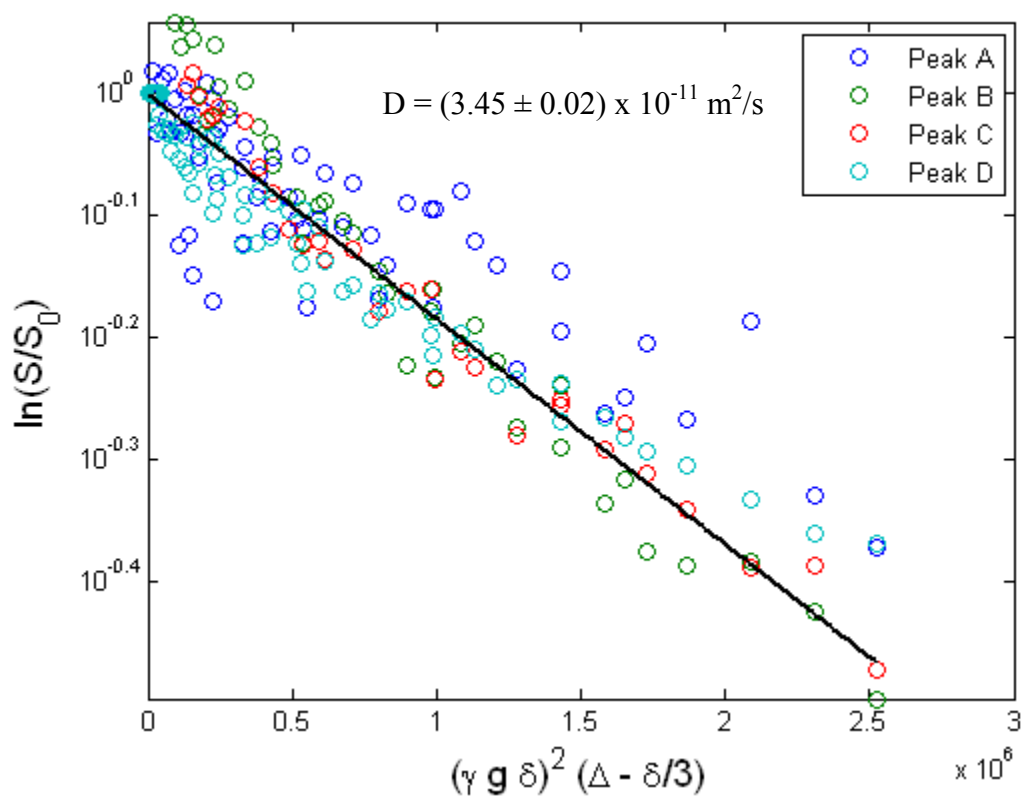
Figure 5.20: Combined PFG plot for methylene blue in PEG-DA

A comparison between the diffusivities found from the microfluidic and NMR methods is shown in Table 5.13. Diffusivity values for rhodamine 6G and crystal violet were not determined by NMR because of time constraints. The samples require time on the order of months to allow for dye to diffuse well into the hydrogel in the tube.

Table 5.13: Comaprison of diffusion coefficients in a PEG-DA hydrogel

Solute	$D \times 10^{-12}$ [m^2/s]		
	Complementary error function	Power law model	NMR
Methylene blue	(17.1 ± 1.5)	(26 ± 2)	(34.5 ± 00.2)
Rhodamine 6g	(4.89 ± 0.09)	(2.5 ± 0.2)	-
Crystal violet	(4.7 ± 0.2)	-	-

5.5 Material Properties

5.5.1 Swelling Studies

Swelling studies were carried out for hydrogel slabs. The water content of the slabs was measured by mass and volume after curing, lyophilization, and after re-swelling. The polymer fraction in the swollen state, $\upsilon_{2,s}$, for 30 vol% PEG-DA hydrogel slabs is shown in Table 5.14. The error reported is the standard deviation of multiple samples; the complete data is presented in Appendix 3.

Table 5.14: Polymer fraction from swelling studies

Condition	Volume	Mass
Cured	0.33 ± 0.01	0.32 ± 0.01
Re-swollen (2 d)	0.42 ± 0.06	0.40 ± 0.05
Re-swollen (8 d)	0.42 ± 0.06	0.43 ± 0.06

There is no statistical difference ($\alpha = 0.05$) between the polymer volume fraction determined by mass or by volume within any condition. There is a noticeable difference between water content before swelling (70 vol%) and after swelling (67 vol%). This indicates the gel excludes a small percentage (~13 %) of water immediately after curing. This agrees with cracking and shrinkage of the gel observed after curing for longer periods of time.

There is a notable increase in polymer volume fraction (or decrease in water content) between curing and re-swelling. This suggests that a population of water is trapped immediately after curing. This is a possibility due to the known high degree of PEG-water interaction. The PEG-DA hydrogel is always cloudy after curing indicating the existence of a separate phase on the length scale that can scatter light. After lyophilization, the PEG-DA slabs became clear; after rehydrating they regained some of their cloudiness, but not all of it. This suggests that water is trapped inside the gel structure and does not have the energy to escape at ambient conditions. The second implication is that water is intimately connected with the PEG-DA hydrogel's optical properties. It was also noted that two water peaks were present on multiple NMR

spectra of cured PEG-DA hydrogels. An example of this is shown in Figure 5.21. The
two peaks could correspond to water existing in two distinct environments in the
hydrogel. What is interesting is that the

The polymer volume fraction can be used to determine other important properties
like molecular weight between crosslinking and mesh size.
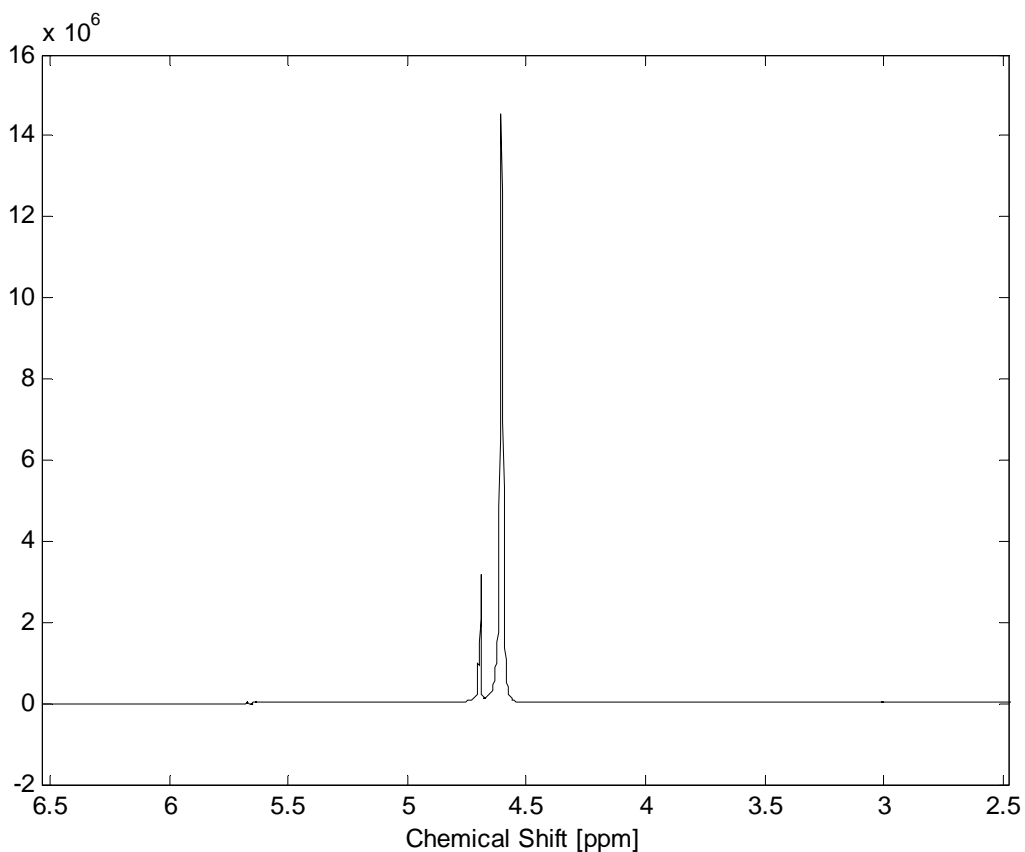
Figure 5.21: Dual water peaks present in cured PEG-DA hydrogel. ^{1}H-NMR Spectra taken in water.

5.5.2 Dynamic Mechanical Analysis

Dynamic Mechanical Analysis (DMA) was performed to determined material
properties, specifically, the shear modulus G. The test was performed while the gel was

swollen. Petroleum gel was used to coat the sample to make sure it did not dehydrate.
The sample was tested over a range of frequencies. The results are shown in Figure 5.22
below. The important results are first that the solid-like component of the shear modulus
is much larger (1 – 2 orders of magnitude) than the liquid-like component. Second, the
solid-like component of the shear modulus is relatively constant over two orders of
magnitude of oscillation frequency. The value of the shear modulus was taken to be 5.5 x
10^5 Pa.
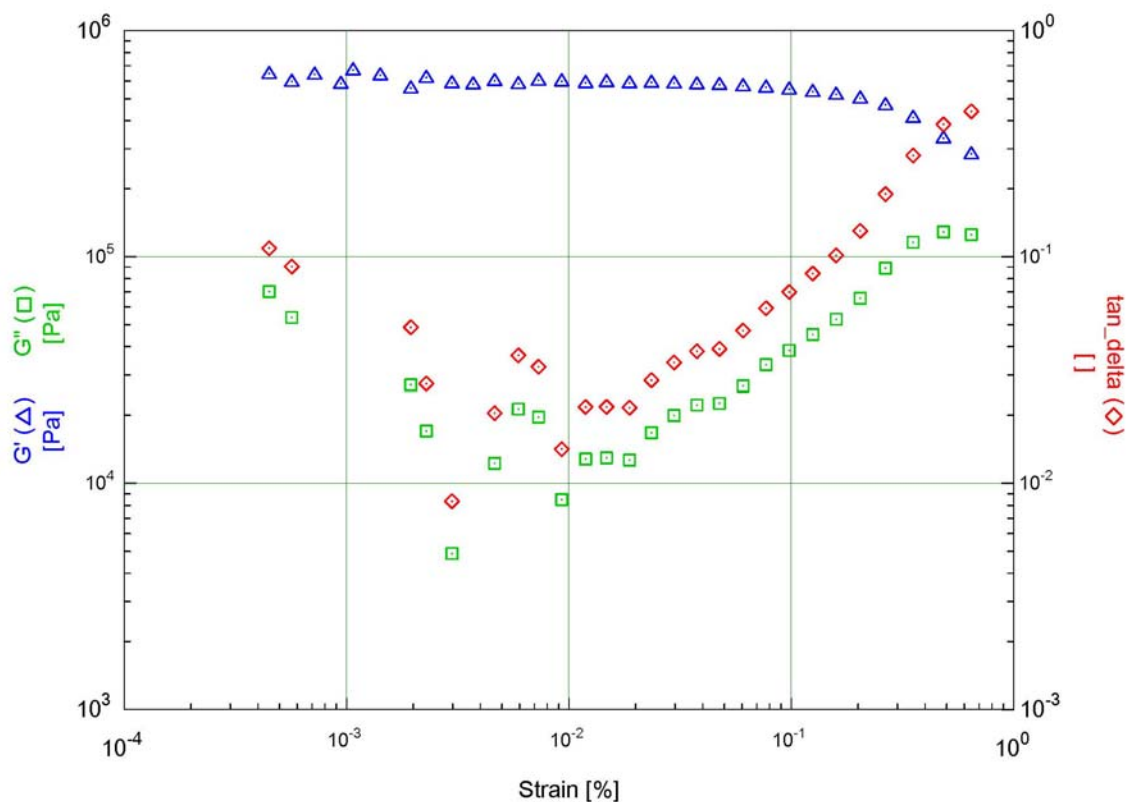
Figure 5.22: DMA analysis of the crosslinked PEG hydrogel slab

This value can be used to calculate a molecular weight between crosslinks, M_c. Using

Equation 2.6, $M_c \approx 270$ g/mol. This value is close to the value of $M_n/2 = 287$ g/mol.

This shows that the gel behaves close to an ideal model.

5.6 References

1. Mayo, D. *Calcium Alginate Encapsulation and Continuous Separation of the capsules through co-laminar flow of the Immiscible Fluids;* Bucknell University: 2008.

2. Amsden, B. *Macromolecules* **1998***, 23,* 8382-8395.

3. Johansson, L.; Skantze, U.; Loefroth, J. E. *Macromolecules* **1991***, 22,* 6019-6023.

4. Tantemsapya, N.; Meegoda, J. N. *Environ. Sci. Technol.* **2004***, 14,* 3950-3957.

5. Teasdale, P. R.; Hayward, S.; Davison, W. *Anal. Chem.* **1999***, 11,* 2186-2191.

6. Lin, H.; Kai, T.; Freeman, B. D.; Kalakkunnath, S.; Kalikas, D. S. *Macromolecules* **2005***, 20,* 8381-8393.

7. Ramos, S.; Vilhena, A.; Santos, L.; Almeida, P. *Magn. Reson. Chem.* **2000***, 6,* 475-478.

8. Devore, J. L.; Farnum, N. R. *Applied statistics for engineers and scientists;* Thomson Brooks/Cole: 2005.

Conclusions

The work performed in this thesis accomplished several goals. Most importantly, a new method was created to measure diffusion in hydrogels. The method employed a microfluidic device with novel features to evaluate the diffusivities of optically active solutes in a hydrogel polymer network. This method is, to the author's knowledge, a new contribution to the field of diffusometry. Advantages of the developed method are that it is noninvasive and does not require expensive equipment.

The fabrication of the device was optimized and limitations were evaluated. The minimum channel resolution of ~500 μm was determined to be caused by PEG-DA radicals diffusing under the photomask to react with other PEG-DA species. Physical properties of the hydrogel were evaluated to determine structural parameters of the hydrogel.
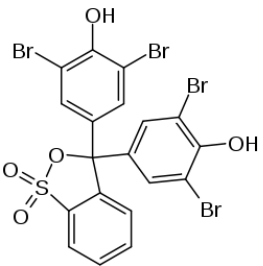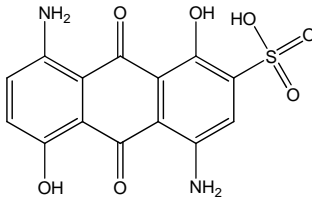
Data analysis and processing procedures were developed to determine diffusion coefficients from optical information. Two models were used to evaluate the diffusion coefficient and quantified how ideal or "Fickian" the diffusion behavior was. The diffusion coefficients of three dyes (methylene blue, rhodamine 6G, and crystal violet) in a hydrogel network were measured using the microfluidic device.
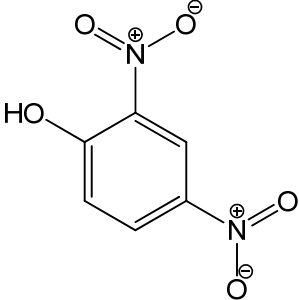
Diffusion coefficients for the dyes in water were found using NMR diffusometry methods. The same methods were used to find diffusion coefficients for the dyes in hydrogels, providing a verification of the microfluidic method. The diffusion coefficient results from the NMR method agree with those collected using the microfluidic method.

Future Directions

The procedures outlined in this research could be used to quantify the diffusive behavior of any optically active solute in a hydrogel. Dyes of different size and charge could be investigated. This includes cationic and anionic dyes. This thesis studied three cationic dyes and one anionic dye for 30 vol% PEG-DA (M_n = 575) in water. More work could be done to investigate anionic dyes, or cationic dyes outside the size range already studied. Some potential water soluble dyes that could be studied are included in Table 7.1.

Table 7.1: Potential solutes to investigate using the microfluidic device

Name	Structure	M_w [g/mol]	Molecular volume [Å^3]	Anionic / Cationic
Bromophenol Blue		670	360.5	-
Acid Blue 43		351	264	-

Sulfur Black 1		184	139	Zwitterionic

The device could be used with fluorescent microscopy to monitor the diffusion of fluorescing solutes. For the PEG-DA hydrogel system, the molecular weight of the polymer and water volume fraction could be systematically varied to determine their relationship with solute diffusivity. Swelling studies performed on the different hydrogels would complement this investigation. The data gathered from such a study would be able to verify hindered diffusion models available in the literature. Insights gained from gathering diffusion data could be used to formulate new models of hindered diffusion that account for variables like polymer-solute interactions, ionic charge, or other factors.

More advanced NMR techniques could be used to examine transport in the PEG-DA hydrogel. Preliminary investigations indicate a time-dependent diffusivity is present for certain species in the PEG-DA hydrogel. This indicates a tortuous network is present. Solutes that have high NMR signals could be used as probes for this hydrogel structure. NMR diffusometry could be applied to isotopes other than hydrogen; nitrogen, phosphorous, or other elements that are magnetically susceptible could be used as probes

in the hydrogel. This would be advantageous because the spectra for the gel is usually crowded and obscures solute peaks readily.

The analytical methodology developed in this research is by no means perfect. The largest source of inaccuracy comes from the empirical correlation between solute concentration in the hydrogel and intensity values from the digital microscope. A study to improve the accuracy of the calibration curve should be carried out. Image colormap information could be analyzed using advanced data exploration techniques like principal component analysis (PCA), or multi dimensional scaling (MDS). This could tease out the variation in image intensity due to concentration from other factors and provide a more precise calibration curve. Other methods of monitoring solute concentration could be investigated as they could improve the accuracy of the method.

The device fabricated in this thesis is robust and highly customizeable. For example, different hydrogels including degradable or erodible gels could be investigated. The device could be loaded with a solute and release studies could be performed. If hydrogels with sufficiently large mesh sizes are used, convective transport through these polymer networks could be investigated.

The scale of microfluidic channels is similar to that in the human body. The *venae cavae* have a diameter of ~2 cm and the smallest capillaries approach 5 μm in diameter. Microfluidic devices can easily be tailored to study flow similar to that in vasculature. Surface modifications including endothelial cell growth or the attachment of a lipid bilayer could provide a more realistic surface. Novel flow conditions such as

pulsatile flow, or flow with particulate matter, could be investigated. This direction would have an immediate application for flow-contacting drug delivery devices.

Other applications could take advantage of the use of PEG or other hydrogels in microfluidic devices. Channels defined by hydrogel walls could be used for myriad purposes. One example would be to use the hydrogel to separate two channels and make a cross-flow filtration device.

Appendix 1: Diffraction of Light Past a Photomask

As light passes the edge of the photomask it diffracts and bends under the mask as shown in Figure A1.1 The magnitude of this effect depends on the wavelength, distance between the photomask and substrate, and distance from the slit. The effect of diffraction due to a photomask has been studied on negative photoresist systems, and can be quantified mathematically.[1]

Exposure UV Light

photomask

Glass Plate

photoresist

- x   0   + x

Si substrate
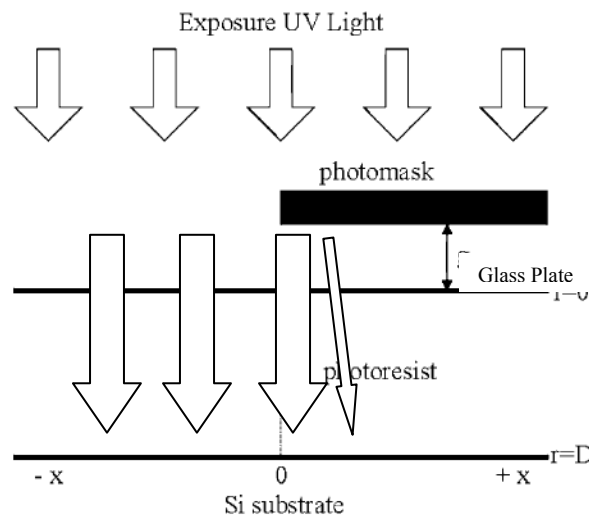
Figure A1.1: Diffraction around a semi-infinite obstacle

The distribution of light intensity after diffusing past a semi-infinite obstacle can be found from the following:

$$\frac{I}{I_0} = \frac{1}{2}\left[\left(\frac{1}{2}-C(u)\right)^2 + \left(\frac{1}{2}-S(u)\right)^2\right]$$

(A1.1)

<div align="right">(A.1)</div>

where $C(u)$ and $S(u)$ are the Fresnel integrals defined below:

$$C(u) = \int_0^u \cos\left(\frac{\pi t^2}{2}\right) dt$$

$$S(u) = \int_0^u \sin\left(\frac{\pi t^2}{2}\right) dt$$

<div align="right">(A1.2)</div>

and u is the fresnel number:

$$u = x\sqrt{\frac{2}{\lambda r}}$$

<div align="right">(A1.3)</div>

where x is the horizontal distance from the photomask boundary, λ is the wavelength of light, and r is the vertical distance from the photomask. Taking $\lambda = 360$ nm, $r = 1.0$ mm as parameters describing the system used, the diffraction pattern is shown in Figure A1.2.

Figure A1.2 shows the distribution of light intensity as a function of distance as it enters the hydrogel. The distribution will spread out even more as light travels through the hydrogel, which for this thesis was 600 or 1200 μm thick. Figure A1.2 shows there is high light intensity near the photomask, and the light intensity is non-zero up to about 20 μm under the photomask. This model not take into account refraction due to the glass slide, which would help offset the stray light from diffraction. The diffraction of light is certainly an important process at small scales, but for channel widths on the order of 900 μm, diffraction will only affect channel resolution by 5-10%.
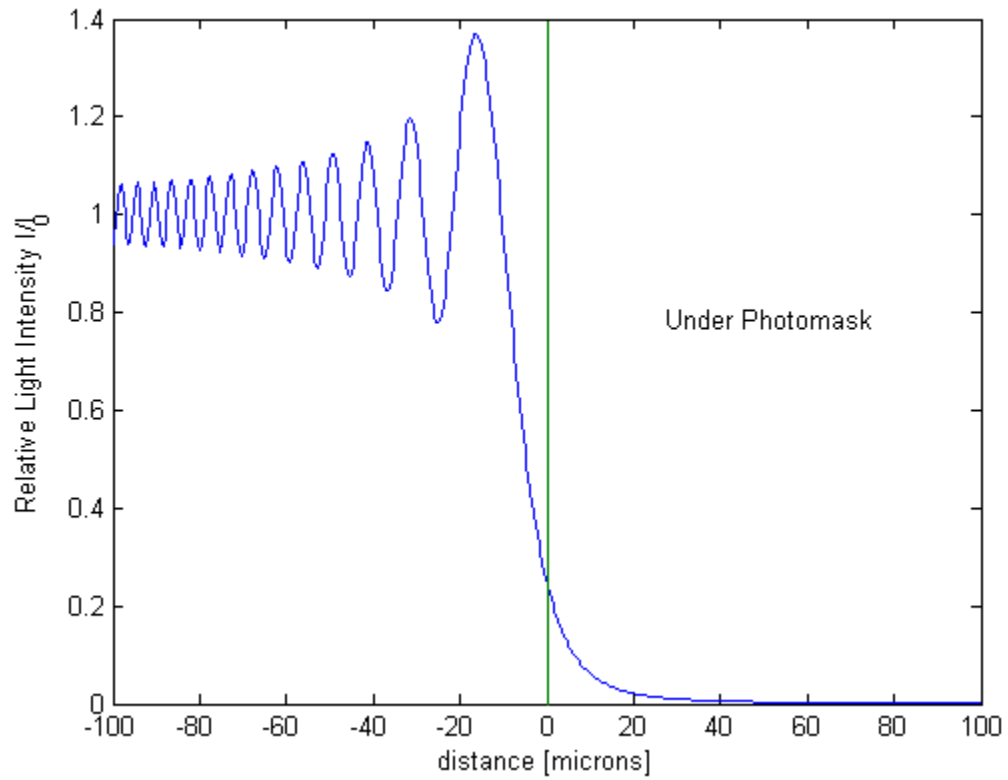
Figure A1.2: Intensity of light diffracting past a photomask

A1.1 References

1. Chuang, Y. J.; Tseng, F. G.; Lin, W. K. *Microsystem technologies* **2002***, 4,* 308-313.

Appendix 2: Derivation of the Power Law Model

It is often easier to gather information about the total amount of analyte diffusing into a slab $M(t)$ rather than the concentration profile, $C(x,t)$. The relation between M(t) and time can provide information about the diffusive process, whether it is Fickian, non-Fickian, and to what extent. For a linear geometry diffusive processes generally obey the following relation:

$$M_t = kt^n \qquad\qquad (A2.1)$$

When $n=0.5$, the process is linear, for $0.5<n<1$, the process is non-Fickian, and for $n=1$, the process is zeroth order (diffusion rate independent of time), and referred as type II behavior.[1] To evaluate the parameter, one can integrate the concentration profile in the x,y, and z dimensions. For diffusion limited to one dimesion, M(t) can be found by the following:

$$M_t(t) = \int C(x,t)dx \qquad\qquad (A2.2)$$

For diffusion into a semi-infinite slab with initial and boundary conditions $C(x,0)=0$; $C(0,t>0)=C_0$; and $C(\infty,t>0)=0$, a theoretical solution to the Fickian diffusion equation takes the following form:[2, 3]:

$$C(x,t) = C_0 erfc\left(\frac{x}{2\sqrt{Dt}}\right) \qquad\qquad (A2.3)$$

Applying equation 3 to equation 2,

$$M_t(t) = \int C_0 erfc\left(\frac{x}{2\sqrt{Dt}}\right) dx \tag{A2.4}$$

The expression can be integrated between the boundaries $x=0$, and $x=\infty$:

$$M_t(t) = \int_0^\infty C_0 erfc\left(\frac{x}{2\sqrt{Dt}}\right) dx \tag{A2.5}$$

which gives the following:

$$M_t(t) = \frac{C_0}{\sqrt{\pi}} 2\sqrt{Dt} \tag{A2.6}$$

This equation has a similar form to eq. 1 where $n=0.5$, and

$$k = 2C_0 \sqrt{\frac{D}{\pi}} \tag{A2.7}$$

Knowing the parameter, k, the diffusion coefficient can be found via the following:

$$D = \frac{\pi}{4}\left(\frac{k}{C_0}\right)^2 \tag{A2.8}$$

Equation 1.8 is only valid under classical Fickian behavior, i.e. when $n=0.5$, to find the diffusion coefficient. It can be useful, for systems where it may be easier to evaluate the total influx of solute instead of the concentration profile.

A2.1 References

1. Muhr, A. H.; Blanshard, J. M. V. *Polymer* **1982**, *1012,* 154.

2. Cengel, Y. A. *Heat and Mass Transfer A Practical Approach;* McGraw-Hill: New York, 2007.

3. R. Byron Bird, Warren E. Stuart, Edwin N. Lightfoot *Transport Phenomena;* John Wiley & Sons Inc: New York, 2007.

Appendix 3: Swelling Data

Table A3.1: Swelling Data for 30 vol% PEG-DA 70 vol% H_2O

Sample	Before Lyophilization				After Lyophilization			
	m [g]	L1 [mm]	L2 [mm]	average L [mm]	m [g]	L1 [mm]	L2 [mm]	ave. L [mm]
S1					0.096	0.93	0.94	0.935
S2					0.09	0.92	0.95	0.935
S3					0.039	0.91	0.94	0.925
S4					0.071	0.95	0.9	0.925
S5	0.287	1.29	1.3	1.295	0.102	0.87	0.88	0.875
S6	0.238	1.26	1.25	1.255	0.083	0.85	0.85	0.85
S7	0.25	1.26	1.27	1.265	0.092	0.86	0.87	0.865
S8	0.218	1.2	1.15	1.175	0.074	0.82	0.8	0.81
	After Reswelling (2 days)				Reswelling 8 days			
	m [g]	L1 [mm]	L2 [mm]	average L [mm]	m [g]	L1 [mm]	L2 [mm]	ave. L [mm]
S1	0.187	1.22	1.22	1.22	0.187	1.24	1.21	1.225
S2	0.164	1.19	1.33	1.26	0.166	1.17	1.2	1.185
S3	-	-	-					
S4	0.124	1.18	1.17	1.175	0.124	1.17	1.16	1.165
S5	0.212	1.21	1.21	1.21	0.215	1.16	1.17	1.165
S6	0.204	1.21	1.22	1.215	0.207	1.22	1.2	1.21
S7	0.192	1.18	1.22	1.2	0.197	1.17	1.18	1.175
S8	0.168	1.13	1.15	1.14	0.172	1.11	1.1	1.105

Denotes broken sample

Appendix 4: Data Processing Scripts

In order to carry out data processing procedures, programming scripts were generated and used extensively. These scripts were developed in a MATLAB programming environment and served to process digital images taken of the microfluidic device, and to create intensity-concentration calibration curves. These scripts should be relatively user friendly; however some previous MATLAB experience is recommended.

To process microfluidic device images, a series of scripts are used. The purpose of the scripts is to take a series of pictures where dye is diffusing through the hydrogel and calculate the diffusivity of the solute. The scripts break this process into several steps, each with its own script file. The steps and associated m-files are presented in Table A4. below:

The fitting routines take advantage of two user generated toolboxes: EZFIT and NATB. These toolboxes are necessary for the scripts to function. EZFIT is useful curve-fitting toolbox available online, while NATB is a custom toolbox generated by Dr. James Maneval (Bucknell University Chemical Engineering Dept). The following is a procedure describing how to make use of the custom scripts for data analysis.

Table A4.1: Overview of MATLAB scripts used in data processing procedure.

Step	File name	Description
1	generic_upload.m	loads the pictures into MATLAB
2	find_conv.m	calculates the physical scale based on a picture of a ruler
3	find_boundary.m	Determines where exactly the boundary between channel and hydrogel is.
4	plot_data_bg_I2C.m	Converts intensity to concentration values, calculates similarity variables, and plots the data
5	collapse2.m	Reduces the noise of the data by fitting a curve to the trend of the data. This is necessary due to the large amount of data generated.
6	erfc_fit.m	Fits a complementary error-function model to the data.
7	exponent.m	Fits a power law model to the data.

Two things are needed before the scripts can be used. First, a set of digital images of dye diffusing through the microfluidic device is required. These images can be acquired by a Motic digital microscope and software. The digital images should be saved with the date and time in the filename, and saved as .png files. If hard drive space is an issue, then the .jpeg format can be used, although the compression method used in the .jpeg format can affect data quality. Second, a picture of the device with a distance calibration image is needed. A distance calibration image could mean a small dot with a known diameter, or more simply, a picture of a ruler placed over the device. Whatever is

used, a calibration picture is required. The calibration picture and the diffusion pictures should be in their own dedicated folder, and a second folder should be created containing the processing scripts.

Once the scripts are placed in the data processing folder, the user can begin to run the scripts. The MATLAB program should be started and the user should move to the data processing folder within MATLAB. The user can now run the first script, generic_upload.m. The script will prompt the user for the location or pathway to the picture folder, the data processing folder, and the name of the device. The user should input this information in the MATLAB environment and press enter to continue. Next, the program will ask the user to choose the picture when the dye first begins to flow through the device. It is important to note that *the first picture in the picture folder is indexed as number 3*, the second picture is number 4 and so on. If the dye appears in the device on the 22nd picture, the user should input 24. Next, the script will ask the user to choose a box in the picture where information will be uploaded. This makes it possible to selectively examine pristine sections of the device while avoiding defects, reflective spots, specks of dirt, and other imperfections. Finally, the script will load the information from all the pictures and save the important information.

The next step calculates the pixel to length conversion factor using the find_conv.m script. This is done by running the find_conv.m script, loading the distance calibration picture, and clicking on two points that are a known distance from each other. Next, the find_boundary.m script determines the location between the hydrogel and the

channel. The script takes an early photograph of the diffusive process and fits a sigmoid

function to the interface between the hydrogel and the channel. The script will show the

boundary locations to the user for approval. To adjust the boundaries, the script must be

opened in MATLAB's mfile editor. To adjust the boundary, the numbers on lines 69 and

70 can be increased or decreased to move the boundary left or right. Sometimes it is

useful to employ the evaluate cell button, or increment value and evaluate cell as shown

in Figure A4.1 below. Click the cursor next to the adjusting numbers on lines 69 or 70.

This will re-plot the graph and show the new boundary location.
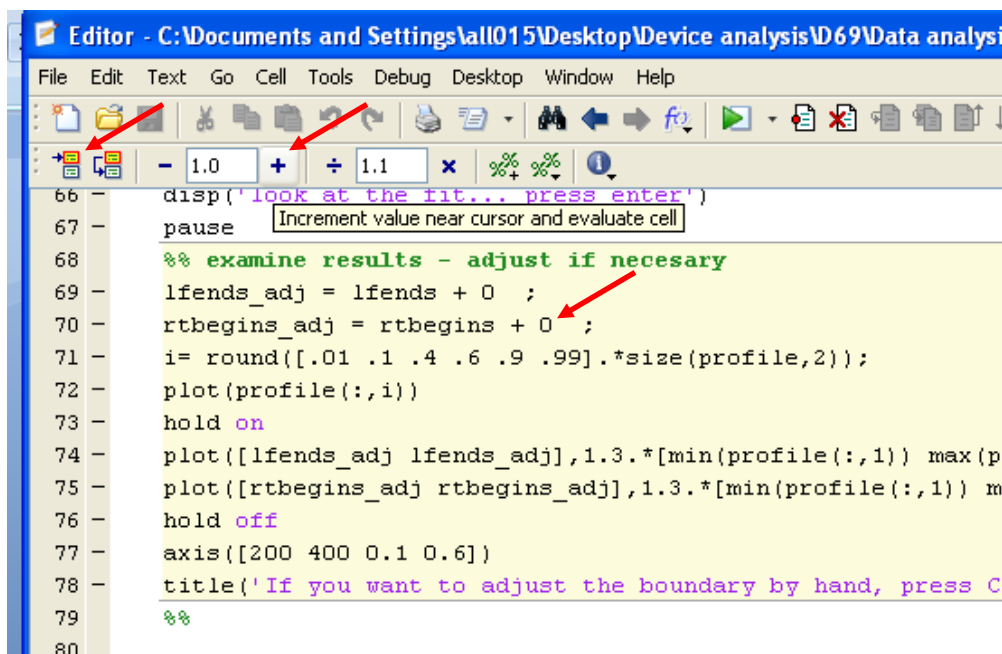
Figure A4.1: Location of the evaluate-cell and increase-value-and-iterate-cell buttons

The next step is to run the plot_data_bg_I2C.m script. This script carries out

multiple tasks. First, it converts the data from intensity to concentration. The data is

normalized and a background is subtracted. The data is collapsed onto the similarity variable and displayed. Plots are generated throughout the process.

The next script file, collapse2.m, takes the similarity variable information and creates a trend through the data. This step is necessary to fit models to data, as datasets can be as large as 250,000 individual points. The final scripts perform data fitting and provide the user with diffusion coefficients. The script Erfc_fit.m fits a complementary errorfunction model to the data and returns a diffusion coefficient. The script exponent.m fits a power law model to the data and returns a value for the exponent, n, as well as the diffusive coefficient, D, which is only valid if n is near 0.5.

To create intensity-concentration calibration curves, a MATLAB script calibration_curve.m was created. This script had to be modified with the concentration and slab thickness values for each curve, but the general template remained the same. To generate a calibration curve using the script, pictures needed to be taken of the dyed hydrogel slabs. The script imported the pictures and recorded the intensity (R, G, and B) values of the images. These intensity values were then plotted against concentration times slab thickness. A logarithmic curve was used to fit some of the data points.

generic_upload.m

```matlab
%%% Upload the Data - Template program file

% Template program file
clear
close all


location = input('where are the pictures located ? ','s'); %location of pictures
home = input('where is the data processing folder located ?','s'); % location of the folder where the
programs are held
cd(location); % Insert location of pictures here.
Devicename = input('what is the device name ? ','s');  % what is the device name
nam = dir;
n0 = char(nam.name);
clear nam
%%% find the first picture
pass =0;
while pass==0
fpic = input('The first picture with dye is # ? (start at 3 and go up) ');
%first pic when dye moves through the channel
% note the 1st picture is the 4th element in n0
 test = imread(n0(fpic,:));
 image(test);

 pass = input('is this the right picture ? Y=1 N=0 ');
end


%%% Find the Box

pass =0;
while pass==0
image(test)
   disp('click on the pic to choose the sides of the box');
[xb yb] = ginput(2);
image(test)
hold
plot([xb(1) xb(1) xb(2) xb(2)], [0 768 768 0],'r','LineWidth',3)
hold
pass = input('is this the right box ? Y=1 N=0 ');
end

clear test
%%% Prepare the load loop
N = length(n0)-fpic; % N = number of picture files - takes into account thumbs.db file
sz = 768; %512 or 768 , 2nd dimension in picture size (i.e. __ x __ pixels)
profile = ones(sz,N);  % pre allocating matrix size
errorprofile = ones(sz ,N); % 768 pixels x number of pictures
names = ones(N,5,1);
```

```
nprofile = ones(sz,N);


 x=1;
%%% Execute the load loop
for k = fpic:(length(n0)-1) %the n0(fpic,:)th pic is when the dye
   ... fully clears the channell/boxed area.
   s0 = imread(n0(k,:));



   prof = s0(:,floor(xb(1)):floor(xb(2)),:);



   clear s0
   prof = rgb2ntsc(prof); %turns to greyscale
   prof = double(prof); %turns integer values into normal values

   prof = prof(:,:,1); %takes only the grayscale element of the picture matrix
   prof = 1 - prof; % makes dark = 1, white = 0
   erprof = std(prof,0,2); %finds the error in the rows in the box
   prof = mean(prof,2); % takes the average accross the rows in the box
   clc
   t = x/N % counter - displays fraction completed
   names(x,1,1) = k ; %this takes the time info out of the filename
   names(x,2,1) = str2double(n0(k,10:11)); %hours
   names(x,3,1) = str2double(n0(k,12:13)); %min
   names(x,4,1) = str2double(n0(k,14:15)); %sec
   names(x,5,1) = str2double(n0(k,7:8));  %days in case you run past midnight
   profile(:,x) = prof; %saves info into the profile matrix
   errorprofile(:,x) = erprof; % saves error info into the error matrix

   % find where the channel is approximately to normalize data
%    nprofile(:,x) = prof./mean(prof(275:325));
   % nprofile is the profile normalised by the channel average
   % profile :  1 column is the profile = profile(:,x)
   %            1 row is change in time = profile(x,:)
   x = x+1;
end

% clear n0


%%% Convert name info into Time
time = names(:,5,1).*(3600*24) + names(:,2,1).*3600 + names(:,3,1).*60 + names(:,4,1); %converts min,
hour to seconds
time = time - time(1); % starting time = 0
x = linspace(1,size(profile,1),size(profile,1)); % makes an array of
% points so you can plot intensity vs pixel number.
x = x';
%%% save important Info
cd(home);
```

```
save data time profile errorprofile x fpic
save loc&nam Devicename location home
% saves something called files with everything inside it.
%% this subsection plots 4 different timepoints of the concentration vs
% pixel#
n = round([.05 .30 .60 .95].*size(nprofile,2));
%

figure, plot(x,profile(:,n(1)) ,':r');
hold on
plot(x,profile(:,n(2)) ,'-g');
plot(x,profile(:,n(3)) ,'-.b');
plot(x,profile(:,n(4)) ,'--k');

xlabel('pixel number');
ylabel('Apparent Intensity');


Y1 = strcat('time = ',mat2str(time(n(1))),' seconds');
Y2 = strcat('time = ',mat2str(time(n(2))),' seconds');
Y3 = strcat('time = ',mat2str(time(n(3))),' seconds');
Y4 = strcat('time = ',mat2str(time(n(4))),' seconds');

legend(Y1,Y2,Y3,Y4,'location','best');
title(['sample concentraction curves Device' Devicename]);
hold off
```

find_conv.m

```matlab
% find a conversion factor for # of pixels to meters.
clear
close all

% need to import location, home, Devicename
load loc&nam

cd(location); %  location of pictures.
nam = dir;
n0 = char(nam.name);
clear nam

rulpic = input('is there a picture with a ruler in the data ? y=1 n=0');
if rulpic == 0
   conv = 1.45e-5;
      % if there is no picture with a ruler, use conv = 1.45e-5;
   % typical values are between 1.44e-5 & 1.47e-5

else

   pass =0;
   while pass == 0
      rulerpic = input('which picture number has the ruler?');   % choose a picture with a ruler
      R = imread(n0(rulerpic,:));
      image(R); % now we look at the pic
      pass = input('is this the ruler picture? Y=1 N=0 ');
   end

   disp('click on two points that are an exact distance from one another')
   [x y] = ginput(2);

   cm = input('how many cm apart were the two points');
   m = cm/100;

   pix = sqrt( (abs(x(2)-x(1)))^2 + (abs(y(2)-y(1)))^2 ); %pythagorean theorem
   conv = m/pix;



end
   % if there is no picture with a ruler, use conv = 1.45e-5;
   % typical values are between 1.44e-5 & 1.47e-5
   % this is about 1 pixel equal to 14.4-14.7 microns
   cd(home);% home address
   save conv conv
disp('OK done!')
```

find_boundary.m


```
% this file helps find the channel boundary
% on both sides and puts the right and
% left side of the data into two new matrices

close all
load data
load loc&nam
load conv

addpath('U:\public\Matlab\ezyfit')

%%  Attempt to fit a sigmoid curve to the profile
% using EZ-Fit
% left side
plot(profile(:,1))  % look at the first picture with dye
disp('click on bottom, then top, then the middle of the left side')
[xi yi] = ginput(3);
disp('select the left boundary with the data brishing tool')
disp('and press enter when done')

pause

a = mat2str(yi(2)-yi(1)); % range up-down (stretchiness up down)
d = mat2str(yi(1)); % y limit as x-> inf (shift up/down)
c=mat2str(xi(3)); % midpoint (shift left/right)
b=mat2str(.2); % stretchiness left right

[xf yf] = pickdata;
plot(xf,yf)

F = ezfit(xf, yf, ['y(xf)=a/(1+exp(-b*(xf-c)))+d;' ' a=' a '; b=' b '; c=' c '; d=' d]);
showfit(F, 'fitcolor', 'red', 'fitlinewidth', 2, 'dispeqboxmode', 'off');
title('Fit of Sigmoid to Left Channel Boundary')
xlabel('pixel')
ylabel('Apparent Intensity')

lfends =round(F.m(3));


disp('look at the fit... press enter')
pause

%% right side
plot(profile(:,1))
disp('click on bottom, then top, then the middle of the right side')
[xi yi] = ginput(3);
disp('select the right boundary with the data brishing tool')
```

```
disp('and press enter when done')

pause

a = mat2str(yi(2)-yi(1));
d = mat2str(yi(1));
c=mat2str(xi(3));
b=mat2str(.2);

[xf yf] = pickdata;
plot(xf,yf)

F = ezfit(xf, yf, ['y(xf)=a/(1+exp(b*(xf-c)))+d;' ' a=' a '; b=' b '; c=' c '; d=' d]);
showfit(F, 'fitcolor', 'red', 'fitlinewidth', 2, 'dispeqboxmode', 'off');
title('Fit of Sigmoid to Right Channel Boundary')
xlabel('pixel')
ylabel('Apparent Intensity')
rtbegins =round(F.m(3));
disp('look at the fit... press enter')
pause
%% examine results - adjust if necesary
lfends_adj = lfends + 0  ;
rtbegins_adj = rtbegins + 0  ;
i= round([.01 .1 .4 .6 .9 .99].*size(profile,2));
plot(profile(:,i))
hold on
plot([lfends_adj lfends_adj],1.3.*[min(profile(:,1)) max(profile(:,end))])
plot([rtbegins_adj rtbegins_adj],1.3.*[min(profile(:,1)) max(profile(:,end))])
hold off
axis([200 400 0.1 0.6])
title('If you want to adjust the boundary by hand, press CTRL+C')
%%

pause
%%
lfends = lfends_adj;
rtbegins = rtbegins_adj;

rtside = profile(rtbegins:end,:); % size = ? by 865
lfside = profile(1:lfends,:); % size = ?? by 865
%%


% make an array to plot intensity vs distance for both sides
L_rt = conv.*linspace(1,size(rtside,1),size(rtside,1));
L_lf = conv.*linspace(1,size(lfside,1),size(lfside,1));


%%
rterror = errorprofile(rtbegins:end,:);
lferror = errorprofile(1:lfends,:);
```

```matlab
lfside = flipud(lfside); % flips the left side to plot easier
lferror = flipud(lferror); % flip the error too.


%%
disp('now saving things')
save data_2_r rtside rterror L_rt rtbegins
save data_2_l lfside lferror L_lf lfends
clc
disp('now you can plot the data!')
```

plot_data_I2C_bg.m

```matlab
%%% this program plots the left and right side

clear
close all
disp('loading data')
load loc&nam
load conv
load data
load data_2_r
load data_2_l
addpath('U:\public\Matlab\ezyfit')

%%% look at the right side
plot(rtside)
title('Right Side Raw Profiles')

%%% convert the right side to concentration via emperical eqn.
rtside = 1/.6*exp((rtside - 1.8106)./0.13606);
figure(2), plot(rtside);
title('Conversion to Concentration - Right Side')

%%% take the user defined last part of the 1st pic and fit a line to it
% edited to have the user select what part of the background to fit
m=size(rtside,2);
i=round(m.*[.01 .1 .25 .5 .75 .9 .99]);
figure, plot(L_rt,rtside(:,i),'.b')
title('Fit a line to the background section')
disp('fit a line to the background signal')
pause
[xf yf] = pickdata;
close
p = polyfit(xf,yf,1);
pv = polyval(p,L_rt);
figure(3), plot(L_rt,rtside(:,i),'.b',L_rt,pv,'r')
title('Fit to Background Signal')
xlabel('pixel')
ylabel('Apparent Intensity')
%%% subtract the background
for n=1:size(rtside,2)
bgs_rt(:,n) = rtside(:,n) - pv';
end
figure(4), plot(bgs_rt)
title('background subtracted - right side')

%%% normalize the data
clc
disp('normalizing right side')
%right side
```

```matlab
figure(4), plot(bgs_rt(:,i));

title('pick the end area to normalize bottom')
pause
[xp yp] = pickdata;
yp = mean(yp);
xp = min(xp);
for j=1:size(rtside,2)
    % normalise data:  data_n = (data -  bottom)/(top - bottom)
    % bottom is the last 10% of data
    % top is the first data point, or the max value of rtside

    bottom = mean(  bgs_rt(xp:end,j)  );
    top = bgs_rt(1,j);
    [ym xm] = max(bgs_rt(:,j));
    top = ym;
        n_bgs_rt(:,j) = ( bgs_rt(:,j)- bottom )./ ( top - bottom );
end
t=5;
figure(5), plot(n_bgs_rt(:,(time>t*60))) %plots everything past 5 mins
title('normalized data - right side')

%% normalize by sqrt(time) and make the nu matrix

for i=1:size(time)
% nu = x/(2 sqrt(t))
    rt_nu(i,:) = L_rt./2./(sqrt(time(i)))';
end
rt_nu = rt_nu';
%% Plot some data taking out first few minutes
t1=0;
figure(6), plot(rt_nu(:,(time>t1*60)),n_bgs_rt(:,(time>t1*60)),'.','markersize',0.2)
title({['collapsed concentration curves - right side. ' Devicename];'If you want to remove the first few
minutes press CNTRL +C'})

figure(7), semilogx(rt_nu(:,(time>t1*60)),n_bgs_rt(:,(time>t1*60)),'.','markersize',0.2)
title({['collapsed concentration curves - right side. ' Devicename];'If you want to remove the first few
minutes press CNTRL +C'})
%%
pause
%% look at the left side
figure(8), plot(lfside)
title('left side raw profiles')

%% convert the left side to concentration via emperical eqn.
lfside = 1/.6*exp((lfside - 1.8106)./0.13606);
figure(9), plot(lfside);
title('Conversion to Concentration - Left Side')

%% take the user defined last part of the 1st pic and fit a line to it
% edited to have the user select what part of the background to fit
```

```matlab
m=size(lfside,2);
i=round(m.*[.01 .1 .25 .5 .75 .9 .99]);
figure(10), plot(L_lf,lfside(:,i),'.b')
title('Fit a line to the background section')
disp('fit a line to the background signal')
pause
[xf yf] = pickdata;
close
p = polyfit(xf,yf,1);
pv = polyval(p,L_lf);
figure(11), plot(L_lf,lfside(:,i),'.b',L_lf,pv,'r')
title('Fit to Background Signal - left side')
xlabel('pixel')
ylabel('Apparent Intensity')

%%  subtract the background
for n=1:size(lfside,2)
bgs_lf(:,n) = lfside(:,n) - pv';
end
figure(11), plot(bgs_lf)
title('background subtracted - left side')

%% normalize the data
clc
disp('normalizing left side')
%left side
figure(12), plot(bgs_lf(:,i));

title('pick the end area to normalize bottom')
pause
[xp yp] = pickdata;
close
yp = mean(yp);
xp = min(xp);
for j=1:size(rtside,2)
   % normalise data:  data_n = (data -  bottom)/(top - bottom)
   % bottom is the last 10% of data
   % top is the first data point, or the max value of rtside

   bottom = mean(  bgs_lf(xp:end,j)  ); % could be min too...
   top = bgs_lf(1,j);
   [ym xm] = max(bgs_lf(:,j));
   top = ym;
      n_bgs_lf(:,j) = ( bgs_lf(:,j)- bottom )./ ( top - bottom );
end
t=5;
figure(12), plot(n_bgs_rt(:,(time>t*60)))
title('normalized data - left side')
```

```matlab
%% normalize by sqrt(time) and make the nu matrix

for i=1:size(time)

    lf_nu(i,:) = L_lf./2./(sqrt(time(i)))';
end
lf_nu = lf_nu';
    %% Plot some data disregarding the first few minutes
t2=0;

figure(13), plot(lf_nu(:,(time>t2*60)),n_bgs_lf(:,(time>t2*60)),'.','markersize',0.2)
title({['collapsed concentration curves - left side. ' Devicename];'If you want to remove the first few
minutes press CNTRL +C'})

figure(14), semilogx(lf_nu(:,(time>t2*60)),n_bgs_lf(:,(time>t2*60)),'.','markersize',0.2)
title({['collapsed concentration curves - left side. ' Devicename];'If you want to remove the first few
minutes press CNTRL +C'})

%%
pause

%% save only the good data - leave out first few minutes...
rt_nu = rt_nu(:,(time>t1*60));
n_bgs_rt = n_bgs_rt(:,(time>t1*60));

lf_nu = lf_nu(:,(time>t2*60));
n_bgs_lf = n_bgs_lf(:,(time>t2*60));
disp('ok saved the good stuff')

%% Save Important Info
cd(home)
disp('saving things')
save files_3I2C lf_nu n_bgs_lf rt_nu n_bgs_rt t1 t2

disp('Done !! ')
return
```

collapse2.m

```matlab
%% Collapse turns the quarter million data points into a single line


disp('loading data')
load loc&nam
load files_3I2C
addpath('../biskit')
%% distill the left data using loess

nf = 200;  % number of points in the fitting mesh
xdat = lf_nu(:);
idx = isfinite(xdat);
xdat=xdat( idx );


ydat = n_bgs_lf(:);
ydat = ydat(idx);



xfit = logspace(log10(min(xdat)),log10(max(xdat)),nf); % logarithmically space the fitting mesh
A = 0.0075;  %fraction of dataset used in fit
lambda = 1; %order of the local fit - use 1
clc
disp('fitting the left side')
tic
[yfit, C] = loess(xdat,ydat,xfit,A,lambda);
toc

% plot the data
figure, semilogx(xdat,ydat,'r.','markersize',0.5)
hold on
plot(xfit,yfit)
hold off

xfit_l = xfit;
yfit_l = yfit;
C_l=C;
%% distill the right data using loess

nf = 200;  % number of points in the fitting mesh
xdat = rt_nu(:);
idx = isfinite(xdat);
xdat=xdat(idx);
ydat = n_bgs_rt(:);
ydat = ydat(idx);


xfit = logspace(log10(min(xdat)),log10(max(xdat)),nf); % logarithmically space the fitting mesh
```

```matlab
A = 0.0075;  %fraction of dataset used in fit
lambda = 1; %order of the local fit - use 1

disp('fitting the right side')
tic
[yfit, C] = loess(xdat,ydat,xfit,A,lambda);
toc

% plot the data
figure, semilogx(xdat,ydat,'r.','markersize',0.5)
hold on
plot(xfit,yfit)
hold off

xfit_r = xfit;
yfit_r = yfit;
C_r = C;


%%
clc
disp('saving things')
save collpdata_I2C xfit_r yfit_r xfit_l yfit_l C_r C_l
disp('done')
return
```

erfc_fit.m

```matlab
% erfc fit. - this program takes the collapsed fitted curves and plots them
% against an errorfucntion.

clear
close all
load collpdata_I2C
load files_3I2C
addpath('U:\public\Matlab\ezyfit')
%%% plot left vs right side
figure, plot(xfit_l,yfit_l,'r',xfit_r,yfit_r,'b');
axis([0 2.5e-5 0 1]);
legend('right side','left side','location','best')

title('Comparison of Left and Right side Data');
ylabel('Normalized Intensity');
xlabel('Similarity Variable \eta [m*s^{-1/2}]');

%%% compare left side to erfc
figure, semilogx(xfit_l,yfit_l,'o');
pause

Diff_l=1e-10;
a = mat2str(1/sqrt(Diff_l));

f = ezfit(xfit_l,yfit_l,['y(xfit_l)=erfc(a*xfit_l);' ' a=' a ';' ]);
showfit(f,'dispeqboxmode', 'off');

semilogx(xfit_l,yfit_l,'o');
showfit(f,'dispeqboxmode', 'off');
Diff_l=mat2str(1/f.m^2);
rsq = mat2str(f.r^2);

title('Complementary Errorfunction fit of the Left Side Data')
xlabel('Similarity Variable \eta [m*s^{-1/2}]');
ylabel('Normalized Intensity');
g1 = ['r^2 = ' rsq(1:6) ];
g2 = ['D = ' Diff_l(1:4) Diff_l(17:end) ' m^2/s'];
gtext({g1,g2});

figure, semilogx(lf_nu,n_bgs_lf,'.k','markersize',0.2)
showfit(f,'fitcolor','red','dispeqboxmode', 'off');
title('Complementary Errorfunction fit of the Left Side Data')
xlabel('Similarity Variable \eta [m*s^{-1/2}]');
ylabel('Normalized Intensity');
gtext({g1,g2});
```

```
%% compare the right side to erfc

figure, semilogx(xfit_r,yfit_r);
pause

Diff_r=1e-10;
a = mat2str(1/sqrt(Diff_r));


f = ezfit(xfit_r,yfit_r,['y(xfit_r)=erfc(a*xfit_r);' ' a=' a ';' ]);
showfit(f,'dispeqboxmode', 'off');

semilogx(xfit_r,yfit_r,'o');
showfit(f,'dispeqboxmode', 'off');
Diff_r=mat2str(1/f.m^2);
rsq = mat2str(f.r^2);

title('Complementary Errorfunction fit of the Right Side Data')
xlabel('Similarity Variable \eta [m*s^{-1/2}]');
ylabel('Normalized Intensity');
g1 = ['r^2 = ' rsq(1:6) ];
g2 = ['D = ' Diff_r(1:4) Diff_r(17:end) ' m^2/s'];
gtext({g1,g2});

figure, semilogx(rt_nu,n_bgs_rt,'.k','markersize',0.2)
showfit(f,'fitcolor','red','dispeqboxmode', 'off');
title('Complementary Errorfunction fit of the Right Side Data')
xlabel('Similarity Variable \eta [m*s^{-1/2}]');
ylabel('Normalized Intensity');
gtext({g1,g2});
```

exponent.m

```
clear
close all
load data
load files_3I2C
load conv
addpath('U:\public\Matlab\ezyfit')

% plot(n_bgs_lf)
% pause
for k=1:size(n_bgs_lf,2)
   C=n_bgs_lf(1:end,k);
   C(C<0.0)=0;

   M_tl(k) = trapz(C);
end

c = size(time,1)-size(M_tl,2)+1;
time2l = time(c:end);
x=1;
figure, loglog(time2l(x:end),M_tl(x:end))
title('left side')
pause
[t M_t] = pickdata;
f1 = ezfit('M_t(t) = k*t^n; n=.5;log');
showfit(f1);
Dl = (conv*f1.m(1))^2*pi/4;
gtext(num2str(Dl));

figure, loglog(t,M_t)
xlabel('time [s]')
ylabel('M_t')
showfit(f1);


   for k=1:size(n_bgs_rt,2)
   C=n_bgs_rt(1:end,k);
   C(C<0.0)=0;
   M_tr(k) = trapz(C);
end
c = size(time,1)-size(M_tr,2)+1;
time2r = time(c:end);
x=1;
figure, loglog(time2r(x:end),M_tr(x:end))
% title('right side')
xlabel('time [s]');
ylabel('Total Integrated Area');
 pause
[t M_t] = pickdata;
```

```
f2 = ezfit('M_t(t) = k*t^n; n=.5;log');
showfit(f2);
Dr = (conv.*f2.m(1))^2*pi/4;
gtext(num2str(Dr));
```

calibration_curve.m

```
% generic calibration curve creator
clear
close all

home=cd;
nam = dir;
n0 = char(nam.name);
clear nam
int=[1:size(n0,1)-3];

cd('U:\public\Matlab')
setup
cd(home);
%%%
for k = 3:6 %adjust for the number of pictures you have
    P = imread(n0(k,:));
    figure(2), image(P)
    axis ij %make the axes like a matrix
    disp('choose where a good area is and click on corners')
    [x,y]=ginput(2);
    x=round(x);
    y=round(y);
    P=P(y(2):y(1),x(1):x(2),:);
    figure(2), image(P)

    x=k-2; % start on 1
    y=x+1;
    figure(1), subplot(3,4,y)
        image(P)
    r = double(P(:,:,1))./256;
    g = double(P(:,:,2))./256;
    b = double(P(:,:,3))./256;
    rm(x) = mean(mean(r),2);
    gm(x) = mean(mean(g),2);
    bm(x) = mean(mean(b),2);

    rer(x) = std(std(r));
    ger(x)= std(std(g));
    ber(x)= std(std(b));

    s0 = rgb2ntsc(P);

    s0 = s0(:,:,1);
    er = std(std(s0));
    s0 = mean(mean(s0),2);
```

```matlab
  gs(x) = s0;
  gser(x) = er;

  % convert to other colormaps?
  Phsv = rgb2hsv(P);
  h = double(Phsv(:,:,1));
  s = double(Phsv(:,:,2));
  v = double(Phsv(:,:,3));

  hm(x) = mean(mean(h),2);
  sm(x) = mean(mean(s),2);
  vm(x) = mean(mean(v),2);

  her(x) = std(std(h));
  ser(x)= std(std(s));
  ver(x)= std(std(v));

  Pntsc = rgb2ntsc(P);
  y = double(Pntsc(:,:,1));
  i = double(Pntsc(:,:,2));
  q = double(Pntsc(:,:,3));

  ym(x) = mean(mean(y),2);
  im(x) = mean(mean(i),2);
  qm(x) = mean(mean(q),2);

  yer(x) = std(std(y));
  ier(x)= std(std(i));
  qer(x)= std(std(q));
end
%%
hold off
conc = [  ]; %mM
path_length = [  ];
path_length=mean(path_length,2); %mm
cPa = conc.*path_length';

rm = 1-rm;
gm = 1-gm;
bm = 1-bm;
gs = 1-gs;
%%
figure(3), errorbar(cPa,rm,rer,'or');
hold on
errorbar(cPa,gm,ger,'og');
   errorbar(cPa,bm,ber,'ob');
   errorbar(cPa,gs,gser,'ok');


   hold off
```

```matlab
    title('Apparent Intensity vs. concentration')
legend('Red','Green','Blue','Grayscale','location','best')
xlabel('Methylene Blue Concentration * Path Length [mM*mm]')
ylabel('Apparent Intensity')


%%% fit the greyscale to a log function
f=ezfit(cPa,gs,'a*log(x)+b; a=.09; b=1.4');
showfit(f,'fitcolor','black','linlogdisp','off','corrcoefmode','r2','dispeqboxmode','off')
%%% try plotting it in another colorspace
figure(4)
 % hsv plot
    hold on
    errorbar(cPa,hm,her,'og');
    errorbar(cPa,sm,ser,'ob');
    errorbar(cPa,vm,ver,'ok');


    hold off
    title('Apparent Intensity vs. concentration - HSV')
    legend('Hue','Saturation','Value','location','best')
    xlabel('Methylene Blue Concentration * Path Length [mM*mm]')
    ylabel('Apparent Intensity')
%     f=ezfit(cPa,sm,'a+b*x+c*x^2; a=.09; b=1.4; c=-2');
     f=ezfit(cPa,sm,'a*log(x)+b; a=.09; b=1.4;');
    showfit(f,'fitcolor','black','linlogdisp','off','corrcoefmode','r2','dispeqboxmode','off')

figure(5) % hsv plot
    hold on
    errorbar(cPa,ym,yer,'og');
    errorbar(cPa,im,ier,'ob');
    errorbar(cPa,qm,qer,'ok');


     hold off
     title('Apparent Intensity vs. concentration - YIQ')
    legend('Luminance','Hue','Saturation','location','best')
    xlabel('Methylene Blue Concentration * Path Length [mM*mm]')
    ylabel('Apparent Intensity')

%%%
```